UC Berkeley
UC Berkeley Electronic Theses and Dissertations

Title

Understanding Photoprotection in Algae through Combined Modeling and Experimental Studies

Permalink

https://escholarship.org/uc/item/9t84f3np

Author

Short, Audrey Higgins

Publication Date

2024

Peer reviewed|Thesis/dissertation

eScholarship.org Powered by the California Digital Library
University of California

Understanding Photoprotection in Algae through Combined Modeling and Experimental Studies

By

Audrey Higgins Short

A dissertation in partial satisfaction of the

requirements for the degree of

Doctor of Philosophy

in

Biophysics

in the

Graduate Division

of the

University of California, Berkeley

Committee in charge:

Professor Graham R. Fleming, Chair

Professor Daniel Fletcher

Professor Anatasios Melis

Professor David Savage

Summer 2024

Copyright 2024
Audrey Higgins Short
All rights reserved.

Abstract
Understanding Photoprotection in Algae through Combined Modeling and Experimental Studies

by

Audrey Higgins Short

Doctor of Philosophy in Biophysics

University of California, Berkeley

Professor Graham R. Fleming, Chair

Photosynthesis utilizes energy from the sun to power photochemical reactions that store energy in chemical bonds, creating the basis of our food chain. As the world population continues to grow, the projected demand for crops is increasing at a higher rate than current agricultural techniques can produce. Altering dynamics around how plants and algae protect themselves from changes in light levels has been proven to increase crop yields. Light levels are constantly changing in nature due to shifts in canopies, weather events, seasons, and photosynthetic organisms need rapidly reversible mechanisms to adjust to sudden changes between high and low light levels. In high light (HL) conditions, excess energy is unable to participate in photochemistry and is instead dissipated through non-photochemical quenching (NPQ) as heat, minimizing reactive oxygen species formation. But, if these NPQ pathways are not de-activated, energy is lost even in low light conditions, leading to an underutilization of light. Plants and algae need to balance photochemistry and photoprotection to maximize efficient energy use in all light conditions. However, NPQ pathways can be slow to turn on and off. By understanding these processes more fully, photosynthesis can be optimized by increasing organisms' responsiveness to light.

In this dissertation, my research focuses on understanding the role that each unique molecular component of NPQ contributes to the overall summation of photoprotection. NPQ is incredibly diverse across photosynthetic organisms—as will be discuss in Chapter 1—yet there are several key features that are nearly universal. These components would be pH-sensing proteins and the xanthophyll cycle. In addition to experiments, we have created a model using these two molecular components as a basis to inform our understanding of the dynamics of these NPQ components in response to all types of light environments, which is explored in Chapter 2. The model is quantitative and predictive, which is helpful in determining the limits of photosynthetic yield improvements when parameterized to a specific organism. The model in turn has highlighted unique attributes of the xanthophyll cycle, particularly the role of antheraxanthin in photoprotective memory (Chapter 3). We explore the effect of two-state verses three-state xanthophyll cycles further in Chapter 4. By creating a flexible model based on the biochemical components of NPQ, we can expand this work to crop plants and other organisms to predict how changes in relevant NPQ pathways might affect the expression and dynamics of photoprotection.

To my family, my friends, and teachers who have helped me reach this goal.

Table of Contents

List of Figures

List of Tables

List of Symbols and Abbreviations

^{1}Car*	singlet excited state of carotenoid
^{1}Chl*	singlet excited state of chlorophyll
$^1O_2$*	singlet excited state of molecular oxygen
^{3}Chl*	triplet excited state of chlorophyll
$^3O_2$	triplet ground state of molecular oxygen
A	antheraxanthin
Car	carotenoid
Chl	chlorophyll
$Chl^{\bullet-}$	chlorophyll radical anion
CT	charge transfer
D	dark
DCBQ	2,6-dichloro-1,4-benzoquinone
DCMU	2-(3,4-dichlorophenyl)-1,1-dimethylurea
Dd	diadinoxanthin
DDE	Dd de-epoxidase
DEP	Dt epoxidase
DES	de-epoxidation state
Dt	diatoxanthin
EET	excitation energy transfer
ESA	excited state absorption
FAD	flavin-adenine dinucleotide
FCP	fucoxanthin-chlorophyll binding protein
FWHM	full width at half-maximum
HL	high light
HPLC	high-performance liquid chromatography
ISC	intersystem crossing
L	lutein
LEP	lutein epoxidase
LHC	light-harvesting complex
LHC	light harvesting complex
LHCSR	light-harvesting complex stress related protein
LHCX	light-harvesting complex stress related protein
LL	low light
Lx	lutein epoxide
NPQ	nonphotochemical quenching
PAM	pulse-amplitude modulation fluorimetry
PC	plastocyanin
PQ	plastoquinone
PS	photosystem
PsbS	photosystem II subunit S protein
PSI	photosystem I
PSII	photosystem II
qE	energy-dependent quenching
qI	photoinhibitory quenching
qT	state-transition quenching

Q_y	chlorophyll excited state
qZ	zeaxanthin-dependent quenching
RC	reaction center
ROS	reactive oxygen species
TA	transient absorption spectroscopy
TCSPC	time-correlated single photon counting
V	violaxanthin
VAZ	violaxanthin-antheraxanthin-zeaxanthin (xanthophyll) cycle
VDE	violaxanthin de-epoxidase enzyme
VDL	VDE-like
Z	zeaxanthin
ZEP	zeaxanthin epoxidase enzyme
ΔpH	proton gradient across thylakoid membrane

Acknowledgements

I am profoundly grateful to all those who I have met and worked with during my PhD. I would not have made it through my PhD program without their encouragement, advice, and support throughout my various endeavors.

First and foremost, I am grateful to have had an excellent research advisor in Graham Fleming. From our first meeting, Graham saw my curiosity and excitement about photosynthesis and encouraged me to always pursue new questions. He also learned firsthand how gregarious I could be, but still took me on as a student, mentoring me and imparting so much of his knowledge, expertise, and wisdom about photosynthesis. With his mentorship, I have made great strides towards becoming the scientist and researcher I hope to be.

Secondly, I would like to thank all my colleagues and collaborators. From the Fleming Lab, I am especially grateful to Collin Steen for mentoring me during my first few years in the lab. He introduced me to the exciting world of non-photochemical quenching and spectroscopic experiments. I have learned so much from Collin, particularly his penchant for organization, though I still strive to become the excellent science communicator that he is. Thien Crisanto, who was a fellow graduate student in the Niyogi Lab, is another amazing role model and brilliant scientist I have had the privilege to work with. She not only grew all the *Nannochloropsis oceanica* algae I used over the years, but also came up with so many fantastic ideas for new projects and approaches to problems. Her creativity and optimism were invaluable during tricky experiments. Much of my work has been supported by the fantastic model created by Tom Fay—a postdoc in the Limmer Lab—who was able to take my observations about photoprotective dynamics and create an elegant model which has greatly added to our understanding of photosynthesis and influenced much of my work. Setsuko Wakao has recently collaborated with me on our diatom project. Her insight and creativity have allowed this project to flourish, and if I had more time, we would likely endeavor to answer even more questions about diatom NPQ. And to Masakazu Iwai, whose guidance and tutelage has made me a better biochemist. Masa has taught me many protocols that have not only expanded my knowledge of the biochemical aspects of photosynthesis, but his attention to detail inspires me to carefully and thoughtfully approach all my projects.

In addition to those mentioned above, I have had the ability to work with many exceptional scientists in the Niyogi Lab. A huge thanks to Ethan Boynton, who helped guide me when I attempted to grow algae myself, and to Nina Marin, who taught me to use the HPLC instrument and always helped when it would (frequently) break. And to all other members of the lab who were always so kind and helpful.

I also would like to thank the Zhang Lab at the University of Cambridge who welcomed me for one summer to work on biophotovoltaics. Robin Scullion was a particular bright spot during my time there as they welcomed me to game nights and taught me about electrodes and cyanobacteria. Without this time in England, I would not have found my passion for applied photosynthetic research. This work was supported by the Winton-Kavli Exchange Scholarship.

My research would not have been possible without the support of my lab mates through the years. Thank you to Kaydren Orcutt who taught me about spectroscopy and lasers and was always there to get coffee with me. To Shane Yang, Lam Lam, and Tsung Yen Lee who I have worked beside for 5 years, thank you for your feedback, your help when the laser would not cooperate, and your support. To Sara Ricks for holding this lab together by organizing all the chaos and paperwork.

And to Johanna Hall who started out as my first summer intern and became my lab mate and close friend. Thank you for always wanting to go on a coffee run or to go piggy dipping or just yapping on top of helping me align lasers when I could not get anything to work. You make coming into lab fun, and I will miss you so much when I leave. I know Graham will finally have peace for one ear, but do not stop yapping off his other!

Thank you to the members—Daniel Fletcher, David Savage, and Anastasios Melis—of my qualifying and dissertation committees at UC Berkeley.

Next, I want to thank those who might not have had a direct role in my research projects, but without whom I certainly could not have made it through grad school. To all my friends who lived with me at the MLK apartments, I will miss our Bachelor/Bridgerton/movie nights. I will miss our parties and Friendsgivings. My next apartment will feel all the more empty without your laughter and friendship. But I most especially want to thank my two best friends Emily Meschke and Logan Thomas. You both took me in when my living situation became untenable, right before Covid hit. Months of quarantining is enough to drive anyone crazy, but our friendship grew. And during our five years in Berkeley, you have become like family to me. You both have helped me grow so much as a researcher but more importantly as a person.

Finally, thank you to my parents, Becky and Steve Short, and my brother and sister-in-law, Spencer and Brittany Short, who have encouraged me and supported me throughout these five years and who will always stand by me. To quote our family motto: “If it’s worth doing, it is worth over-doing.” I think I nailed that one on the head.

Funding Statement: The work presented in this dissertation was supported by the U.S. Department of Energy, Office of Science, Basic Energy Sciences, Chemical Sciences, Geosciences, and Biosciences Division under the field work proposal 449B.

Chapter 1

Introduction to Photoprotective Pathways and Mechanisms

Sections of this chapter are reproduced with permission from the following publications:

C.J. Steen, J.M. Morris, A.H. Short, K.N. Niyogi, G.R. Fleming
"Complex Roles of PsbS and Xanthophylls in the Regulation of
Nonphotochemical Quenching in *Arabidopsis thaliana* under Fluctuating Light"
J. Phys. Chem. B (2020)124, 46, 10311–10325
DOI: 10.1021/acs.jpcb.0c06265. Copyright © 2020American Chemical Society

C.J. Steen, A. Burlacot, A.H. Short, K.N. Niyogi, G.R. Fleming
"Interplay between LHCSR proteins and state transitions governs the NPQ
response in intact cells of Chlamydomonas during light fluctuations"
Plant Cell Environ (2022) 45, 2428-2445
DOI: 10.1101/2021.12.31.474662. Copyright © 2022 Authors

1.1 Motivation

Oxygenic photosynthesis is one of the most important biochemical processes on earth; it has completely altered our atmosphere and is the basis of our food chain. With increasing populations, the demand for food is outpacing current projections for what farmers can produce[1,2]. One way of addressing this issue is to increase the yield per field for all crop plants. Up to 30% of canopy carbon fixation is lost because of the slow relaxation dynamics of photoprotection[2]. Altering photoprotective pathways through related protein expression is speculated to increase crop yields[3–5]. Recently, Long et al showed this to be true in soybeans. By increasing the expression level of three genes related to photoprotection, they were able to increase yields by ~25%[6]. However, in these experiments, it is unknown if the increased ratio of these three genes is providing the maximum improvement to yields in crop plants and biofuel algae. Improving the responsiveness of plants to light conditions—increasing protection in high light (HL) or turning off dissipative pathways in limiting light conditions—will allow plants to utilize the energy available more efficiently, thereby maximizing the rate of carbon fixation without incurring damage[7,8]. Figure 1-1 depicts what this might look like if photosynthetic organisms were genetically modified to rapidly respond to changes in light levels.

Within this introduction, I will mainly discuss the model organisms that I have studied throughout my thesis work: *Arabidopsis thaliana*[9], *Chlamydomonas reinhardtii*[10], *Nannochloropsis oceanica*[11,12], and *Thalassiosira pseudonana.* These organisms cover some of the diversity found in photosynthetic, eukaryote taxa—broadly categorized as vascular plants, green algae, eustigmatophyte algae, and diatoms. While photoprotection research is mainly motivated by improving crop yields, understanding NPQ across the photosynthetic landscape is beneficial in determining which specific proteins are the most effective in their role as well as giving insight into the diversity of photoprotective mechanisms found in nature. Additionally, algae and diatoms account for 25% of primary production[13] and 40% of oceanic carbon fixation[13–15], indicating how

important these organisms are for maintaining our climate and can be utilized for biofuel production[16–18].

By studying natural photosynthetic systems in fluctuating systems, a better understanding of how plants and algae protect themselves in HL can be gained. With this information, a universal model can be created to predict how photosynthetic organisms may respond to fluctuating light conditions thereby allowing scientists to make predictions of which photoprotective components to target. However, this endeavor is made difficult by the complexity of photoprotection. Below, I will describe what photosynthesis is, the role and pathways of photoprotection, and how the components of photoprotection are species dependent.

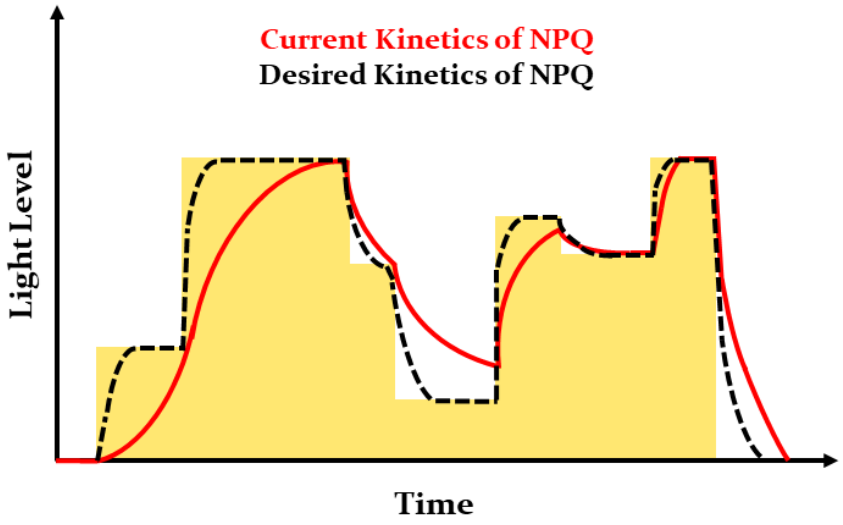

Figure 1-1. Cartoon representation of the goal for photoprotection research. The red line shows a typical NPQ response to altering levels of high light that might be encountered in nature. In the HL periods, photosynthetic organisms are under-protected, meaning more energy than required is absorbed by photosynthetic apparatuses, leading to damage and cell death. Meanwhile, when organisms are in sub-saturating or lower light levels, NPQ mechanisms dissipate more energy than is used to saturate photosynthesis pathways. In these low light periods, organisms are unable to utilize the limited light energy to capture CO_2. Schematic adapted from Ruban *Nature* 2017, *541*,36-37[8].

1.2 Photosynthesis

Within eukaryotic photosynthetic organisms are organelles called chloroplasts where the light and dark reactions of photosynthesis occur. Within chloroplasts are thylakoid membrane which is a continuous membrane that forms stacked regions called grana and unstacked regions connecting the grana referred to as the stroma lamellae[19]. The thylakoid membrane is integral to photosynthesis as both photosystem (PS) I and II are embedded in the lipid bilayer. Additionally, the thylakoid membrane encloses an aqueous spaced called the lumen, which allows for a pH gradient to form, powering ATP synthase[19,20] (Figure 1-2a,b). Photosynthesis uses energy from the sun to split water and store energy in the chemical bonds of NADPH and ATP[20,21]. NADPH and ATP are then utilized in the Calvin-Benson Cycle, also known as the dark reaction, to form

carbohydrates[22]. While we understand the overall process and its impact on our world, we are still trying to understand the complexities of various aspects of photosynthesis such as oxygen evolution, energy transfer within PS, and photoprotection. This thesis will focus on the latter: understanding the role and importance of photoprotection and how photoprotection impacts the overall efficiency of photosynthesis.

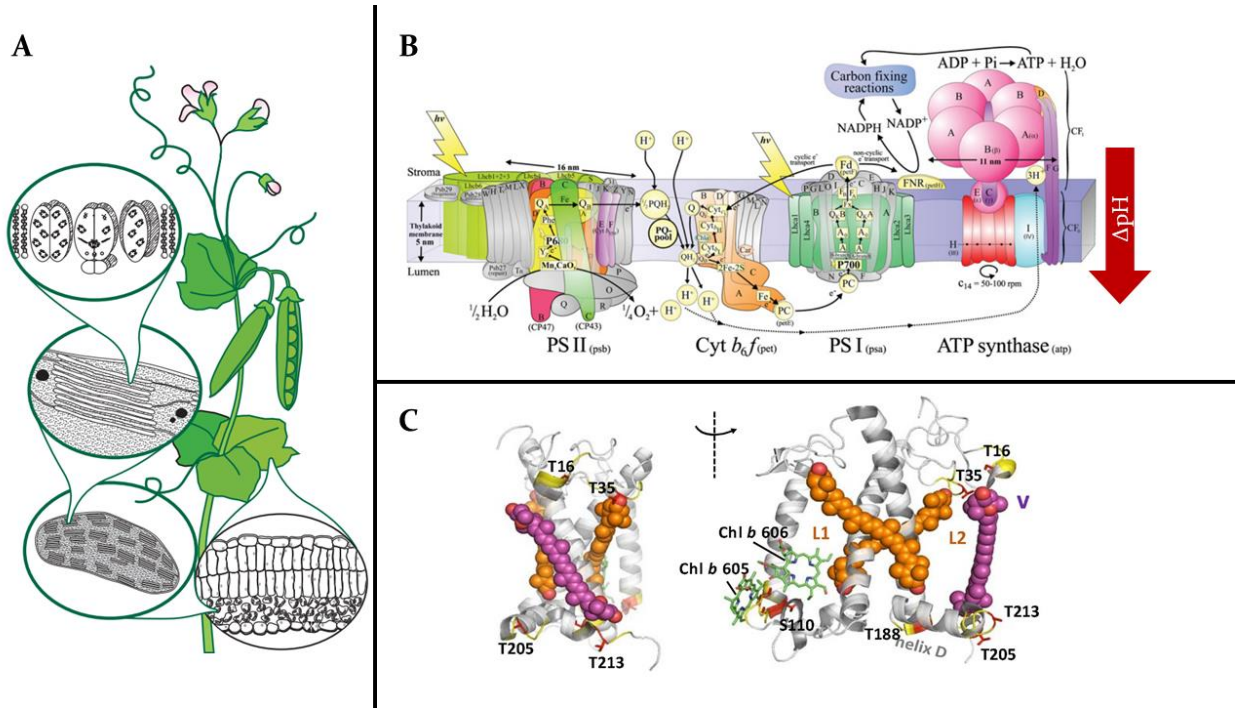

Figure 1-2. Illustration of the photosynthetic structures from a macro to micro level. Pane **A** depicts the cellular structure of photosynthetic organelles in plants by zooming into smaller lengths scales from whole leaf to the cellular to the chloroplast to the grana and finally to the thylakoid membrane. Panel **B** shows a more detailed depiction of the thylakoid membrane and the multitude of proteins that are relevant to photosynthesis. Image **A** and **B** adapted from Blankenship, R. *Molecular Mechanisms of Photosynthesis*, 2021[22]. Panel **C** shows the monomer subunit of the LHCII trimer. Image borrowed from Azadi-Chengi et al. *Biophys J* 2020, *120*, 270-283[23].

In ideal conditions, plants and algae will capture energy from the sun, using the energy to excite an electron from the specialized chlorophyll (Chl) pair known as the reaction center (RC) to an acceptor molecule which will funnel the electron through the electron transport chain[22]. The RC is surrounded by an antenna composed of additional light harvesting complexes (LHC) which contain Chl and carotenoids (Car)[24]. The most abundant protein in world[25] and in thylakoid membranes is LHCII, which is a heterotrimer containing LHCII binds 14 Chl, 2 lutein, 1 neoxanthin, and sub-stoichiometric amounts of violaxanthin per monomer[19,26,27]. LHCII has four binding sites for Car, but as violaxanthin as a lower affinity for LHCII compared to other Car, during purification it is often lost[27] (Figure 1-2c). Cars like lutein, neoxanthin, and violaxanthin are accessory pigment molecules that can extend the usable wavelengths and transfer the energy to nearby Chls. Additionally, Cars also aid in structure and photoprotective mechanisms to dissipate excess energy as heat[28,29]. The role that Car play in photoprotection will be discussed in greater detail in section 1.3.2. While the core RCs are well conserved between all oxygenic photosynthetic organisms, the surrounding antenna can differ[30]. In other species, the light

harvesting complexes surrounding the RCs are known as fucoxanthin-chlorophyll binding proteins (FCP)[31]. FCPII are typically trimers[32] or tetramers[30] or nonamers[33], depending on the species. FCP monomers and dimers also have been observed[32]. FCPII functions similarly to LHCII.

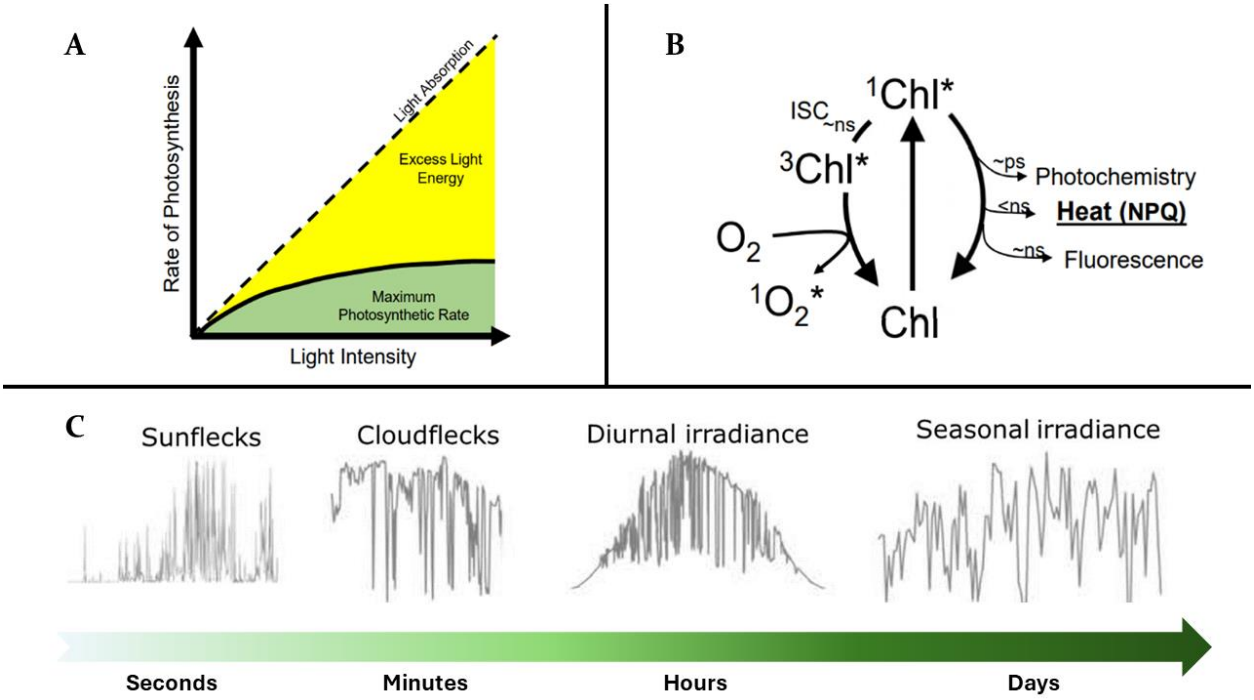

Figure 1-3. Schematics depict several aspects of photoprotection. **A** represents how increasing light intensity leads to an abundance of excess light that cannot be utilized as photosynthetic processes are entirely saturated. This figure is adapted from Ruban *Nature* 2017, *541*, 36-37[8] **B** shows the multiple pathways that excitation energy from photons can be dissipated, returning Chl to its ground state. In ideal light conditions, the main pathway is through photochemistry while intersystem crossing (ISC) and NPQ become more important in excess light. This figure is adapted from Müller et al. *Plant Physiology* 2001, *124,* 1558-1566[34] **C** represents the fluctuating light patterns organisms experience of multiple timescales ranging from seconds to seasonal changes. This is adapted from Morales and Kaiser *Front. Plant. Sci* 2020, *11*[35].

In the linear electron transport chain, starting from PSII, energy is harvested by the antenna and transferred to PSII's RC, referred to as P680[36]. This energy is used to excite an electron, which is then passed to plastoquinone (PQ)[20]. The electron is replaced by splitting a water molecule into molecular oxygen and hydrogen ions in the oxygen evolving complex connected to PSII[37]. PQ will pick up two electrons from PSII before it moves to cytochrome b_6f[20]. Cytochrome b_6f will transfer the electrons to PSI via the soluble electron carrier plastocyanin (PC)[20] found in the lumen. These electrons will replace the electrons that are excited from the PSI RCs. In PSI, the electron is moved from P700—PSI's RC—to ferredoxin (Fd) to ferredoxin-NADP+ reductase (FNR), where NADPH is formed[38]. As electrons move along the electron transport chain, a pH gradient will form as more H+ are pumped into the lumen. This electrochemical gradient (ΔpH) powers ATP synthase by moving H+ back across the thylakoid membrane through ATPase[39] (Figure 1-2b).

However, changes in the environment can induce stress to the photosynthetic machinery, limiting their efficiencies. Sunlight can be a dual edged sword for photosynthetic organisms. In most crop

plants, photosynthesis is saturated at about a quarter of the maximum intensity of full sunlight[4]. Above this level, energy from the sun is wasted and can cause irreversible damage and even cellular death[40,41] (Figure 1-3a). These effects are exacerbated when organisms must rapidly switch between HL and low light conditions. Within a day, plants and algae are exposed to several orders of magnitude of light intensities as well as fluctuations due to weather (i.e. cloud coverage), lens effects from water, or fluctuations in canopies[35,42–44] (i.e. sunflecks) (Figure 1-3c).

As the kinetic limit for CO_2 fixation and electron transportation are approached, there is excess energy that cannot be utilized by the RCs[44]. This can occur when light levels exceed an organism's maximum photosynthetic rate (Figure 1-3a), which arises because energy transfer into a RC is much faster (fs-ps timescale) than the diffusion rate of electron carriers like PQ or PC (ms)[45]. This leads to 'closed' or saturated RCs which are unable to accept capture energy from the surrounding antenna as the RC is unable to transfer the excited electron to PQ or replenish depleted RCs like in PSI. PSI has ways of preventing this excess energy from being wasted through the cyclic electron transport chain, which is a necessary pathway to increase the concentration of ATP[46,47], but PSII does not have a way of quickly recycling its electron acceptors. Additionally, since the oxygen-evolving complex is contained within PSII, there is a higher local concentration of reactive oxygen species (ROS), which can lead to protein degradation and PSII inactivation[48].

Over millennia, plants and algae have developed alternative pathways to dissipate this excessive energy that cannot be utilized by RCs[49]. In ideal light conditions the majority of excited Chl are returned to the ground state via photochemistry as described above. Additionally, ^{1}Chl* also relaxes back to the ground state via fluorescent decay, admitting a photon in the 600 nm to 700 nm range on a ~ns timescale[22] (Figure 1-3b). Chl *a* fluoresces at 680 nm. Both pathways occur at all light intensities. However, in HL regimes—which are species- dependent but typically occur at light levels greater than 600 μE[50]— ^{1}Chl* state may undergo intersystem crossing to become ^{3}Chl* (~ns). In the excited triplet state, ^{3}Chl* can interact with ground state oxygen ($^3O_2$) to become singlet oxygen ($^1O_2{}^*$)[51]. To minimize ROS formation, photosynthetic organisms have evolved to prioritize photoprotective pathways collectively referred to as non-photochemical quenching (NPQ) pathways in times of high light (HL) and other stressor events[34]. With NPQ, excess energy is dissipated as heat[52]. There are many pathways and mechanisms that fall into this category[44], which are discussed in the following section.

1.3 Photoprotection

NPQ pathways are classified based on their time scale and involved molecular components, which can lead to confusion in what photoprotective mechanisms are being activated or contributing to NPQ at any given time (Figure 1-4). There are five main NPQ pathways that are referred to as qE, qZ, qI, qT, and qH. Since there is overlap in the molecular actors participating in the NPQ pathways, it is easier to discuss the role of each individual molecular actor regardless of which NPQ pathway it falls into when creating a universal model. However, before we discuss the contributions of the molecular components, I will describe the characteristics of each pathway.

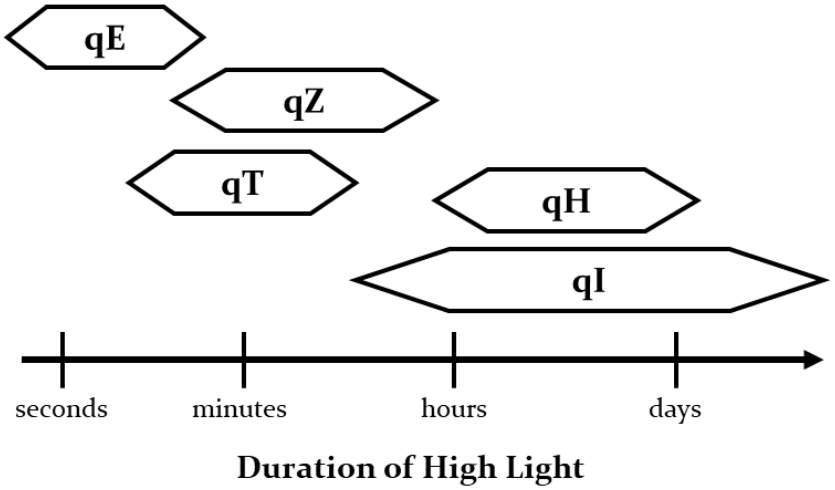

Figure 1-4. Schematic describing the relative activation and deactivation timescales of NPQ pathways. Many of these processes overlap in timescales and in molecular actors making NPQ difficult to alter. Adapted from Erickson *et al*. *Plant Journal* 2015, *82*, 449-465[53].

(1) Energy-dependent quenching (qE) is responsible for ~85% of NPQ. qE is known to be rapidly reversible, activating and deactivating with ~1 minute[53,54]. It is associated with lumen acidifying as the pH gradient across the membrane increases and requires a pH-sensing protein in association with a de-epoxidated Car[55]. This pathway likely is activated by a conformational change of the pH sensing protein that causes the Cars to switch roles from light harvesting to photoprotection[56]. The identity of the pH-sensing protein is species-dependent as well as the mechanisms for how energy is quenched.

(2) Zeaxanthin-dependent quenching (qZ) is associated with the accumulation of zeaxanthin (Z), a de-epoxidized Car[28]. Z is formed through the violaxanthin-antheraxanthin-zeaxanthin (VAZ) cycle, where violaxanthin de-epoxidase (VDE) converts V to A to Z[57,58]. This pathway also has a pH-dependent component as VDE is activated when the lumen acidifies[59]. Zeaxanthin epoxidase (ZEP) reverses this process back to the V, which is the Car best suited for light harvesting. Generally, the accumulation of Z takes about 5-15 minutes of high light (HL) exposure[60]. qZ is a slowly relaxing process, but individual reactions in the cycle may activate faster, as will be discussed in Chapter 3. Not all photosynthetic species contain Z. Two other xanthophyll cycles exist which may induce similar effects to qZ. All three xanthophyll cycles will be explored in further detail below (Figure 1-8).

(3) State transitions (qT) refer to the movement of LCHII trimers from PSII to PSI and vice versa depending on which PS is being preferentially excited. In State I, PSII is preferentially excited; this causes an over reduction of the PQ pool, activating a kinase, which is bound to cyt b_6f[19]. The kinase—a number of which have been identified and are species dependent[61]—phosphorylates LCHII causing the trimer to migrate to PSI[62], increasing the light harvesting antennae size around PSI. When PSI is more favorably excited, known as State II, LHCII is de-phosphorylated and returns to PSII[61] (Figure 1-9).

(4) Photoinhibition (qI) occurs whenever there is damage to the photosystems, though PSII is more often affected[63]. PSII is involved in qI since water oxidation occurs at this

protein complex, increasing the likelihood of ROSs damaging the D1 protein where water oxidation happens. PSII is then completely deconstructed until the D1 subunit is repaired[44,54,64]. This can lead to further damage as less PSII's are able to participate in linear electron flow[44].

(5) qH is a sustained relax photoprotective pathway that is independent of ΔpH[65–67]. This process is typically found in colder climates with long exposure to HL such as in evergreens[68]. However, based on the experiments I have conducted for my thesis this process does not contribute to photoprotection and will not be discussed in detail.

In many crop plants, these processes are started simultaneously and contribute varying amounts depending on the duration and intensity of HL. The quenching mechanisms of each pathway are complex and highly debated, thus making it difficult to make a model of the NPQ response which could provide insight into the biochemical processes. Through understanding how each unique biochemical component contributes simultaneously and/or independently to photoprotection, we can create models to guide our efforts to improve crop yields. With information about which mechanisms are impacting NPQ activation and deactivation rates, we can predict how to improve the responsiveness of NPQ. Long et al. was able to increase soybean yields by 24.5% by increasing the expression of VDE, ZEP, and the plant pH-sensing protein, PsbS[6]. Utilizing a model that could inform researchers which molecular components are the best to target for NPQ could lead to even larger increases in crop productivity. Additionally, not all NPQ pathways are found in all species of photosynthetic organisms, and even shared pathways utilize difference proteins, which may result in difference effects. This can make it difficult to construct a model to understand the role of photoprotection across photosynthetic organisms. In the next section, I will address the three main molecular components involved across the board in NPQ and how different species utilize certain molecular actors as well as the different proteins that occupy the same role to motivate why it is important to study multiple species to fully understand photoprotection.

1.3.1 pH-sensing Proteins

The first indication of HL stress occurs when the PQ pool is over reduced; the lumen acidifies which acts to trigger the start of NPQ mechanisms[69]. This effect can be proven by the use of de-coupler chemicals like nigericin or ammonium chloride, which prove a pH-gradient is needed to trigger photoprotection[47,70]. However, without a pH gradient, even with the accumulation of de-epoxidated Car, qE does not occur[71]. A pH sensing protein is therefore required to induce necessary changes to induce rapid and reversible quenching upon acidification of the lumen. So far three pH-sensing proteins have been identified in photosynthetic organisms.

1.3.1.1 Vascular Plants

In most vascular plants, the involvement of the pH-sensing protein, PsbS, is widely recognized[71–73]. This 22 kDa protein is a subunit of PSII[74,75] and has four transmembrane helices with two lumen exposed glutamates, which can be protonated when the lumen is acidified in high light[72]. The role of PsbS can be seen in Figure 1-5, which depicts several mutant lines of *A. thaliana*. In *A. thaliana*, two mutants exist that effect PsbS expression: *npq4*[71] (red line) is deficient in PsbS while *L17*[76] (orange line) is a PsbS-overexpressing mutant. In the PsbS-containing strains (WT, *npq1, stt7, L17*), there is an oscillatory response to changes in the light environment. PsbS allows for the dynamic switch between photoprotection and light-harvesting. There is minimal modulation of NPQτ in the *npq4* mutant as the system cycles between light and dark phases. During dark phases, NPQτ increases for *npq4*, likely arising from photoinhibition or potentially state transitions[10].

Interestingly, the overexpressor, *L17*, has significantly increased NPQτ values compared to the WT (blue line). This indicates that PsbS also modulates the extent of quenching in plants. PsbS is not able to bind pigments yet has a substantial impact on quenching in plants[56]. The exact quenching mechanism induced by PsbS is debated, but likely when protonated by the pH-gradient, PsbS switches from its inactive dimeric form to its active monomeric form to force LHCII into a quenched state[77–81] by distancing the trimer from the supercomplex[56]. This process is reversed in the dark when PsbS is de-protonated. While PsbS is indispensable to all vascular plants for photoprotection, it is only active in this lineage and therefore does not provide a full image of pH-sensing proteins involved in photoprotection.

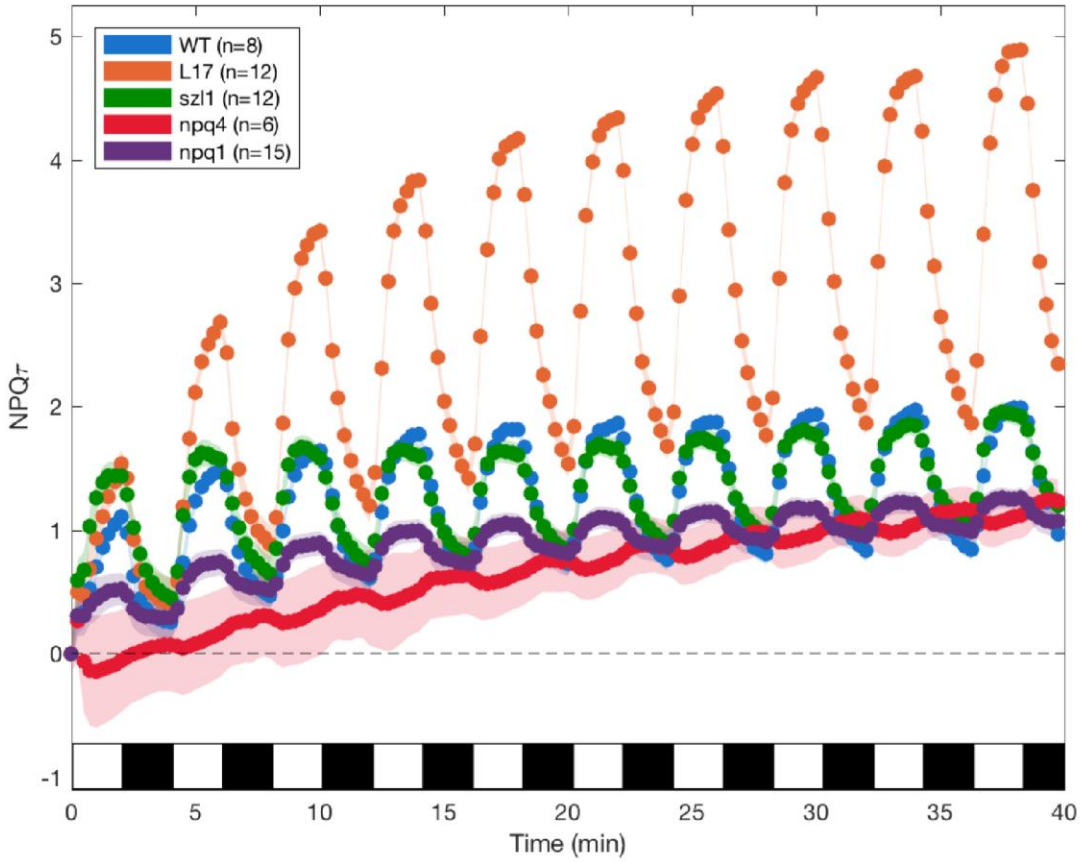

Figure 1-5. Comparison of NPQτ traces for each strain: WT (blue), *L17* (orange), *szl1* (green), *npq4* (red), and *npq1* (purple). The PsbS-containing lines (WT, *L17*, *szl1*, and *npq1*) show oscillatory quenching induction and relaxation within each period. The PsbS-deficient mutant *npq4* does not show strong oscillatory behavior and the Zea-deficient mutant *npq1* shows a dampened oscillatory behavior. Data are presented as the mean NPQτ value, and the shaded regions represent the standard error. The number of independent leaf samples measured for each genotype is indicated in the legend. The white boxes represent two minutes of HL while the black boxes represent the two-minute dark period.

1.3.1.2 Green Algae

In green algae, qE is mediated by the light harvesting complex stress related (LHCSR) proteins—formally referred to as LI1818[82]. The LHCSR protein is known to bind pigments[83,84] as well as contain three transmembrane helices with protonatable residues[85] exposed to the lumen which can

trigger NPQ[86–88]. LCHSRs are of particular interest because they can bind pigments, allowing them act as the quenching location as well as the pH-sensing proteins[85,89]. Two homologues of LHCSR proteins—LHCSR3 and LHCSR1—exist, which both bind pigments and contribute to NPQ[89,90], but LHCSR3 is considered the main molecular actor in qE[83,91]. Since quenching occurs on LHCSR3, it is a simple system to study NPQ. However, LHSCRs must be induced to accumulate to produce a significant photoprotective response to HL[83]. Therefore, to study NPQ associated with LHSCRS, organisms like *C. reinhardtii* are exposed to prolonged HL before experiments. Interestingly, the *psbs* gene is found in *C. reinhardtii*, but the protein is not expressed or accumulated[83,92].

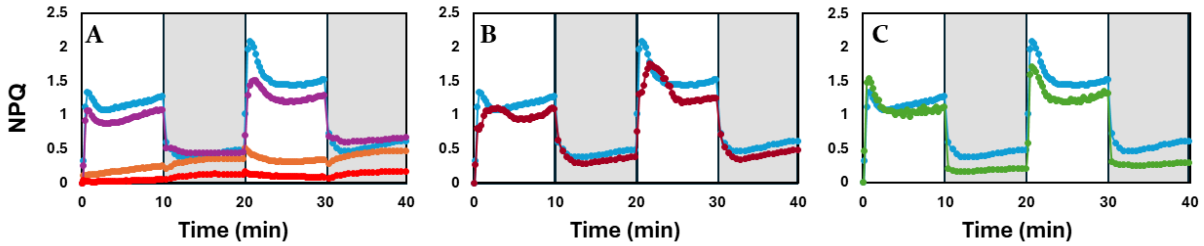

Figure 1-6. Comparison of *C. reinhardtii* NPQ traces for each strain: WT (blue), *lhcsr1* (purple), *npq4* (orange), *npq4lhcsr1* (red), *stt7* (green), *stt7npq4* (pink). **A** Comparison of the pH-sensing mutations (*lhcsr1*, *npq4*, *npq4lhcsr1*) to WT. *lhcsr1* has a minute effect on NPQ expression while the two *npq4* strains are significantly impacted. **B** The traces of WT and *npq1*, showing the minimal effect of removing Z accumulation. **C** The comparison of WT and *stt7*, which highlights the impact of state transitions in the dark phases. The white boxes represent the 10 min HL periods while the gray boxes show the 10 min dark phases.

In *C. reinhardtii*, the mutant strain knocking out LHCSR3 is referred to as *npq4*[83], though it does not knockout the PsbS gene, while *lhcsr1* refers to mutants without LHCSR1 present[93]. When comparing WT with the LHCSR double mutant, *npq4lhcsr1*, there is a significant difference in the NPQ response with only a minimal increase in NPQ during HL phases while in the light to dark transition there is an increase in NPQ during the dark phases. Comparing the two single pH-sensing mutant knockouts shows that *lhcsr1* has a phenotype similar to WT, indicating its minor role in photoprotection. Meanwhile *npq4* is notably impaired in its response, though reaches higher NPQ values during light phases than the double mutant, indicating that both proteins are needed to produce maximum photoprotection (Figure 1-6A).

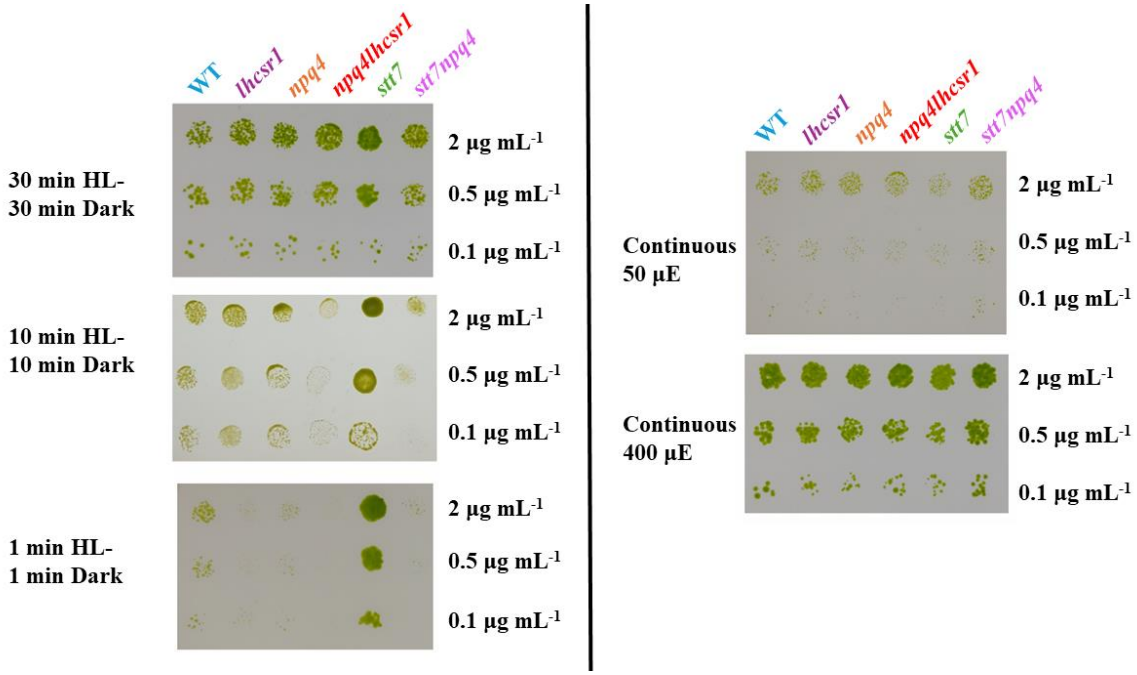

Figure 1-7. Growth of *C. reinhardtii* strains {WT (blue), *lhcsr1* (purple), *npq4* (orange), *npq4lhcsr1* (red), *stt7* (green), *stt7npq4* (pink)} in fluctuating light and continuous light conditions. On the left, the comparison of the difference strains in 30 minutes, 10 minutes, and 1 minute of HL fluctuations. In rapid (1 min HL- 1 min D), the strains that do not contain the pH-sensing proteins (*lhcsr1*, *npq4*, *npq4lhcsr1*, *stt7npq4*) are unable to grow. However, in the 10 min HL- 10 min dark, only the two double mutants (*npq4lhcsr1, stt7npq4*) exhibit decreased growth. In the slow light fluctuations, there is no significant change between WT and the mutant strains. On the right, continuous light inhibits cells' ability to grow in 50 µE while all strains are able to grow significantly more in HL.

The relationship between NPQ capacities and growth have remained puzzling in Chlamydomonas, because only some light fluctuation regimes have consistently been shown to impair growth[10,83,94,95]. While all mutants, including mutants deficient in one (*lhcsr1, npq4, stt7npq4*) or both LHCSRs (*npq4lhcsr1*), grow well in continuous light, especially at 400 µE, pH-sensing mutants were not able to grow well in rapid fluctuating light sequences (1 min HL-1 min D) (Figure 1-7). In the intermediate 10 min HL- 10 min dark light pattern, the double mutant *npq4lhcsr1* grew poorly while the single LCHSR mutants were comparable to WT with *npq4* performing worse than *lhcsr1*. This trend was absent under the slowest fluctuating light sequence (30 min HL- 30 min D), appearing very similar to continuous light growth. There seems to be a good relationship between defect of NPQ and growth deficiency under rapid fluctuations when considering *npq4lhcsr1* and *stt7npq4* mutants (Figure 1-7), clearly showing that LHCSR-dependent qE is critical for growth when light fluctuates within a short period of time.

1.3.1.3 Eustigmatophyte Algae and Diatoms

In diatoms like *Thalassiosira pseudonana* or *Phaeodactylum tricornutum* and the Eustigmatophyte, *Nannochloropsis oceanica,* LHCX proteins mediate qE. LHCXs are homologues to LHCSRs found in green algae. The LHCX proteins are able to modulate NPQ in diatoms. In *Nannochloropsis*, LHCX-like proteins, specifically LHCX1, are necessary for an NPQ response[96,97]. In diatoms, LHCX1 is upregulated, leading to a high NPQ phenotype[98–100]. LHCX4

and LHCX6 are also upregulated in HL exposure, indicating that they may also play a role in photoprotection[101]. LHCX proteins have three membrane-spanning helices like LHCSRs[98]. However, unlike LHSCR3, LHCX1 in *P. tricornutum* does not bind pigments, nor does it sense lumen pH as its protonatable residues, D95 and E205, do not affect NPQ when mutated[98]. Whether LHCX1 can bind pigments or sense a change in pH is highly debated and still under investigation[97,98,102–106].

1.3.2 Xanthophyll Cycles and De-epoxidated Carotenoids

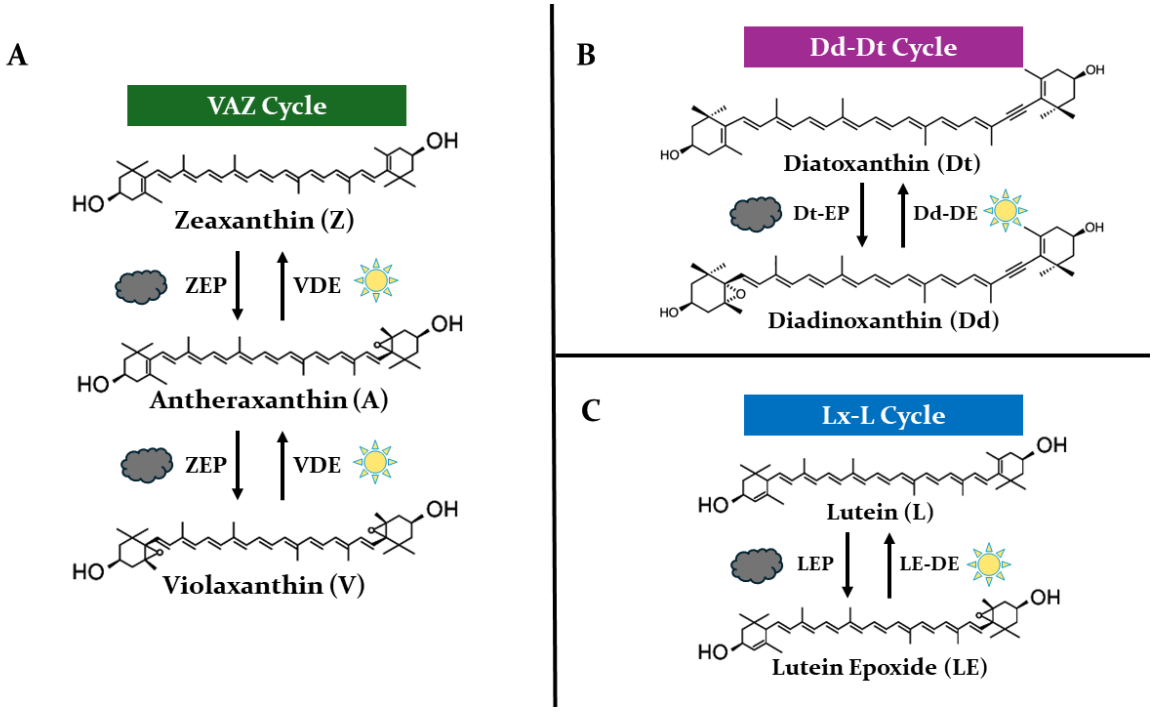

Figure 1-8. Schematic of the three xanthophyll cycles, which convert pigments to and from preferential light harvesting configurations (epoxidated) to photoprotection (de-epoxidated). **A** The VAZ cycle requires two steps to transform V, the pigment associated with light-harvesting, to Z, the pigment typically involved in photoprotection. **B** The Dd-Dt cycle only needs one step to convert between Dd to Dt when the lumen is acidified. **C** The Lx-L cycle results in the accumulation of L in vascular plants.

Carotenoids play a dual role in photosynthesis as light-harvesting pigments, enhancing photochemistry by extending the range of wavelengths that can be utilized by photosystems and in photoprotection. In their role in photoprotection, carotenoids can dissipate excess energy as heat and quench ROSs, acting as an antioxidant in many other systems besides photosynthetic membranes[28]. Carotenoids are hydrocarbons containing eight isoprenoid units that join two cyclic end groups. Specific carotenoids called xanthophylls will have modifications to this base structure which gives their unique attributes[107,108]. Xanthophylls are a class of carotenoids that contain oxygen and are the main carotenoids involved in photosynthesis. There are two precursors to xanthophylls called α- and β-carotene from which xanthophylls are derived[109]. α-carotene is converted into lutein and lutein epoxide while β-carotene is transformed into zeaxanthin and then antheraxanthin and violaxanthin[57,109]. In diatoms, β-carotene not only is converted into the VAZ pool but violaxanthin is further modified to become diadinoxanthin (Dd) and diatoxanthin (Dt)[110]. These oxygenated carotenoids switched between epoxidated and de-epoxidated states with the help

of enzymes which either add or remove an epoxide group (Figure 1-8). These enzymes, which are species dependent, can be activated by a change in pH gradient as will be discussed below.

There are three known xanthophyll cycles: the violaxanthin-antheraxanthin-zeaxanthin (VAZ), the diadinoxanthin-diatoxanthin (Dd-Dt), and the lutein epoxide-lutein (Lx-L) cycle (Figure 1-8). The VAZ cycle is found in all green algae, brown algae, diatoms, plants as well as some moss. The Dd-Dt cycle is found in diatoms[82,104]. The Lx-L cycle is found almost exclusively in plants[111]. In many species, there is a linear relationship between the accumulation of de-epoxidated carotenoids and photoprotection[31,104,112]. However, some species like *C. reinhardtii* do not depend on xanthophyll cycles for photoprotection, even if the pigments are present[10,89,113]. Currently, it is not fully understood why three unique cycles have evolved in photosynthetic organisms. Below I explore the differences between each cycle and their potential impact on photoprotection.

1.3.2.1 VAZ cycle

The most studied xanthophyll cycle is the VAZ cycle as it is found in most photosynthetic organisms. It was first characterized by Yamamoto in 1962[57]. In this cycle V is de-epoxidized by violaxanthin de-epoxidase (VDE), which requires two ascorbates as a co-substrates[114]. VDE is a water-soluble protein in neutral pHs, but when the lumen acidifies VDE binds tightly to MDGD enriched areas of the thylakoid membrane, which typically surround LCHII trimers[115,116]. The active form of VDE is thought to be a dimer[82]. De-epoxidation is a first-order reaction[58], and VDE has a higher affinity for A over V[117]. Additionally, V is converted at different rates depending on binding location in LHC proteins[26]. The epoxidation reaction is catalyzed by zeaxanthin epoxidase (ZEP)[118]. ZEP is located at the stromal side of the thylakoid membrane and its optimal activity is between pH 7.4-7.8[118]. ZEP requires O_2, NADPH, and flavin-adenine dinucleotide (FAD) to complete the transfer of one oxygen molecule to Z or A[119,120]. Epoxidation reactions are much slower than de-epoxidation, though Z→A is faster than the A→V reaction[11,121].

The role of V in the photosynthetic antenna is to extend the usable wavelengths available to organisms. Carotenoids can transfer energy to Chl from their S_2 state or S1[122,123]. S2 goes to Chl Q_x but transfer needs to be quick as the S_2-S_1 internal conversion is fast, so must occur within 100 fs[27]. Ultrafast energy transfer requires proximity and spectral overlap, which is seen with the two L in LHCII; V can participate in excitation energy transfer but not electron transfer from the S_1 state to Chl[124]. However, in HL, V is converted to Z to switch the system into a photoprotective state[26,125]. This is because of the extended π system of Zea (11 conjugated double bounds); its S_1 state is below most Chl a S_1[126]. Therefore, energy is transfer to Z and cannot be transferred back to Chl, dissipating the energy as heat by a non-radiative decay[27].

Much about the mechanisms of xanthophyll cycles still remains to be discovered. For example, the mechanism for how VDE removes V from LHCII or LHC monomers is still not understood. Violaxanthin has a lower binding affinity than Z for the V1 binding spot in LHCII[26,27]. V likely equilibrates with a pool of free carotenoids in the membrane where it can be converted into Z[27]. This would also explain how Z is able to act as a lipid protector and an antioxidant in addition to dissipating excess energy[127]. When Z is incorporated into the LCHII or other bind cites, it can lead to conformational changes that enable NPQ[82]. Typically, in plants acclimated in higher light intensity, up to 50% of the total xanthophyll pool is converted into Z and A; however, in low light grown plants, up to 80% of V because Z and A[29].

In *Physcomitrella patens*, a moss with both PsbS and LHCSRs, Z-accumulation has major effects on LHCSR-dependent NPQ because LHCSRs can bind pigments even when the majority of V is replaced with Z[128]. However, not all organisms utilize the complete VAZ cycle. Organisms like *Mantoniella squamata* or *Ostreococcus lucimarinus*[82,129,130] are only able to convert V to A. This is in part due to an extremely slow reaction from A to Z in these organisms[130]. Concurrently, the reaction from Z to A is fast, effectively erasing any newly formed Z. In the incomplete xanthophyll cycle, A is able to replace Z in terms of inducing a strong NPQ phenotype[117]. The reason for the incomplete VAZ cycle is attributed to a significantly reduced affinity for A in the VDE enzyme[130]. This particular VDE has a higher affinity for di-epoxide carotenoids like V, which is in contrast to the VDE found in typical land plants which have a higher affinity for A or other mono-epoxides[82]. Another hypothesis is that the VDE in *M. squamata* or *O. lucimarinus* are unable to bind ascorbate, limiting the ability to convert both epoxy groups[131]

1.3.2.2 Dd-Dt cycle

The VAZ cycle is the major xanthophyll cycle across the photosynthetic taxon. It is also present in diatoms; however, the VAZ cycle does not typically contribute to NPQ unless exposed to extreme HL[104,132]. Instead, violaxanthin is the precursor to Dd and Dt[110]. Similar to the VAZ cycle, Dd is converted to Dt when the lumen is acidified, activating a VDE enzyme (often referred to as Dd epoxidase, DDE)[133,134]. Though the optimal pH for DDE is slightly shifted towards a more neutral pH[134,135]. The ZEP (or Dt epoxidase EP, DEP) transforms Dt back to Dd. DDE and DEP have similar structures and are encoded by the same genes. The diatom VDE enzyme participates both in the VAZ and the Dd-Dt cycle[136,137]. DDE converts Dd to Dt faster than the conversion of V in plants, which may be due to DDE's higher affinity for ascorbate[134]. In addition to DDE, diatoms also have VDE-like (VDL) enzymes present which may participate in the xanthophyll cycles but mainly related to neoxanthin and fucoxanthin formation[136,137]. In contrast to plants, DEP is regulated by the ΔpH across the thylakoid membrane while ZEP is considered constitutively active. When the pH-gradient is established, DEP is inactivated. However, DEP might also be inactive in dark periods due to a lack of NADPH[112]. DEP is almost 20 times faster than the ZEP enzyme in plants or green algae[121]. Additionally, diatom species have 2 (in centric diatoms like *T. pseudonana*) or 3 (in pennate diatoms like *P. tricornutum*) DEP genes compared to the one in plants[82].

The roles of Dt and Z are very similar in diatoms and plants/green algae. The Dd pigment has 10 conjugated π bonds but contains a triplet carbon bond unlike the VAZ pigments. Interestingly, Dd has the same number of conjugated bonds as A while Dt is equivalent to Z[138]. Both pigments can bind to the photosynthetic antenna, facilitating NPQ, but they can also be soluble in the lipid membrane to act as antioxidants[82,134]. As with the conversion of V to Z, converting Dd to Dt lowers the lifetimes of the S_2 and S_1 states, therefore making Dt more suitable for energy dissipation[138]. The lifetime changes of the S_2 and S_1 state are smaller in diatoms than in organisms with the VAZ cycle[138].

1.3.2.3 Lutein Epoxide-Lutein cycle

Lutein is derived from the α-carotene branch[108,139]. Because of this, the Lx-L cycle is typically only found in vascular plants with a few exceptions[111]. Lutein is usually present in large amounts, and its concentration relative to Chl *a* and *b* does not alter much depending on the growth conditions, though the concentration of α-carotene does increase in shade-acclimated plants[29,140,141]. Like A and Z, lutein can participate in thermal dissipation[140,142]. However, the

quenching efficiency of L is ten times lower than Z[143]. The enzymes that participate in the VAZ cycle also can convert Lx to L and back, but the regeneration of Lx is extremely slow, suggesting ZEP (or LEP) has a low affinity for L[139,144]. Lx is often accumulated in deeply shaded leaves[141].

In mutants like *suppressor of zeaxanthin-less (szl1)*[145] in *A. thaliana*, which accumulate high levels of L and little to no VAZ pigments, there is a rapid response to HL that peaks and then decreases back to a steady state value[143]. This response can be seen when comparing *szl1* (green line) to WT (blue line) in Figure 1-5. In this figure, the *szl1* mutant is able to respond more rapidly to the sudden transition into the light while the WT strain more gradually builds up an NPQτ response, which is likely correlated with the accumulation of Z. The *szl1* and WT NPQ traces are very similar indicating that the overaccumulation of L can compensate for the lack of Z[109] (Figure1-5).

1.3.3 State transitions

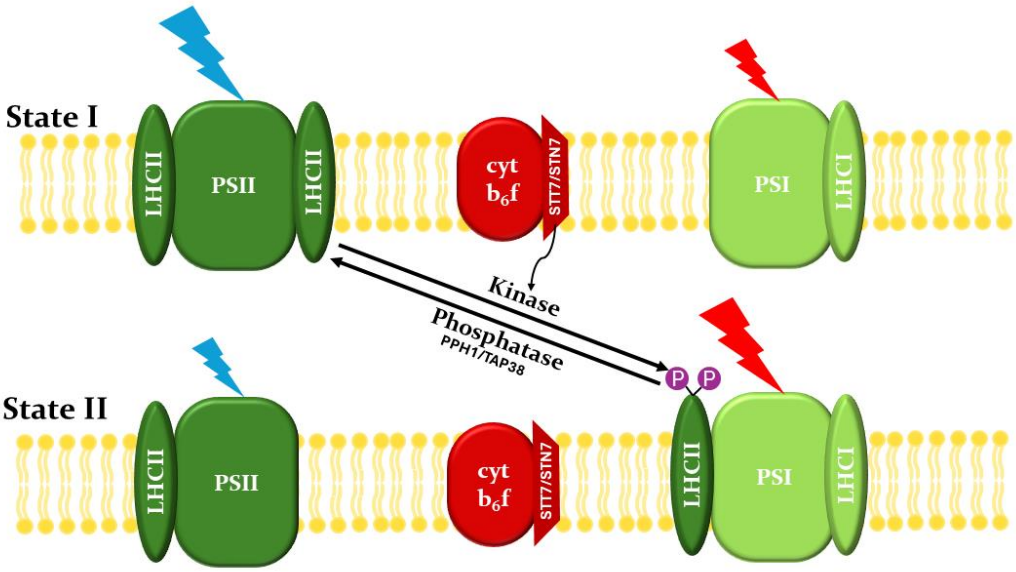

Figure 1-9. Schematic of state transitions in algae and plants. When PSII is preferentially excited, the PQ pool is over reduced, which activates STT7/STN7, phosphorylating LCHII, which then migrates to PSI. When LCHII is attached to PSI, this is referred to as State II. The transition to State I occurs when PSI is preferentially excited by far-red light. LCHII is then de-phosphorylated by PPH1/TAP38, returning to PSII. This figure is adapted from Subramanyam and Madireddi *Adv Photosynth Respir*. 2021, *47*, 303-320[146].

State transitions—as described above—occur when one PS is preferentially excited, activating mechanisms to balance this light distribution by changing the antenna size around PSI or PSII. State transitions occur within minutes of HL stress and require the phosphorylation or de-phosphorylation of LHC[62,147,148]. While xanthophyll cycles and pH-sensing proteins rely on a pH-gradient to be activated, state transition are triggered by the overexcitation of PSI or PSII. State I occurs when LHCII trimers are primarily bound to PSII, but the transition to State II ensues when PSII is preferentially excited by blue light. This leads to the accumulation of reducing agents in the thylakoid membrane which activated serine/threonine-protein kinase (STT7)[61,149–151]. In green algae, the phosphorylating protein is STT7, but its homologue in vascular plants is STN7[152]. STT7/STN7 phosphorylate LHCII, enabling it to move from PSII to PSI. The transition back to

State I occurs when PSI is preferentially excited by light enriched in the far-red regions[61]. In plants, LHCII is de-phosphorylated by PPH1[153]/TAP38[154], which are phosphorylases.

While state transitions only occur in plants and green algae, its impact on NPQ can be large. In plants, 15-20% of LHCII are mobile during state transitions[152]. Absence of STN7 will limit the growth of plants when grown in fluctuating light conditions[152]. In *Chlamydomonas*, state transitions have an even larger impact as 80% of their LHCII trimers dissociate from PSII, though only 15% of these LHCII are then bound to PSI[146]. Because of the significant role state transitions play in *C. reinhardtii*, it is a comply used model system for qT research. STT7 is responsible for 42% of NPQ[10]. However, this contribution is even greater when considering photoprotection during darkness (60%) or during illumination (36%). State transitions contributed more to NPQ after 20 minutes of light fluctuations. Interestingly, the contributions of LCHSR3 to NPQ were increased when STT7 was present. The inverse is also true, indicating the synergistic cooperation of photoprotective components. Because quenching related to LHCSRs can take a few hours to be induced[83], it has been hypothesized that state transitions may substitute for other NPQ pathways[155]. Additionally, state transitions appear to accumulate during the dark periods of the light fluctuations, allowing it to play a role in NPQ during subsequent light exposures. In Figure 1-10, the *stt7* mutant (green line) has no significant increase in NPQ during the dark phases while WT (Figure 1-6c) and LHCSR-mutants (Figure 1-10) do. State transitions could be 'anticipating' the next HL exposure, which provide effective photoprotection during rapid, unpredictable fluctuating light environments.

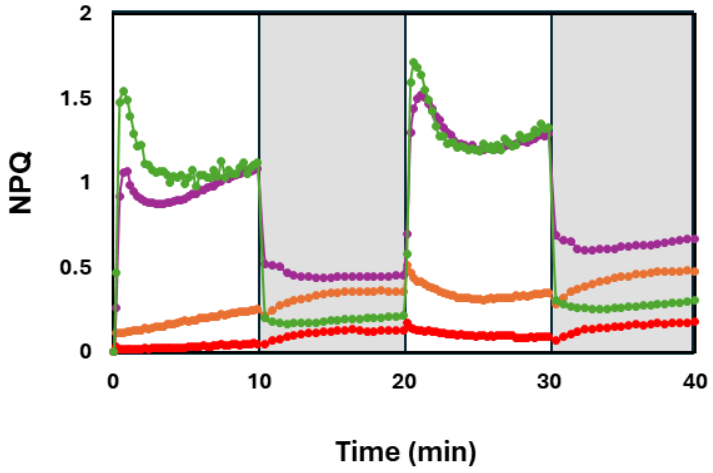

Figure 1-10. Comparison of NPQ traces of *C. reinhardtii* mutant strains: *stt7* (green), *lhscr1* (purple), *npq4* (orange), and *npq4stt7* (red). The white boxes represent the 10 min HL periods while the gray boxes show the 10 min dark phases.

1.4 Method for Studying Photoprotection

Since non-photochemical quenching is the release of excess energy as heat, it can be difficult to directly measure this phenomenon. Figure 1-3b shows the multiple pathways for excited energy to be released, returning Chl *a* to its ground state. Some energy is lost as a fluorescent photon that peaks around 680 nm for Chl *a*[22,156]. The rate of decay for energy to photochemistry and fluorescence is consistent, but when other pathways such as ISC and NPQ are introduced, less energy is lost as fluorescence, shortening the fluorescence lifetime of the system. The fluorescence

of a system can be monitored to see how the fluorescence lifetime or yield changes. A perk of this technique is that it is non-invasive, which allows us to make measurements without influencing NPQ[157].

1.4.1 Time-Correlated Single Photon Counting

In time-correlated single photon counting (TCSPC), the fluorescence yield is tracked. Directly measuring the fluorescence lifetimes in snapshots allows for us to focus only on the processes that quench chlorophyll excitation. Methods like pulse-amplitude modulation (PAM) fluorimetry measure fluorescence quantum yields, which are influenced by light scattering, chloroplast movement, and photobleaching[156]. These things can lower the fluorescence yield but do not result from Chl being quenched[157,158].

TCSPC works by detecting single photons and recording their arrival times with respect to a precisely timed reference signal. By accumulating these arrival times over many photon events, TCSPC builds a histogram that reveals the distribution of photon arrival times, providing insights into the fluorescence lifetime or dynamics of the sample. The histogram is then fit with the equation 1 to a biexponential (in the case of my experiments) to get an average fluorescence lifetime referred to as τ_{avg}. This method is able to capture subtle changes in the fluorescence lifetime over very short timescales.

With snapshot TCSPC, a dark-adapted fluorescence lifetime ($\tau_{avg,dark}$) is gathered from an organism that has been in a dark environment for long enough to de-activate any photoprotective mechanisms that may have been triggered. This dark-adapted lifetime will then be used in reference to all other snapshot lifetimes ($\tau_{avg,light}$) collected as a function of an actinic light sequence. Using the equation 2, the unitless value of NPQτ can be determined which represents the change in photoprotection.

$$\tau_{avg} = \frac{\sum_i A_i \tau_i}{\sum_i A_i} \tag{1}$$

$$NPQ_\tau = \frac{\tau_{avg,dark} - \tau_{avg,light}}{\tau_{avg,light}} \tag{2}$$

1.4.2 Actinic Light Sequences

As discussed above, light levels are always changing in nature, which has led photosynthetic organisms to develop mechanisms to optimize growth in inconsistent light environments. Yet, this can introduce a level of complexity that makes it difficult to study NPQ. For example, the PsbS mutant *npq4* in *A. thaliana* is unable to rapidly respond to changing light levels, but when grown in continuous light is nearly identical to the wild type; it is only under fluctuating light, which reveals the mutation[159]. Including fluctuating light sequences in experiments is important to not only see how long-term application of fluctuating light might affect growth but also in how immediate response might be impaired.

By adding in fluctuating light sequences, this also allows for the disentangling of the overlapping timescale of NPQ components. Alternating dark and HL periods over a series of cycles allows one to measure how the rapid response evolves as the slower components simultaneously move towards their steady state behavior. Increasing the complexity of light sequences by introducing aperiodic or irregular light sequences will more closely match light dynamics seen in nature.

1.5 Conclusions

As can be seen, there is great diversity among the molecular components contributing to NPQ across multiple species. Understanding the benefits of each system could help guide modifications in biofuel algae or in crop plants to maximize total photosynthetic productivity leading to higher yields. In the following chapters, I will discuss my work mostly with *Nannochloropsis* understanding its NPQ components and mechanisms as it contains the fewest photoprotective components. With this work, we created a simple model based on the biochemically relevant components of the pH-gradient and the xanthophyll cycle to predict changes in NPQ based on the light environment. By increasing the complexity of the light sequences and experimental species, we hope to approximate NPQ responses in crop plants then to calculate which components should be genetically modified and in what ratio.

1.6 References

1. Clayton, C. Global Food Gap Growing. https://www.dtnpf.com/agriculture/web/ag/news/article/2018/10/17/group-warns-food-supply-meet-future (2018).
2. Murchie, E. H., Pinto, M. & Horton, P. Agriculture and the new challenges for photosynthesis research. *N. Phytol.* **181**, 532–552 (2009).
3. Kromdijk, J. *et al.* Improving photosynthesis and crop productivity by accelerating recovery from photoprotection. *Science* **354**, 857-861 (2016).
4. Long, S. P., Zhu, X., Naidu, S. L. & Ort, D. R. Can improvement in photosynthesis increase crop yields? *Plant, Cell Environ.* **29**, 315–330 (2006).
5. Bailey-Serres, J., Parker, J. E., Ainsworth, E. A., Oldroyd, G. E. D. & Schroeder, J. I. Genetic strategies for improving crop yields. *Nature* **575**, 109-118 (2019).
6. Souza, A. P. D. *et al.* Soybean photosynthesis and crop yield are improved by accelerating recovery from photoprotection. *Science* **377**, 851–854 (2022).
7. Ruban, A. V. & Saccon, F. Chlorophyll a de-excitation pathways in the LHCII antenna. *J Chem Phys* **156**, 070902 (2022).
8. Ruban, A. V. Crops on the fast track for light. *Nature* **541**, 36–37 (2017).
9. Steen, C. J., Morris, J. M., Short, A. H., Niyogi, K. K. & Fleming, G. R. Complex Roles of PsbS and Xanthophylls in the Regulation of Nonphotochemical Quenching in Arabidopsis thaliana under Fluctuating Light. *J Phys Chem B* **124**, 10311–10325 (2020).
10. Steen, C. J., Burlacot, A., Short, A. H., Niyogi, K. K. & Fleming, G. R. Interplay between LHCSR proteins and state transitions governs the NPQ response in Chlamydomonas during light fluctuations. *Plant Cell Environ* **45**, 2428–2445 (2022).
11. Short, A. *et al.* Kinetics of the xanthophyll cycle and its role in photoprotective memory and response. *Nat. Commun.* **14**, 6621 (2023).
12. Short, A. H. *et al.* Xanthophyll-cycle based model of the rapid photoprotection of Nannochloropsis in response to regular and irregular light/dark sequences. *J Chem Phys* (2022) doi:10.1063/5.0089335.
13. Falkowski, P. G., Barber, R. T. & Smetacek, V. Biogeochemical Controls and Feedbacks on Ocean Primary Production. *Science* **281**, 200–206 (1998).
14. Smetacek, V. Diatoms and the Ocean Carbon Cycle. *Protist* **150**, 25–32 (1999).
15. Bowler, C., Vardi, A. & Allen, A. E. Oceanographic and Biogeochemical Insights from Diatom Genomes. *Mar. Sci.* **2**, 333–365 (2010).
16. Benedetti, M., Vecchi, V., Barera, S. & Dall'Osto, L. Biomass from microalgae: the potential of domestication towards sustainable biofactories. *Microb Cell Fact* **17**, 173 (2018).
17. Perin, G. & Jones, P. R. Economic feasibility and long-term sustainability criteria on the path to enable a transition from fossil fuels to biofuels. *Curr Opin Biotech* **57**, 175–182 (2019).
18. Vecchi, V., Barera, S., Bassi, R. & Dall'Osto, L. Potential and Challenges of Improving Photosynthesis in Algae. *Plants* **9**, 67 (2020).
19. Kouřil, R., Dekker, J. P. & Boekema, E. J. Supramolecular organization of photosystem II in green plants. *Biochim. Biophys. Acta (BBA) - Bioenerg.* **1817**, 2–12 (2012).
20. Rochaix, J.-D. Regulation of photosynthetic electron transport. *Biochim. Biophys. Acta (BBA) - Bioenerg.* **1807**, 375–383 (2011).
21. Nelson, N. & Ben-Shem, A. The complex architecture of oxygenic photosynthesis. *Nat. Rev. Mol. Cell Biol.* **5**, 971–982 (2004).
22. Blankenship, R. E. *Molecular Mechanisms of Photosynthesis*. (John Wiley & Sons, 2021).

23. Azadi-Chegeni, F. *et al.* Conformational dynamics of Light-Harvesting Complex II in a native membrane environment. *bioRxiv* 288860 (2020) doi:10.1101/288860.
24. Papageorgiou, G. C. & Govindjee. Non-Photochemical Quenching and Energy Dissipation in Plants, Algae and Cyanobacteria. *Proceedings of 17th International Symposium on Discharges and Electrical Insulation in Vacuum* **1**, (2014).
25. Barros, T. & Kühlbrandt, W. Crystallisation, structure and function of plant light-harvesting Complex II. *Biochim. Biophys. Acta (BBA) - Bioenerg.* **1787**, 753–772 (2009).
26. Jahns, P., Wehner, A., Paulsen, H. & Hobe, S. De-epoxidation of Violaxanthin after Reconstitution into Different Carotenoid Binding Sites of Light-harvesting Complex II*. *J. Biol. Chem.* **276**, 22154–22159 (2001).
27. Standfuss, J., Scheltinga, A. C. T. van, Lamborghini, M. & Kühlbrandt, W. Mechanisms of photoprotection and nonphotochemical quenching in pea light-harvesting complex at 2.5 Å resolution. *Embo J* **24**, 919–928 (2005).
28. Demmig-Adams, B. Carotenoids and photoprotection in plants: A role for the xanthophyll zeaxanthin. *Biochimica Et Biophysica Acta Bba - Bioenergetics* **1020**, 1–24 (1990).
29. Demmig-Adams, B. & Adams, W. W. Carotenoids in Photosynthesis. 206–251 (1993) doi:10.1007/978-94-011-2124-8_7.
30. Nagao, R. *et al.* Structural basis for different types of hetero-tetrameric light-harvesting complexes in a diatom PSII-FCPII supercomplex. *Nat. Commun.* **13**, 1764 (2022).
31. Büchel, C. Light harvesting complexes in chlorophyll c-containing algae. *Biochim. Biophys. Acta (BBA) - Bioenerg.* **1861**, 148027 (2020).
32. Arshad, R., Calvaruso, C., Boekema, E. J., Büchel, C. & Kouřil, R. Revealing the architecture of the photosynthetic apparatus in the diatom Thalassiosira pseudonana. *Plant Physiol.* **186**, 2124–2136 (2021).
33. Gundermann, K., Wagner, V., Mittag, M. & Büchel, C. Fucoxanthin-Chlorophyll Protein Complexes of the Centric Diatom Cyclotella Meneghiniana Differ in Lhcx1 and Lhcx6_1 Content. *Plant Physiol* **179**, 1779–1795 (2019).
34. Müller, P., Li, X.-P. & Niyogi, K. K. Non-Photochemical Quenching. A Response to Excess Light Energy. *Plant Physiol* **125**, 1558–1566 (2001).
35. Morales, A. & Kaiser, E. Photosynthetic Acclimation to Fluctuating Irradiance in Plants. *Front. Plant Sci.* **11**, 268 (2020).
36. Barber, J. P680: what is it and where is it? *Bioelectrochemistry* **55**, 135–138 (2002).
37. Yocum, C. F. Photosystem 2 and the oxygen evolving complex: a brief overview. *Photosynth. Res.* **152**, 97–105 (2022).
38. Webber, A. N. & Lubitz, W. P700: the primary electron donor of photosystem I. *Biochim. Biophys. Acta (BBA) - Bioenerg.* **1507**, 61–79 (2001).
39. Junge, W. & Nelson, N. ATP Synthase. *Annu. Rev. Biochem.* **84**, 1–27 (2015).
40. Gao, Y. & Erdner, D. L. Cell death responses to acute high light mediated by non-photochemical quenching in the dinoflagellate Karenia brevis. *Sci. Rep.* **12**, 14081 (2022).
41. Demmig-Adams, B., Stewart, J. J., López-Pozo, M., Polutchko, S. K. & Adams, W. W. Zeaxanthin, a Molecule for Photoprotection in Many Different Environments. *Molecules* **25**, 5825 (2020).
42. Demmig-Adams, B., Polutchko, S. K., Stewart, J. J. & Adams, W. W. History of excess-light exposure modulates extent and kinetics of fast-acting non-photochemical energy dissipation. *Plant Physiol. Rep.* **27**, 560–572 (2022).

43. Pearcy, R. W. Sunflecks and Photosynthesis in Plant Canopies. *Annu. Rev. Plant Physiol. Plant Mol. Biol.* **41**, 421–453 (1990).
44. Long, S. P., Humphries, S. & Falkowski, P. G. Photoinhibition of Photosynthesis in Nature. *Annu Rev Plant Phys* **45**, 633–662 (1994).
45. Murchie, E. H. & Ruban, A. V. Dynamic non-photochemical quenching in plants: from molecular mechanism to productivity. *Plant J* **101**, 885–896 (2020).
46. Joliot, P. & Joliot, A. Cyclic electron flow in C3 plants. *Biochimica Et Biophysica Acta Bba - Bioenergetics* **1757**, 362–368 (2006).
47. Joliot, P. & Johnson, G. N. Regulation of cyclic and linear electron flow in higher Plants. *Proc National Acad Sci* **108**, 13317-3322 (2011).
48. Bethmann, S., Melzer, M., Schwarz, N. & Jahns, P. The zeaxanthin epoxidase is degraded along with the D1 protein during photoinhibition of photosystem II. *Plant Direct* **3**, e00185 (2019).
49. Niyogi, K. K. & Truong, T. B. Evolution of flexible non-photochemical quenching mechanisms that regulate light harvesting in oxygenic photosynthesis. *Curr Opin Plant Biol* **16**, 307–314 (2013).
50. Lohr, M. & Wilhelm, C. Photosynthesis: Mechanisms and Effects, Volume I–V: Proceedings of the XIth International Congress on Photosynthesis, Budapest, Hungary, August 17–22, 1998. 2313–2316 (1998) doi:10.1007/978-94-011-3953-3_542.
51. Asada, K. Production and Scavenging of Reactive Oxygen Species in Chloroplasts and Their Functions. *Plant Physiol.* **141**, 391–396 (2006).
52. Demmig-Adams, B. & III, W. W. A. Photoprotection and Other Responses of Plants to High Light Stress. *Annu Rev Plant Phys* **43**, 599–626 (1992).
53. Erickson, E., Wakao, S. & Niyogi, K. K. Light stress and photoprotection in Chlamydomonas reinhardtii. *Plant J.* **82**, 449–465 (2015).
54. Krause, G. H. & Weis, E. Chlorophyll Fluorescence and Photosyntehsis: The Basics. *Annu. Rev. Plant Physiol. Plant Mol. Biol.* **42**, 313–49 (1991).
55. Horton, P., Ruban, A. V. & Wentworth, M. Allosteric regulation of the light-harvesting system of photosystem II. *Philosophical Transactions Royal Soc Lond Ser B Biological Sci* **355**, 1361–1370 (2000).
56. Iwai, M., Patel-Tupper, D. & Niyogi, K. K. Structural Diversity in Eukaryotic Photosynthetic Light Harvesting. *Annu. Rev. Plant Biol.* **75**, (2024).
57. Yamamoto, H. Y., Nakayama, T. O. M. & Chichester, C. O. Studies on the light and dark interconversions of leaf xanthophylls. *Arch. Biochem. Biophys.* **97**, 168–173 (1962).
58. Yamamoto, H. Y. Biochemistry of the violaxanthin cycle in higher plants. *Pure Applied Chemistry* 639–648 (1979) doi:10.1016/b978-0-08-022359-9.50017-5.
59. Yamamoto, H. Y. [34] Xanthophyll cycles. *Methods Enzym.* **110**, 303–312 (1985).
60. Nilkens, M. *et al.* Identification of a slowly inducible zeaxanthin-dependent component of non-photochemical quenching of chlorophyll fluorescence generated under steady-state conditions in Arabidopsis. *Biochim. Biophys. Acta (BBA) - Bioenerg.* **1797**, 466–475 (2010).
61. Lemeille, S. & Rochaix, J.-D. State transitions at the crossroad of thylakoid signalling pathways. *Photosynth. Res.* **106**, 33–46 (2010).
62. Allen, J. F. Protein phosphorylation in regulation of photosynthesis. *Biochimica Et Biophysica Acta Bba - Bioenergetics* **1098**, 275–335 (1992).
63. Sonoike, K. Photoinhibition of photosystem I. *Physiol. Plant.* **142**, 56–64 (2011).

64. Niyogi, K. K., Grossman, A. R. & Björkman, O. Arabidopsis Mutants Define a Central Role for the Xanthophyll Cycle in the Regulation of Photosynthetic Energy Conversion. *Plant Cell* **10**, 1121–1134 (1998).
65. Roach, T., Na, C. S., Stöggl, W. & Krieger-Liszkay, A. The non-photochemical quenching protein LHCSR3 prevents oxygen-dependent photoinhibition in Chlamydomonas reinhardtii. *J Exp Bot* **71**, 2650–2660 (2020).
66. Long, S. P. *et al.* Into the Shadows and Back into Sunlight: Photosynthesis in Fluctuating Light. *Annu. Rev. Plant Biol.* **73**, 617–648 (2022).
67. Sohbat, Z. I. Non-photochemical quenching of chlorophyll fluorescence and its components – recent advances. *Journal of Life Sciences and Biomedicine* **4**, 76–83 (2022).
68. Malnoë, A. Photoinhibition or photoprotection of photosynthesis? Update on the (newly termed) sustained quenching component qH. *Environ. Exp. Bot.* **154**, 123–133 (2018).
69. Briantais, J.-M., Vernotte, C., Picaud, M. & Krause, G. H. A quantitative study of the slow decline of chlorophyll *a* fluorescence in isolated chloroplasts. *Biochim. Biophys. Acta (BBA) - Bioenerg.* **548**, 128–138 (1979).
70. Ruban, A. *et al.* The super-excess energy dissipation in diatom algae: comparative analysis with higher plants. *Photosynth. Res.* **82**, 165 (2004).
71. Li, X. P. *et al.* A pigment-binding protein essential for regulation of photosynthetic light harvesting. *Nature* **403**, 391-395 (2000).
72. Li, X.-P. *et al.* Regulation of Photosynthetic Light Harvesting Involves Intrathylakoid Lumen pH Sensing by the PsbS Protein*. *J Biol Chem* **279**, 22866–22874 (2004).
73. Demmig-Adams, B. *et al.* Modulation of PsbS and flexible vs sustained energy dissipation by light environment in different species. *Physiol Plantarum* **127**, 670–680 (2006).
74. Kim, S. *et al.* Characterization of a spinach psbS cDNA encoding the 22 kDa protein of photosystem II. *FEBS Lett.* **314**, 67–71 (1992).
75. Wedell, N., Klein, R., Ljungberg, U., Andersson, B. & Herrmann, R. G. The single-copy gene psbS codes for a phylogenetically intriguing 22 kDa polypeptide of photosystem II. *FEBS Lett.* **314**, 61–66 (1992).
76. Li, X.-P., Müller-Moulé, P., Gilmore, A. M. & Niyogi, K. K. PsbS-dependent enhancement of feedback de-excitation protects photosystem II from photoinhibition. *Proc. Natl. Acad. Sci.* **99**, 15222–15227 (2002).
77. Jahns, P., Latowski, D. & Strzalka, K. Mechanism and regulation of the violaxanthin cycle: The role of antenna proteins and membrane lipids. *Biochimica Et Biophysica Acta Bba - Bioenergetics* **1787**, 3–14 (2009).
78. Correa-Galvis, V., Poschmann, G., Melzer, M., Stühler, K. & Jahns, P. PsbS interactions involved in the activation of energy dissipation in Arabidopsis. *Nat Plants* **2**, 15225 (2016).
79. Johnson, M. P. & Ruban, A. V. Arabidopsis plants lacking PsbS protein possess photoprotective energy dissipation. *Plant J* **61**, 283-289 (2009).
80. Ware, M. A., Giovagnetti, V., Belgio, E. & Ruban, A. V. PsbS protein modulates non-photochemical chlorophyll fluorescence quenching in membranes depleted of photosystems. *J Photochem Photobiology B Biology* **152**, 301–307 (2015).
81. Chiariello, M. G., Grünewald, F., Zarmiento-Garcia, R. & Marrink, S. J. pH-Dependent Conformational Switch Impacts Stability of the PsbS Dimer. *J Phys Chem Lett* **14**, 905–911 (2023).
82. Goss, R. & Lepetit, B. Biodiversity of NPQ. *J Plant Physiol* **176**, 13–32 (2014).

83. Peers, G. *et al.* An ancient light-harvesting protein is critical for the regulation of algal photosynthesis. *Nature* **462**, 518–521 (2009).
84. Rochaix, J.-D. & Bassi, R. LHC-like proteins involved in stress responses and biogenesis/repair of the photosynthetic apparatus. *Biochem J* **476**, 581–593 (2019).
85. Ballottari, M. *et al.* Identification of pH-sensing Sites in the Light Harvesting Complex Stress-related 3 Protein Essential for Triggering Non-photochemical Quenching in *Chlamydomonas reinhardtii*. *J. Biological Chem.* **291**, 7334–7346 (2016).
86. Kondo, T. *et al.* Single-molecule spectroscopy of LHCSR1 protein dynamics identifies two distinct states responsible for multi-timescale photosynthetic photoprotection. *Nat Chem* **9**, 772–778 (2017).
87. Liguori, N., Roy, L. M., Opacic, M., Durand, G. & Croce, R. Regulation of Light Harvesting in the Green Alga *Chlamydomonas reinhardtii*: The C-Terminus of LHCSR Is the Knob of a Dimmer Switch. *J Am Chem Soc* **135**, 18339–18342 (2013).
88. Troiano, J. M. *et al.* Identification of distinct pH-and zeaxanthin-dependent quenching in LHCSR3 from *Chlamydomonas reinhardtii*. *Elife* **10**, e60383 (2021).
89. Bonente, G. *et al.* Analysis of LhcSR3, a Protein Essential for Feedback De-Excitation in the Green Alga *Chlamydomonas reinhardtii*. *Plos Biol* **9**, e1000577 (2011).
90. Perozeni, F., Beghini, G., Cazzaniga, S. & Ballottari, M. *Chlamydomonas reinhardtii* LHCSR1 and LHCSR3 proteins involved in photoprotective non-photochemical quenching have different quenching efficiency and different carotenoid affinity. *Sci Rep-uk* **10**, 21957 (2020).
91. Girolomoni, L. *et al.* LHCSR3 is a nonphotochemical quencher of both photosystems in *Chlamydomonas reinhardtii*. *Proc National Acad Sci* **116**, 201809812 (2019).
92. Bonente, G., Howes, B. D., Caffarri, S., Smulevich, G. & Bassi, R. Interactions between the Photosystem II Subunit PsbS and Xanthophylls Studied *in Vivo* and *in Vitro*. *J Biol Chem* **283**, 8434–8445 (2008).
93. Truong, T. B. Investigating the role(s) of LHCSRs in *Chlamydomonas reinhardtii*. (Berkeley: University of California, 2011).
94. Roach, T. LHCSR3-Type NPQ Prevents Photoinhibition and Slowed Growth under Fluctuating Light in *Chlamydomonas reinhardtii*. *Plants* **9**, 1604 (2020).
95. Cantrell, M. & Peers, G. A mutant of Chlamydomonas without LHCSR maintains high rates of photosynthesis, but has reduced cell division rates in sinusoidal light conditions. *Plos One* **12**, e0179395 (2017).
96. Vieler, A. *et al.* Genome, Functional Gene Annotation, and Nuclear Transformation of the Heterokont Oleaginous Alga *Nannochloropsis oceanica* CCMP1779. *Plos Genet* **8**, e1003064 (2012).
97. Park, S. *et al.* Chlorophyll–carotenoid excitation energy transfer and charge transfer in *Nannochloropsis oceanica* for the regulation of photosynthesis. *Proc National Acad Sci* **116**, 3385-3390 (2019).
98. Giovagnetti, V. *et al.* Biochemical and molecular properties of LHCX1, the essential regulator of dynamic photoprotection in diatoms. *Plant Physiol* (2021) doi:10.1093/plphys/kiab425.
99. Lepetit, B., Goss, R., Jakob, T. & Wilhelm, C. Molecular dynamics of the diatom thylakoid membrane under different light conditions. *Photosynth. Res.* **111**, 245–257 (2012).
100. Bailleul, B. *et al.* An atypical member of the light-harvesting complex stress-related protein family modulates diatom responses to light. *Proc. Natl. Acad. Sci.* **107**, 18214–18219 (2010).

101. Zhu, S.-H. & Green, B. R. Photoprotection in the diatom *Thalassiosira pseudonana*: Role of LI818-like proteins in response to high light stress. *Biochim. Biophys. Acta (BBA) - Bioenerg.* **1797**, 1449–1457 (2010).
102. Buck, J. M. *et al.* Lhcx proteins provide photoprotection via thermal dissipation of absorbed light in the diatom *Phaeodactylum tricornutum*. *Nat Commun* **10**, 4167 (2019).
103. Taddei, L. *et al.* Dynamic Changes between Two LHCX-Related Energy Quenching Sites Control Diatom Photoacclimation. *Plant Physiol.* **177**, 953–965 (2018).
104. Lacour, T., Babin, M. & Lavaud, J. Diversity in Xanthophyll Cycle Pigments Content and Related Nonphotochemical Quenching (NPQ) Among Microalgae: Implications for Growth Strategy and Ecology. *J. Phycol.* **56**, 245–263 (2020).
105. Buck, J. M., Kroth, P. G. & Lepetit, B. Identification of sequence motifs in Lhcx proteins that confer qE-based photoprotection in the diatom *Phaeodactylum tricornutum*. *Plant J.* **108**, 1721–1734 (2021).
106. Lavaud, J. & Goss, R. Non-Photochemical Quenching and Energy Dissipation in Plants, Algae and Cyanobacteria. *Adv Photosynth Respir* 421–443 (2014) doi:10.1007/978-94-017-9032-1_20.
107. Britton, G. Structure and properties of carotenoids in relation to function. *FASEB J.* **9**, 1551–1558 (1995).
108. Namitha, K. K. & Negi, P. S. Chemistry and Biotechnology of Carotenoids. *Crit. Rev. Food Sci. Nutr.* **50**, 728–760 (2010).
109. Li, Z. *et al.* Lutein Accumulation in the Absence of Zeaxanthin Restores Nonphotochemical Quenching in the *Arabidopsis thaliana npq1* Mutant. *Plant Cell* **21**, 1798–1812 (2009).
110. Dambek, M. *et al.* Biosynthesis of fucoxanthin and diadinoxanthin and function of initial pathway genes in Phaeodactylum tricornutum. *J. Exp. Bot.* **63**, 5607–5612 (2012).
111. Esteban, R., Becerril, J. M. & García-Plazaola, J. I. Lutein epoxide cycle, more than just a forest tale. *Plant Signal. Behav.* **4**, 342–344 (2009).
112. Blommaert, L., Chafai, L. & Bailleul, B. The fine-tuning of NPQ in diatoms relies on the regulation of both xanthophyll cycle enzymes. *Sci Rep-uk* **11**, 12750 (2021).
113. Girolomoni, L. *et al.* Evolutionary divergence of photoprotection in the green algal lineage: a plant-like violaxanthin de-epoxidase enzyme activates the xanthophyll cycle in the green alga Chlorella vulgaris modulating photoprotection. *N. Phytol.* **228**, 136–150 (2020).
114. Hager, A. & Perz, H. Veränderung der Lichtabsorption eines Carotinoids im Enzym (De-epoxidase)-Substrat(Violaxanthin)-Komplex. *Planta* **93**, 314–322 (1970).
115. Yamamoto, H. Y. & Higashi, R. M. Violaxanthin de-epoxidase Lipid composition and substrate specificity. *Arch Biochem Biophys* **190**, 514–522 (1978).
116. Hager, A. & Holocher, K. Localization of the xanthophyll-cycle enzyme violaxanthin de-epoxidase within the thylakoid lumen and abolition of its mobility by a (light-dependent) pH decrease. *Planta* **192**, 581–589 (1994).
117. Goss, R., Lepetit, B. & Wilhelm, C. Evidence for a rebinding of antheraxanthin to the light-harvesting complex during the epoxidation reaction of the violaxanthin cycle. *J Plant Physiol* **163**, 585–590 (2006).
118. Siefermann, D. & Yamamoto, H. Y. Properties of NADPH and oxygen-dependent zeaxanthin epoxidation in isolated chloroplasts A transmembrane model for the violaxanthin cycle. *Arch. Biochem. Biophys.* **171**, 70–77 (1975).
119. Yamamoto, H. Y., Bugos, R. C. & Hieber, A. D. The Photochemistry of Carotenoids. *Adv. Photosynth. Respir.* 293–303 (2004) doi:10.1007/0-306-48209-6_16.

120. Büch, K., Stransky, H. & Hager, A. FAD is a further essential cofactor of the NAD(P)H and O_2-dependent zeaxanthin-epoxidase. *FEBS Lett.* **376**, 45–48 (1995).
121. Goss, R., Pinto, E. A., Wilhelm, C. & Richter, M. The importance of a highly active and ΔpH-regulated diatoxanthin epoxidase for the regulation of the PS II antenna function in diadinoxanthin cycle containing algae. *J. Plant Physiol.* **163**, 1008–1021 (2006).
122. Polívka, T. & Sundström, V. Ultrafast Dynamics of Carotenoid Excited States−From Solution to Natural and Artificial Systems. *Chem. Rev.* **104**, 2021–2072 (2004).
123. Holt, N. E., Kennis, J. T. M., Dall'Osto, L., Bassi, R. & Fleming, G. R. Carotenoid to chlorophyll energy transfer in light harvesting complex II from *Arabidopsis thaliana* probed by femtosecond fluorescence upconversion. *Chem Phys Lett* **379**, 305–313 (2003).
124. Dreuw, A., Fleming, G. R. & Head-Gordon, M. Charge-Transfer State as a Possible Signature of a Zeaxanthin−Chlorophyll Dimer in the Non-photochemical Quenching Process in Green Plants. *J Phys Chem B* **107**, 6500–6503 (2003).
125. Färber, A. & Jahns, P. The xanthophyll cycle of higher plants: influence of antenna size and membrane organization. *Biochim. Biophys. Acta (BBA) - Bioenerg.* **1363**, 47–58 (1998).
126. Frank, H. A. *et al.* Photophysics of the carotenoids associated with the xanthophyll cycle in photosynthesis. *Photosynth Res* **41**, 389-395 (1994).
127. Havaux, M., Dall'Osto, L., Cuiné, S., Giuliano, G. & Bassi, R. The Effect of Zeaxanthin as the Only Xanthophyll on the Structure and Function of the Photosynthetic Apparatus in Arabidopsis thaliana *. *J Biol Chem* **279**, 13878–13888 (2004).
128. Pinnola, A. *et al.* Zeaxanthin Binds to Light-Harvesting Complex Stress-Related Protein to Enhance Nonphotochemical Quenching in *Physcomitrella patens*. *Plant Cell* **25**, 3519–3534 (2013).
129. Goss, R., Böhme, K. & Wilhelm, C. The xanthophyll cycle of *Mantoniella squamata* converts violaxanthin into antheraxanthin but not to zeaxanthin: consequences for the mechanism of enhanced non-photochemical energy dissipation. *Planta* **205**, 613–621 (1998).
130. Frommolt, R., Goss, R. & Wilhelm, C. The de-epoxidase and epoxidase reactions of *Mantoniella squamata (Prasinophyceae*) exhibit different substrate-specific reaction kinetics compared to spinach. *Planta* **213**, 446–456 (2001).
131. Schaller, S. *et al.* The investigation of violaxanthin de-epoxidation in the primitive green alga *Mantoniella squamata (Prasinophyceae*) indicates mechanistic differences in xanthophyll conversion to higher plants. *Phycologia* **51**, 359–370 (2012).
132. Lohr, M. & Wilhelm, C. Algae displaying the diadinoxanthin cycle also possess the violaxanthin cycle. *Proc National Acad Sci* **96**, 8784–8789 (1999).
133. Lepetit, B. *et al.* High Light Acclimation in the Secondary Plastids Containing Diatom *Phaeodactylum tricornutum* is Triggered by the Redox State of the Plastoquinone Pool. *Plant Physiol.* **161**, 853–865 (2012).
134. Bertrand, M. Carotenoid biosynthesis in diatoms. *Photosynth. Res.* **106**, 89–102 (2010).
135. Kuczynska, P. *et al.* The xanthophyll cycle in diatom *Phaeodactylum tricornutum* in response to light stress. *Plant Physiol. Biochem.* **152**, 125–137 (2020).
136. Gaidarenko, O., Mills, D. W., Vernet, M. & Hildebrand, M. Overexpression of *Thalassiosira pseudonana* violaxanthin de-epoxidase-like 2 (VDL2) increases fucoxanthin while stoichiometrically reducing diadinoxanthin cycle pigment abundance. *bioRxiv* 2020.01.06.896316 (2020) doi:10.1101/2020.01.06.896316.
137. Dautermann, O. *et al.* An algal enzyme required for biosynthesis of the most abundant marine carotenoids. *Sci Adv* **6**, eaaw9183 (2020).

138. Kagatani, K. *et al.* Excitation relaxation dynamics of carotenoids constituting the diadinoxanthin cycle. *Photosynth. Res.* **154**, 13–19 (2022).
139. García-Plazaola, J. I., Matsubara, S. & Osmond, C. B. The lutein epoxide cycle in higher plants: its relationships to other xanthophyll cycles and possible functions. *Funct. Plant Biol.* **34**, 759–773 (2007).
140. Demmig-Adams, B. *et al.* Non-Photochemical Quenching and Energy Dissipation in Plants, Algae and Cyanobacteria. *Adv. Photosynth. Respir.* 531–552 (2014) doi:10.1007/978-94-017-9032-1_24.
141. Esteban, R. & García-Plazaola, J. I. Non-Photochemical Quenching and Energy Dissipation in Plants, Algae and Cyanobacteria. *Adv. Photosynth. Respir.* 277–295 (2014) doi:10.1007/978-94-017-9032-1_12.
142. Niyogi, K. K. *et al.* Photoprotection in a zeaxanthin- and lutein-deficient double mutant of *Arabidopsis*. *Photosynth Res* **67**, 139–145 (2001).
143. Leuenberger, M. *et al.* Dissecting and modeling zeaxanthin- and lutein-dependent nonphotochemical quenching in *Arabidopsis thaliana*. *Proc National Acad Sci* **114**, E7009–E7017 (2017).
144. Matsubara, S., Morosinotto, T., Osmond, C. B. & Bassi, R. Short- and Long-Term Operation of the Lutein-Epoxide Cycle in Light-Harvesting Antenna Complexes. *Plant Physiol.* **144**, 926–941 (2007).
145. Cazzaniga, S., Li, Z., Niyogi, K. K., Bassi, R. & Dall'Osto, L. The *Arabidopsis szl1* Mutant Reveals a Critical Role of β-Carotene in Photosystem I Photoprotection. *Plant Physiol* **159**, 1745–1758 (2012).
146. Subramanyam, R. & Madireddi, S. K. Photosynthesis: Molecular Approaches to Solar Energy Conversion. *Adv Photosynth Respir* 303–320 (2021) doi:10.1007/978-3-030-67407-6_11.
147. Nagy, G. *et al.* Chloroplast remodeling during state transitions in *Chlamydomonas reinhardtii* as revealed by noninvasive techniques in vivo. *Proc. Natl. Acad. Sci.* **111**, 5042–5047 (2014).
148. Nawrocki, W. J., Santabarbara, S., Mosebach, L., Wollman, F.-A. & Rappaport, F. State transitions redistribute rather than dissipate energy between the two photosystems in *Chlamydomonas*. *Nat Plants* **2**, 16031 (2016).
149. Lemeille, S., Turkina, M. V., Vener, A. V. & Rochaix, J.-D. Stt7-dependent Phosphorylation during State Transitions in the Green Alga *Chlamydomonas reinhardtii*. *Mol. Cell. Proteom.* **9**, 1281–1295 (2010).
150. Depège, N., Bellafiore, S. & Rochaix, J.-D. Role of Chloroplast Protein Kinase Stt7 in LHCII Phosphorylation and State Transition in *Chlamydomonas*. *Science* **299**, 1572–1575 (2003).
151. Bennett, J., Steinback, K. E. & Arntzen, C. J. Chloroplast phosphoproteins: regulation of excitation energy transfer by phosphorylation of thylakoid membrane polypeptides. *Proc. Natl. Acad. Sci.* **77**, 5253–5257 (1980).
152. Bellafiore, S., Barneche, F., Peltier, G. & Rochaix, J.-D. State transitions and light adaptation require chloroplast thylakoid protein kinase STN7. *Nature* **433**, 892–895 (2005).
153. Shapiguzov, A. *et al.* The PPH1 phosphatase is specifically involved in LHCII dephosphorylation and state transitions in *Arabidopsis*. *Proc. Natl. Acad. Sci.* **107**, 4782–4787 (2010).

154. Pribil, M., Pesaresi, P., Hertle, A., Barbato, R. & Leister, D. Role of Plastid Protein Phosphatase TAP38 in LHCII Dephosphorylation and Thylakoid Electron Flow. *PLoS Biol.* **8**, e1000288 (2010).
155. Allorent, G. *et al.* A Dual Strategy to Cope with High Light in *Chlamydomonas reinhardtii*. *Plant Cell* **25**, 545–557 (2013).
156. Sylak-Glassman, E. J., Zaks, J., Amarnath, K., Leuenberger, M. & Fleming, G. R. Characterizing non-photochemical quenching in leaves through fluorescence lifetime snapshots. *Photosynth Res* **127**, 69-76 (2016).
157. Kalaji, H. M. *et al.* Frequently asked questions about in vivo chlorophyll fluorescence: practical issues. *Photosynth. Res.* **122**, 121–158 (2014).
158. Baker, N. R. Chlorophyll Fluorescence: A Probe of Photosynthesis In Vivo. *Annu. Rev. Plant Biol.* **59**, 89–113 (2008).
159. Grieco, M., Tikkanen, M., Paakkarinen, V., Kangasjärvi, S. & Aro, E.-M. Steady-State Phosphorylation of Light-Harvesting Complex II Proteins Preserves Photosystem I under Fluctuating White Light. *Plant Physiol.* **160**, 1896–1910 (2012).

Chapter 2

Modeling Photoprotection in *Nannochloropsis* under Fluctuating Irregular and Regular Light/Dark Sequences

This chapter is reproduced with permission from

Audrey H. Short, Thomas P. Fay, Thien Crisanto, Johanna Hall, Collin J. Steen, Krishna K. Niyogi, David T. Limmer, Graham R. Fleming

"Xanthophyll-cycle based model of the rapid photoprotection of Nannochloropsis in response to regular and irregular light/dark sequences:
J Chem Phys (2022)
DOI:10.1063/5.0089335. Copyright © 2022 Authors

2.1 Abstract

We explore the photoprotection dynamics of *Nannochloropsis oceanica* using time-correlated single photon counting under regular and irregular actinic light sequences. The varying light sequences mimic natural conditions, allowing us to probe the real-time response of non-photochemical quenching (NPQ) pathways. Durations of fluctuating light exposure during a fixed total experimental time and prior light exposure of the algae are both found to have a profound effect on NPQ. These observations are rationalized with a quantitative model based on the xanthophyll cycle and the protonation of LHCX1. The model accurately describes the dynamics of non-photochemical quenching across a variety of light sequences. The combined model and observations suggest that the accumulation of a quenching complex, likely zeaxanthin bound to a protonated LHCX1, is responsible for the gradual rise in NPQ. Additionally, the model makes specific predictions for the light sequence dependence of xanthophyll concentrations that are in reasonable agreement with independent chromatography measurements taken during a specific light/dark sequence.

2.2 Introduction

Under ideal conditions of low light, photosynthesis is a highly efficient metabolic process[1]. When subjected to non-ideal environmental conditions such as high light (HL) exposure, most photosynthetic organisms rely on protective pathways to prevent damage that occurs when reactive oxygen species form[2–4]. Non-photochemical quenching (NPQ) pathways can quench excess energy and dissipate it as heat. However, since these protective pathways are not instantaneously activated or de-activated with changing light levels, organisms can be left under- or over-protected. Light levels can change rapidly over the course of a day, leading to inefficient energy use and damage[5,6]. Previous studies have shown that optimizing the photoprotective pathways used to combat excessive light can increase an organism's biomass yields[7,8]. In addition, the suite of mechanisms used by plants and algae overlap in timescale and known biochemical components, making delineation of specific mechanisms difficult. Here, we study an organism with an apparently simpler, but substantial, response to a variety of light/dark exposures and build a model based on known biochemical actors with which to confront the data.

Interest in understanding the photoprotective pathways in *Nannochloropsis oceanica* is growing due to its high lipid production, which can be utilized in the biofuel industry[9,10]. *N. oceanica* has a high NPQ capacity, a comparatively simple pigment composition[11,12], as well as a small diameter of ~3 μm, making it amenable to spectroscopy and thus a promising organism for mechanistic studies of NPQ pathways. *N. oceanica* contains only chlorophyll (Chl) *a* in its antenna, as well as the xanthophyll (VAZ) cycle pigments, violaxanthin (V), antheraxanthin (A), and zeaxanthin (Z), and the carotenoid vaucheriaxanthin[13,14]. It does not contain the carotenoid, lutein, that is commonly found in other algal and plant species, which enables more direct analysis of the carotenoids involved in quenching. The xanthophylls are interconverted via the VAZ cycle, which requires the enzymes violaxanthin de-epoxidase (VDE) and zeaxanthin epoxidase (ZEP), with A being an intermediate in the conversion of V to Z[15]. Triggering of the NPQ response in oxygenic photosynthetic organisms generally involves a ΔpH-sensing protein. In *N. oceanica* this role is likely played by LHCX1[14]. Finally, *N. oceanica* does not exhibit pronounced state transitions, which are prominent in *C. reinhardtii*[16–18]. Because we are considering the short-time response, we have opted not to use conventional divisions into rapidly reversible (qE) or Z-dependent (qZ) processes and instead simply refer to NPQ. Longer timescale studies may need to delineate qE and qZ[12]. In our previous live-cell snapshot transient absorption spectroscopic studies of wild-type *N. oceanica* and two mutants lacking either VDE or LHCX1, we found a very small response to excess light if either VDE or LHCX1 was absent[11]. In addition, we found clear signals from both the Z S_1 state and the Z radical cation when NPQ was turned on, but no such signal in the VDE mutant nor the LHCX1 mutant even though it contained Z in high light. These observations suggest the importance of a joint action of LHCX1 and Z, with Z binding to a pigment-protein complex (putatively LHCX1) to create the quencher.

In this study, we explore NPQ in *N. oceanica* via fluorescence lifetime snapshot measurements under regular and irregular fluctuating light sequences and their description via a biochemically informed model based on the VAZ cycle and the protonation/de-protonation of a pH sensor. By changing the light intensity over one to several minutes, we aim to simulate the dynamic fluctuations experienced in natural environments. The model makes specific predictions for

xanthophyll concentrations that are compared with some preliminary snapshot HPLC measurements taken under identical conditions to the fluorescence lifetime snapshots.

2.3 Experimental Setup

2.3.1 *Algal growth conditions*

Nannochloropsis oceanica CCMP1779[13] was obtained from the National Center for Marine Algae and Microbiota (https://ncma.bigelow.org/) and cultivated in F2N medium[19]. Liquid cultures were grown to 2-5 x 10^7 cells/ml in continuous light at a photon flux density of 60 µmol photons m^{-2} s^{-1} at 22°C. We refer to these cells as LL-grown cells. For HL-grown cells, liquid cultures were transferred to HL for 24 hours at 350 µmol photons m^{-2} s^{-1} at 22°C.

2.3.2 *Time-correlated single photon counting*

Time-correlated single photon counting results in a histogram of Chl *a* fluorescence decay, which is then fit to a biexponential decay function yielding a lifetime (τ_{avg}). These fluorescence lifetimes were captured at 15 second intervals, resulting in snapshots of fluorescence trajectory that track the changes in the fluorescence lifetime as a function of HL exposure. The amplitude-weighted average lifetime of the Chl *a* fluorescence decay is converted into a unitless form, similar to that measured in the conventional pulse-amplitude modulation technique using the following equation: $NPQ_\tau(t) = \frac{\tau_{avg}(0)-\tau_{avg}(t)}{\tau_{avg}(t)}$ [20] where $\tau_{avg}(0)$ and $\tau_{avg}(t)$ are the average lifetimes in the dark and at any time point *t* during the HL exposure, respectively.

An ultrafast Ti:sapphire coherent Mira 900f oscillator was pumped using a diode laser (Coherent Verdi G10, 532 nm). The center wavelength of the oscillator was 808 nm with a full width at half maximum of 9 nm. After frequency doubling the wavelength to 404 nm with a β-barium borate crystal, the beam was split between a sync photodiode, which was used as a reference for snapshot measurements, and the sample. To control exposure of the sample to the actinic light, three synchronized shutters located in the laser path, actinic light path, and path between the sample and the microchannel plate-photomultiplier tube detector (Hamamatsu R3809U) were controlled by a LABVIEW software sequence. The detector was set to 680 nm to measure Chl *a* emission. During each snapshot, the laser and detection shutters were opened, allowing an excitation pulse with a power of 1.7 mW to saturate the reaction center for 1 second while the emission was recorded. During HL periods, samples were exposed to white light with an intensity of 885 µmol photons m^{-2} s^{-1} (Leica KL 1500 LCD, peak 648 nm, FWHM 220 nm) by opening the actinic light shutter.

1 mL of *N. oceanica* culture was pelleted for 10 minutes at room temperature at 14000 x RMP, flash frozen, thawed at room temperature, and broken using FastPrep-24 at 6.5 m/s for 60 seconds. The pellet was flash frozen and broken two more times. Chlorophyll was extracted from the broken cells using 1 mL of 80% acetone, and total chlorophyll in the culture was quantified according to Porra et al[21]. The culture was then concentrated to ~40 µg Chl mL^{-1} by centrifuging for 5 minutes at room temperature at 4000 RPM. Samples were then dark-acclimated for 30 minutes prior to the experiment and placed in the custom-built sample holder on a sample stage. The LABVIEW sequence was altered for each regular and irregular sequence run to control exposure to light fluctuations.

2.3.3 *High performance liquid chromatography*

Aliquots of *N. oceanica* algae in F2N media were taken at various time points during several irregular and regular actinic light sequences. Samples were then flash frozen in liquid nitrogen. After thawing, the aliquots of the same time point were pooled by centrifuging for 5 minutes at 4 °C at 14000 x RPM to reach a cell count of ~45 x 10^6. The cells were washed twice with H_2O and pelleted at 14,000 x RPM for 5 minutes. Then, the cells were again flash frozen and thawed at room temperature followed by breaking the cells using FastPrep-24 (MP Biomedicals LLC) at 6.5 m/s for 60 seconds. The bead beating step was repeated once before adding 300 µL of 100% cold acetone. The samples were centrifuged for 10 minutes (14000 x RPM, 4 °C), and the supernatant was filtered (0.2 µm nylon filter) into HPLC vials. The supernatant was separated on a Spherisorb S5 ODS1 4.6- x 250 mm cartridge column (Waters, Milford, MA) at 30°C. Analysis was completed using a modification of García-Plazaola and Becerril[22]. Pigments were extracted with a linear gradient from 14% solvent A (0.1M Tris-HCl pH 8.0 ddH_20), 84% (v/v) solvent B (acetonitrile), 2.0% solvent C (methanol) for 15 minutes, to 68% solvent C and 32% solvent D (ethyl acetate) for 33 min, and then to 14% solvent A (0.1M Tris-HCl pH 8.0 ddH2O), 84% (v/v) solvent B (acetonitrile) , 2.0% solvent C (methanol) for 19 min/ The solvent flow rate was 1.2 mL min^{-1}. Pigments were detected by A445 with reference at 550 nm by a diode array detector. Standard curves were prepared from concentrated pigments. The HPLC peaks were normalized to the total Chl *a* concentration.

2.4 Results

2.4.1 *General kinetic features of* **N. oceanica** *photoprotective response*

During the first HL exposure for the LL-grown cells, the photoprotective response as quantified by NPQ_τ has an exponential growth, which gradually slows with continued exposure to HL. The maximum NPQ_τ values for each successive HL period, separated by periods of darkness, trace out a sigmoidal curve. In the subsequent exposures to HL, the response to the transition from dark to light is immediate (Figure 2-1A). In the light to dark transition, the relaxation rate of NPQ_τ is also rapid. When the dark period is less than or equivalent to the duration of the initial HL period, the cells appear to retain a memory of the previous NPQ_τ activation level (Figure 2-1A). However, when the dark period increases, the subsequent HL exposure begins at a much lower NPQ_τ value than in the preceding period (Figure 2-1B and 2-1C). As a result, the photoprotective mechanism seems to reset, causing the NPQ_τ curve during the second HL exposure to increase exponentially rather than grow more gradually (Figure 2-1B and 2-1C).

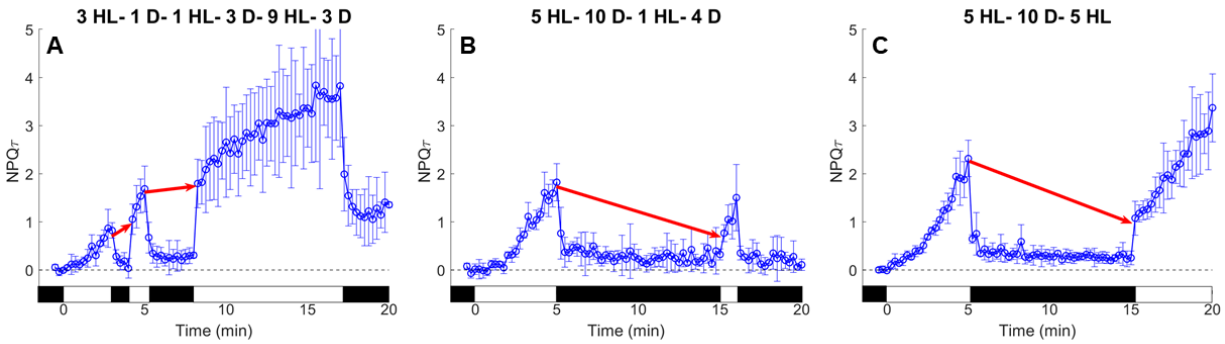

Figure 2-1. Select irregular sequence NPQ_τ traces for LL-grown cells, which demonstrate the cells' apparent memory is dependent on the duration of the dark period. **A)** 3 min HL- 1 min dark- 1 min HL – 3 min dark- 9 min HL- 3 min dark sequence demonstrates that when the dark relaxation period is shorter than the total prior HL exposure, the cells retain a memory of the proceeding NPQ_τ level before the light to dark transition. **B)** 5 min HL-10 min dark-1 min HL-4 min dark and **C)** 5 min HL-10 min dark-5 min HL show that when the dark period is longer than the HL period the initial step in subsequent HL period is reduced. 95% confidence intervals are represented by error bars for n=3. The red arrows connect the last HL point to the top of the initial response in the subsequent HL period. The black boxes at the bottom of each plot represent the dark periods while the white boxes represent HL exposure.

To understand what molecular actors might be involved in the photoprotective pathways of *N. oceanica*, we acquired data for the HL-grown cells using the same light/dark sequences. This results in increased Z concentration, [Z]. In the LL-grown cells, when the initial HL exposure is less than 2 minutes, the response is minimal (Figure 2-2A). Yet, HL-grown cells show a strong and increased NPQ_τ response. The curvature also differs from convex in LL-grown cells to concave in HL-grown cells during the first HL period (Figure 2-2). While the second HL period shown in Fig 2A exhibits a sigmoidal growth for LL-grown cells, the HL-grown cells show an immediate, significant NPQ_τ response. Interestingly, the maximum NPQ_τ value reached in each HL exposure remains approximately the same for LL- and HL-grown cells. The relaxation dynamics in the dark are also consistent regardless of the [Z]. In the light to dark transition, the cells for both treatments respond very rapidly and relax at the same rate to approximately equal NPQ_τ values.

2.4.2 *A xanthophyll cycle-based NPQτ model*

In order to understand the origin of the timescales of the experimental NPQ_τ response in its complex form, we propose a kinetic model based on the xanthophyll cycle. Specifically, we sought to construct a minimal model constrained by known biochemical processes that was consistent with four common kinetic effects observed across the varied light conditions studied. The general kinetic features revealed in Figures 2-1 and 2-2 include the rapid decay of NPQ_τ on transition to the dark and the presence of a slow decay following longer HL exposures is similar between the two treatments of algae. After a period of HL exposure, the slow increase in the NPQ_τ over the course of subsequent light exposures and the short induction period for response to initial light exposure are also similar for both samples.

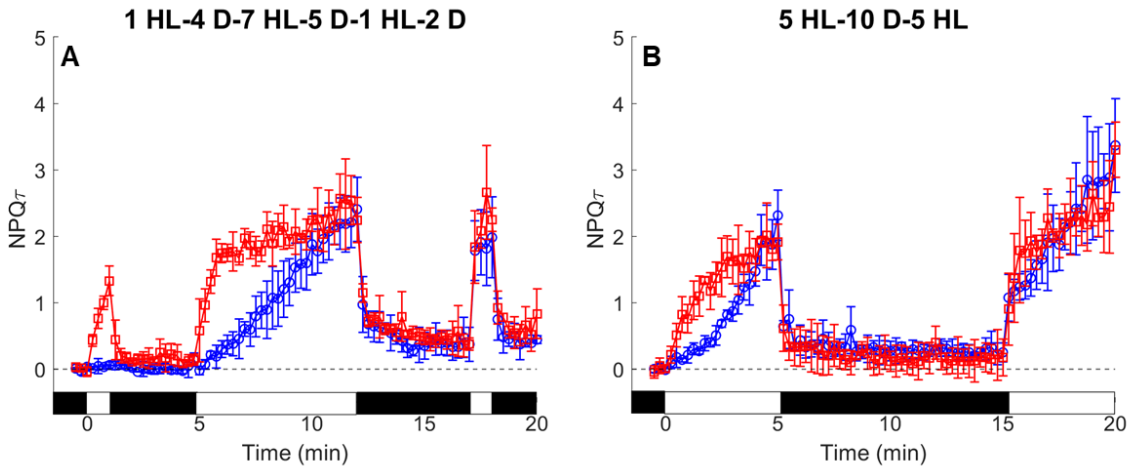

Figure 2-2. HL-grown cells (red squares) compared to LL-grown cells (blue circles) for **A)** 1 min HL-4 min dark-7 min HL-5 min dark-1 min HL-2 min dark and B) 5 min HL-10 min dark-5 min HL sequences. The LL-grown cells exposed to the fluctuating light sequence in **A)** show no significant response to the first HL stimulus. Conversely, HL-grown cells exhibit an immediate response. **B)** The initial 5-minute HL exposure results in different curvatures which are dependent on the pretreatment. HL-grown cells show an immediate, concave response to the first light period rather than a more gradual increase in NPQ_τ for LL-grown cells. In both **A)** and **B)**, the maximum NPQ_τ values, as well as the extent and rate of recovery, are consistent between HL- and LL-grown cells. 95% confidence intervals are represented by error bars (n=3). The black boxes at the bottom of each plot represent the dark periods while the white boxes represent HL exposure.

First, the rapid decay and recovery of NPQ_τ to light after a period of HL exposure suggests that some quencher is produced in a primed state, which rapidly switches between an active and inactive form. The fast timescale is likely related to the lumen pH that is known to rapidly respond to light[23]. The "inactive" quencher must be relatively long lived in the dark phases for the NPQ_τ to retain a memory of previous light exposure. Second, the slow increase in the NPQ_τ over the course of light exposure suggests that the quencher must be formed during the light phases in a second light-dependent process. These observations could be explained by the formation of a Z-bound protein complex that acts as a quencher in response to a low lumen pH. Likely the complex is between LHCX1 and Z given the known importance of both to NPQ in *Nannochloropsis*[11]. The formation of these quenchers is mediated by the xanthophyll cycle since we assume the LHCX1 also binds V. To de-epoxidize V to Z, any complexed V must first unbind from LHCX1. In the HL-grown algae, we expect a higher initial concentration of Z, which leads to a faster initial onset of quenching. Third, the minimal NPQ_τ response we see in LL-grown cells in 1-minute of initial light exposure could be explained by a delay in the activation and deactivation of the conversion of V to Z. In our model we account for this delay by including an activation step for the VDE enzyme, which mediates the V de-epoxidation. A response time in the light and dark phases of the conversion between the active and inactive forms on the order of 1 minute would account for the induction time. Finally, the slow decay of the NPQ_τ during long dark phases suggests that we need to include the reverse step of the xanthophyll cycle, in which Z is epoxidized back to V by ZEP. This process would remove quenchers in the dark phases, which would account for the decrease in NPQ_τ after long dark phases.

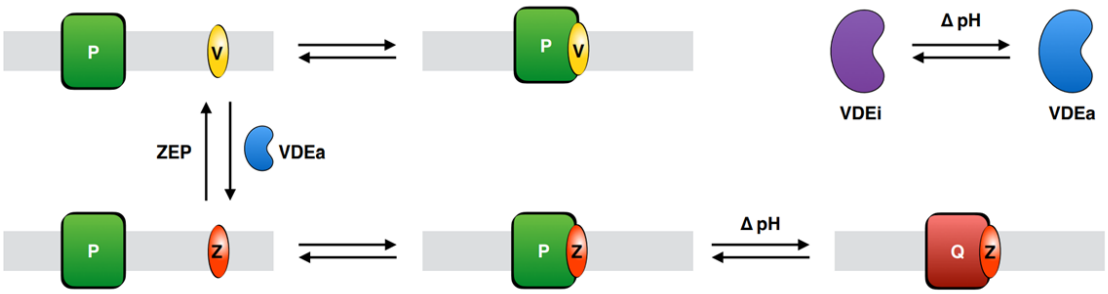

Figure 2-3. Schematic of the model, showing the VAZ cycle and the involvement of VDE and ZEP (the intermediate step of A is omitted from the VAZ cycle for simplicity, and P is assumed to represent LHCX1, though the model does not require this). The activation of VDE and the conversion of PZ to Q (eq 7) occur in response to ΔpH.

Synthesizing these ingredients, we arrive at the following model, illustrated schematically in Figure 2-3. Protein-violaxanthin complexes (PV) establish an equilibrium with dissociated V and protein (P). VDE in its active form (VDEa), irreversibly catalyzes the de-epoxidation of V to Z. The activation of the de-epoxidation is mediated by light, due to changes in lumen pH. Z and unbound protein are in equilibrium with a protein-zeaxanthin (PZ) complex, the inactive quencher. Under HL conditions this PZ complex converts to an active quencher Q in response to changes in pH, and in darkness it rapidly converts back to its inactive form. This likely reflects a protonation due to altered lumen pH. To reduce the model complexity and the number of parameters needed, we have chosen to neglect the A intermediate in the xanthophyll cycle. These specific kinetic processes are

$$\mathrm{P} + \mathrm{V} \underset{k_{\mathrm{PV},b}}{\overset{k_{\mathrm{PV},f}}{\rightleftharpoons}} \mathrm{PV}$$

$$\mathrm{P} + \mathrm{Z} \underset{k_{\mathrm{PZ},b}}{\overset{k_{\mathrm{PZ},f}}{\rightleftharpoons}} \mathrm{PZ}$$

$$\mathrm{V} + \mathrm{VDEa} \xrightarrow{k_{\mathrm{V}}} \mathrm{Z} + \mathrm{VDEa}$$

$$\mathrm{Z} \xrightarrow{k_{\mathrm{Z}}} \mathrm{V}$$

$$\mathrm{VDEi} \underset{k_{\mathrm{VDE},b}(I(t))}{\overset{k_{\mathrm{VDE},f}(I(t))}{\rightleftharpoons}} \mathrm{VDEa}$$

$$\mathrm{PZ} \underset{k_{\mathrm{Q},b}(I(t))}{\overset{k_{\mathrm{Q},f}(I(t))}{\rightleftharpoons}} \mathrm{Q}.$$

where to obtain the model kinetic equations, we treat each step in the above scheme as an elementary process with rates defined by the arrows.

Our proposed model includes two light intensity, $I(t)$, dependent equilibria. Given that the lumen pH is known to respond on a much faster timescale than the kinetics that these experiments probe, we model the light intensity $I(t)$ dependent steps as instantaneously switching between a dark-phase value and a HL phase value,

$$k\big(I(t)\big) = \begin{cases} k_{\text{dark}}, \text{if } I(t) = 0 \\ k_{\text{light}}, \text{if } I(t) > 0 \end{cases} \quad (1)$$

for each light-dependent rate in the kinetic scheme. We assume the system is initially in its dark-phase steady state, which leaves only three free concentrations, $[\text{VDE}]_{\text{tot}} = [\text{VDEa}] + [\text{VDEi}]$, $[\text{X}]_{\text{tot}} = [\text{V}] + [\text{Z}] + [\text{PV}] + [\text{PZ}] + [\text{Q}]$, and $[\text{P}]_{\text{tot}} = [\text{P}] + [\text{PV}] + [\text{PZ}] + [\text{Q}]$. To obtain the NPQ_τ from this model, we assume that the fluorescence lifetime of chlorophyll *a* is given by

$$\frac{1}{\tau_F} = k_R + k_{NR} + k_Q[\text{Q}], \quad (2)$$

where k_R is the radiative rate of Chl *a*, k_{NR} is the rate for de-excitation by other non-radiative processes, and k_Q is the quenching rate. With this we model NPQ_τ as

$$\text{NPQ}_\tau = \tau_{F,0} k_Q [\text{Q}] - \tau_{F,0} k_Q [\text{Q}]_0 \quad (3)$$

where $\tau_{F,0}$ is the initial fluorescence lifetime and $[\text{Q}]_0$ is the initial concentration of the Q species.

To solve these kinetic equations numerically, we employ a system of dimensionless variables defined by $\widetilde{[\text{A}]} = \tau_{F,0} k_Q [\text{A}]$, to eliminate the k_Q parameter. In these reduced variables, the NPQ_τ signal is simply $\text{NPQ}_\tau = \widetilde{[\text{Q}]} - \widetilde{[\text{Q}]}_0$. In order to allow for consistent comparison between the parameters obtained in fitting the LL-grown algae datasets and HL-grown algae datasets, the NPQ_τ model value has to be scaled by the ratio of the fluorescence lifetimes under HL and LL conditions, which within the model is simply $1/\big(1 - \widetilde{[\text{Q}]}_0^{\text{LL}} + \widetilde{[\text{Q}]}_0\big)$, where $\widetilde{[\text{Q}]}_0^{\text{LL}}$ is the initial value $\widetilde{[\text{Q}]}$ obtained for the LL-grown dataset. Overall then the HL-grown dataset NPQ_τ is given by

$$\text{NPQ}_\tau^{\text{HL}} = \frac{\tau_{F,0}^{\text{HL}}}{\tau_{F,0}^{\text{LL}}} \big(\widetilde{[\text{Q}]} - \widetilde{[\text{Q}]}_0\big) = \frac{\widetilde{[\text{Q}]} - \widetilde{[\text{Q}]}_0}{1 - \widetilde{[\text{Q}]}_0^{\text{LL}} + \widetilde{[\text{Q}]}_0}. \quad (4)$$

Furthermore, there is some parametric redundancy in fitting the model to the NPQ_τ data, because this signal depends only on $k_{\text{V}}[\text{VDEa}]$, so k_{V} can be scaled arbitrarily provided the total VDE concentration is scaled down by the same amount. In order to circumvent this problem, we fit the parameters $k_{\text{V}}[\text{VDEa}]_{\text{light}}^{\text{eq}}$, and $k_{\text{V}}[\text{VDEa}]_{\text{dark}}^{\text{eq}}$, and we only explicitly treat the relative activity of the VDE enzyme, $\alpha_{\text{VDE}} = [\text{VDEa}]/[\text{VDEa}]_{\text{light}}^{\text{eq}}$, as a kinetic variable. Here $[\text{VDEa}]_{\text{light/dark}}^{\text{eq}}$ are the steady-state values of [VDEa] in the light and dark phases of the experiment.

The remaining 15 model parameters were obtained by performing a least-squares fit to the experimental NPQ_τ data. Details are available in Appendix 1. Due to variation between the experiments and shortcomings of the model, we could not find a parameter set that consistently captures the maximum NPQ_τ in both the periodic and irregular sequence datasets, so the model was fitted separately to these two datasets. Because longer timescale NPQ components were not included in the model, the 1-1 periodic sequence was found to heavily skew the model fitting with the periodic sequence data, so this was excluded in the fitting procedure. Additional simplified models were also tested in which various components of the current model were removed, for example models in which VDE is assumed to respond instantaneously and models in which the Z to V conversion is neglected were tested. These simplified models did not adequately capture the NPQ_τ response to light fluctuations, and the model presented was found to be the minimal model

that could describe the NPQ_τ responses. Further details of the model implementation, fitting, and error analysis are given in Appendix 1.

2.4.3 *NPQ response to regular and irregular light*

When *N. oceanica* is exposed to periodic light fluctuations, the intensity of response is dependent on time as well as the duration of the HL periodic exposure. The NPQ_τ data and model fits for the regular light fluctuations are presented in Figure 2-4, and the model parameters are given in Tables 2-1 through 2-3. The regular light fluctuations fall into two regimes, fast and slow, depending on the sequence duration. Sequences 1-1 and 2-2 (Figure 2-4A and 2-4B) are considered fast fluctuations, while sequences 4-4, 5-5, and 10-10 (Figure 2-4C-E) have a qualitatively different appearance, and we term them slow fluctuations. The fast fluctuations have higher max NPQ_τ values of 4.73 and 4.34, respectively, which is caused by a raising baseline as a result of incomplete relaxation of NPQ. Within the slow fluctuations, 5-5 and 10-10 have equivalent total HL exposure as the fast fluctuations, but do not exhibit a rising baseline, giving maximum NPQ_τ values that are lower at 3.76 and 3.79, respectively (Figure 2-4D and 2-4E). While the model succeeds in capturing the NPQ_τ values in HL periods for the slow fluctuations, it underestimates these values in the fast fluctuation, likely as a result of neglect of slower relaxation of long-timescale NPQ components.

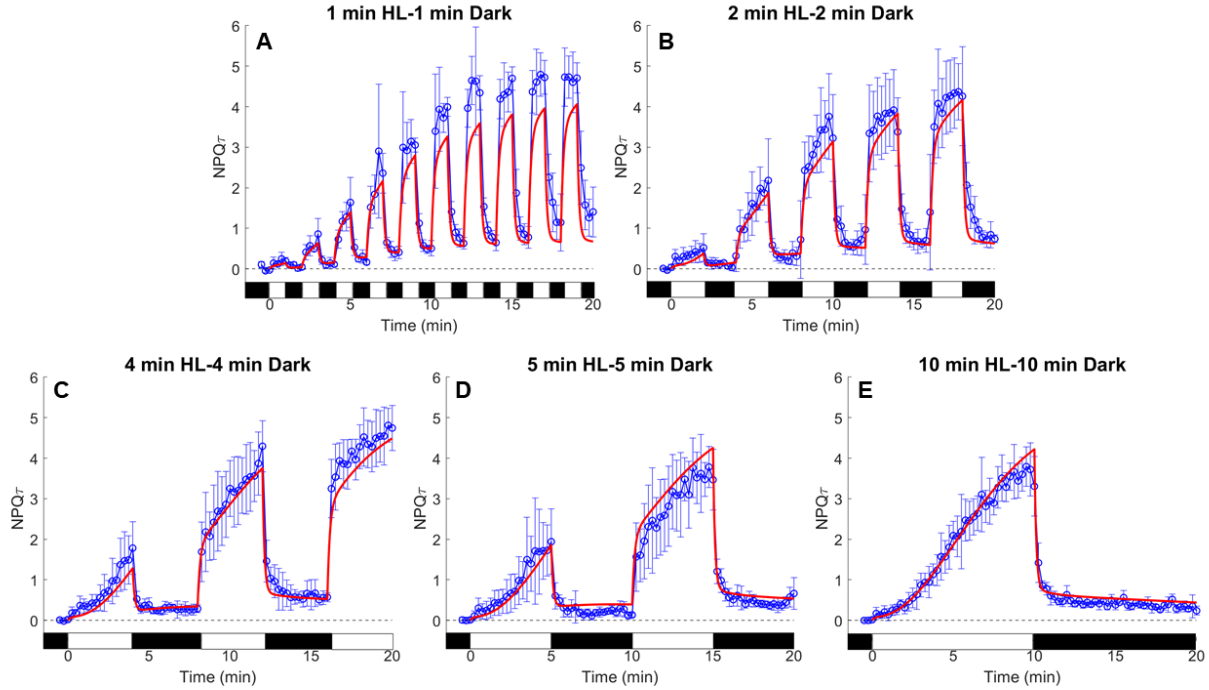

Figure 2-4. NPQ_τ traces for each regular fluctuating light sequence for LL-grown cells. The model predicted NPQ_τ traces are shown as the red lines. Rapid fluctuating sequences, **A)** and **B)**, show an increasing recovery baseline compared to slow fluctuating sequences **C)**, **D)**, **E),** indicating slower timescale NPQ components might not be able to relax in **A)** and **B)**. Because of incomplete recovery in the 1 min HL-1 min dark sequence, this sequence was not included in the parameter fitting, which may be why the model underestimates NPQ_τ for this sequence. 95% confidence intervals are represented by error bars (n=5). The black boxes at the bottom of each plot represent the dark periods while the white boxes represent HL exposure.

Parameter	LL periodic	Error (2σ)	LL irregular	Error (2σ)	HL all sequences	Error (2σ)
$k_{PZ,f}$	5.86	2.5	6.28	2.6	3.91	1.5
$k_{PZ,b}$	0.325	7.2 x10^{-2}	0.364	7.7 x10^{-2}	0.861	0.23
$k_{PV,f}$	115	48	101	70	127	34
$k_{PV,b}$	5.09	1.0	6.00	3.4	5.72	0.68
$k_{Q,f,light}$	6.55	2.1	10.9	7.1	9.78	1.2
$k_{Q,b,light}$	2.14 x10^{-2}	2.6 x10^{-4}	1.51 x10^{-2}	4.9 x10^{-3}	2.00 x10^{-3}	6.6 x10^{-4}
$k_{Q,f,dark}$	1.60	3.5 x10^{-3}	1.13	0.28	12.2	2.5
$k_{Q,b,dark}$	7.34	0.57	3.88	0.66	11.6	2.8
$k_{V,light}$ [a]	0.156	3.3 x10^{-2}	0.158	7.0 x10^{-2}	9.21 x10^{-2}	1.2 x10^{-2}
$k_{V,dark}$ [a]	1.13 x10^{-3}	8.7 x10^{-4}	4.53 x10^{-4}	1.1 x10^{-4}	1.30 x10^{-3}	2.6 x10^{-4}
$k_{Z,dark}$	5.29 x10^{-2}	2.1 x10^{-2}	6.21 x10^{-2}	4.7 x10^{-3}	1.10 x10^{-3}	2.6 x10^{-4}
$k_{VDE,light}$ [b]	3.84	1.6	1.84	0.72	3.58	1.1
$k_{VDE,dark}$ [b]	0.615	0.12	1.42	0.50	0.857	0.33

Table 2-1. Fitted rate constants for the NPQ models for LL regular, LL irregular and HL datasets. All model parameters refer to the reduced variable model, with parameters in min^{-1}.[a] $k_{\mathrm{V,light/dark}} = k_{\mathrm{V}}[\mathrm{VDEa}]^{\mathrm{eq}}_{\mathrm{light/dark}}$ is the maximum rate of V to Z conversion in the light/dark phases. [b] $k_{\mathrm{VDE}} = k_{\mathrm{VDE},f} + k_{\mathrm{VDE},b}$ is the recovery rate for the the VDE activation to its light/dark phase equilibrium value.

Parameter	LL periodic	Error (2σ)	LL irregular	Error (2σ)	HL all sequences	Error (2σ)
K_{PV}	22.7	9.5	16.8	10	22.3	4.0
K_{PZ}	18.1	9.5	17.3	8.0	4.54	1.6
$K_{X,dark}$ [a]	2.13 x10^{-2}	1.7 x10^{-2}	7.29 x10^{-3}	1.9 x10^{-3}	1.25	0.36
$K_{X,light}$ [a]	2.94	1.7	2.55	1.2	86.2	21
$K_{Q,dark}$	0.217	1.7 x10^{-2}	0.292	3.7 x10^{-2}	1.05	0.16
$K_{Q,light}$	306	99	721	350	4790	1600
$K_{PZ,eff,dark}$ [b]	22.0	12	22.3	10	9.28	2.7
$K_{PZ,eff,light}$ [b]	5550	2800	12500	6900	21700	12000

Table 2-2. Equilibrium constants obtained for various equilibria in the model in reduced variables. [a] $K_{\mathrm{X}} = [\mathrm{Z}]_{\mathrm{eq}}/[\mathrm{V}]_{\mathrm{eq}}$. [b] $K_{\mathrm{PZ,eff}} = ([\mathrm{PZ}]_{\mathrm{eq}} + [\mathrm{Q}]_{\mathrm{eq}})/[\mathrm{P}]_{\mathrm{eq}}[\mathrm{Z}]_{\mathrm{eq}}$.

Parameter	LL periodic	Error (2σ)	LL irregular	Error (2σ)	HL all sequences	Error (2σ)
$[V]_0$	32.1	6.6	27.0	17	13.2	0.26
$[Z]_0$	0.684	0.55	0.197	0.14	16.5	4.8
$[PZ]_0$	8.60 x10^{-2}	6.4 x10^{-2}	2.88 x10^{-2}	1.6 x10^{-2}	1.78	0.61
$[Q]_0$	1.87 x10^{-2}	1.4 x10^{-2}	8.40 x10^{-3}	4.7x10^{-3}	1.86	0.82
$[PV]_0$	5.06	0.40	3.85	0.10	6.99	2.2
$[P]_0$	6.96 x10^{-3}	3.3 x10^{-3}	8.46 x10^{-3}	6.6 x10^{-3}	2.38 x10^{-2}	9.9 x10^{-3}
$[X]_{tot}$	37.9	6.8	31.1	18	40.3	7.7
$[P]_{tot}$	5.17	0.41	3.90	0.10	10.6	3.6
NPQ_{max}	5.13	0.40	3.88	0.10	8.79	2.8

Table 2-3. Initial concentrations and the theoretical maximum NPQ_τ for the models fitted to the different datasets. All values are given for the reduced variable model, as described in the text, and as such all concentrations are unitless.

The initial response to the first HL period clearly differs between the two fluctuation regimes. Examining the 10-10 sequence, the NPQ_τ curve has a sigmoidal shape with an inflection point at about 5 minutes, exhibiting an NPQ_τ value of 2. In sequences 4-4 and 5-5, the first HL period has a convex shape which reaches an NPQ_τ value of approximately 2. However, the fast fluctuations have different initial responses to HL. In these cases, the initial photoprotective response is minimal. Several light/dark cycles must pass before the fast fluctuations exhibit rapid responses to the dark to light transition with concave curvature. When examining the HL period segments, they form a sigmoidal curve similar to the continuous HL curve in 10-10. Even with a variety of durations, the model correctly generates the convex curvature for the first HL period and the changes in the subsequent HL periods to a more gradual NPQ_τ increase.

In addition to the regular periodic sequences, irregular light fluctuations were also used (Figure 2-5). Here, the limits of the model were probed by seemingly random light/dark durations, which more closely mimic random light changes in nature. Overall, the model was able to capture the immediate response the cells have in the light-to-dark and dark-to-light transitions as seen in both the regular and irregular sequences. The predicted NPQ_τ response also retains an apparent memory of HL when dark durations are less than preceding HL exposure (Figure 2-5A-F, I, J). The same sigmoidal shape can be seen in both the model and experimental data for the HL periodic segments except in two sequences: 5-10-1-4 and 5-10-5 (Figure 2-5G and 2-5H). Particularly in the 5-10-1-4 sequence, the model overestimates the NPQ_τ response in the second HL exposure. A similar issue can be seen in Figure 2-5A when the first HL period is 1 minute, which does not elicit a response in LL-grown cells. The experimental data show the sigmoidal growth in maximum NPQ_τ in the second HL period, indicating the quenching mechanism was not fully turned on during the first minute of HL.

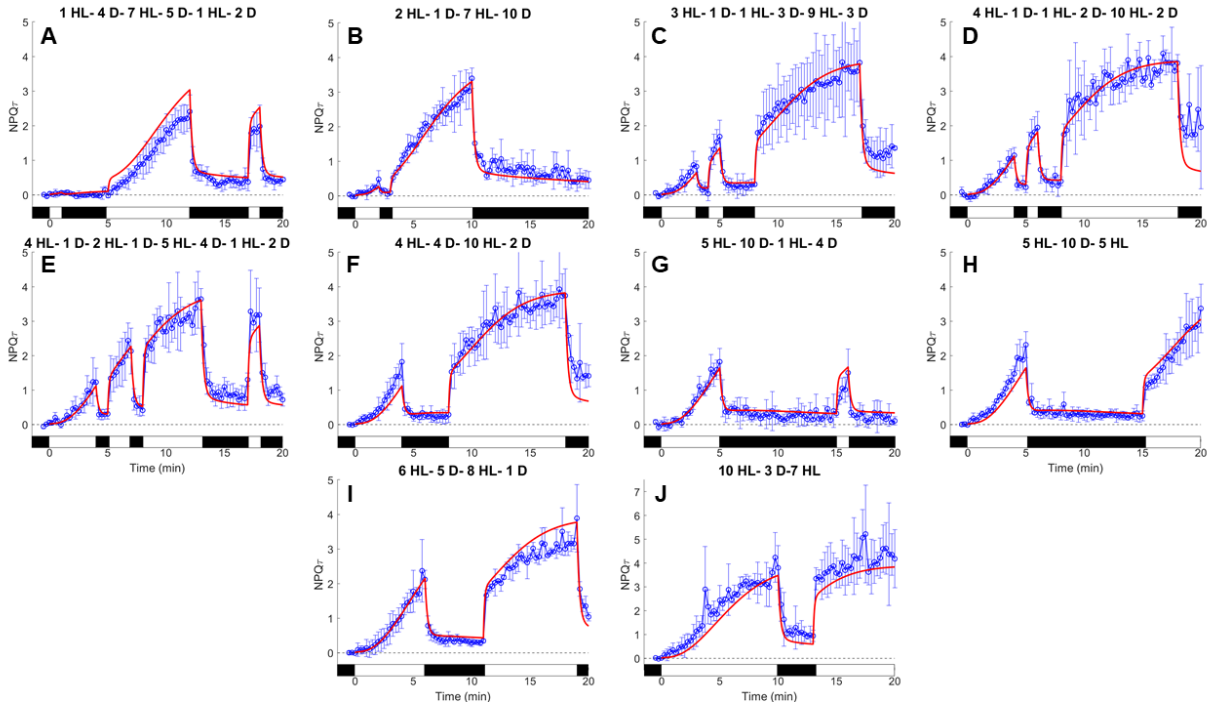

Figure 2-5. NPQ_τ traces for each irregular fluctuating light sequence for LL-grown cells. The model predicted NPQ_τ curve (red line) is also shown. Experimental NPQ_τ and predicted NPQ_τ curve for **A)** 1 min HL- 4 min dark- 7 min HL- 5 min dark- 1 min HL- 2 min dark, **B)** 2 min HL- 1 min dark- 7 min HL- 10 min dark, **C)** 3 min HL- 1 min dark- 1 min HL- 3 min dark- 9 min HL- 3 min dark, **D)** 4 min HL- 1 min dark- 1 min HL- 2 min dark- 10 min HL- 2 min dark, **E)** 4 min HL- 1 min dark- 2 min HL- 1 min dark- 5 min HL- 4 min dark- 1 min HL – 2min dark, **F)** 4 min HL- 4 min dark- 10 min HL- 2 min dark, **G)** 5 min HL- 10 min dark- 1 min HL- 4 min dark, **H)** 5 min HL- 10 min dark- 5 min HL, **I)** 6 min HL- 5 min dark- 8 min HL- 1 min dark, **J)** 10 min HL- 3 min dark- 7 min HL. As can be seen in **A)** the model overestimates the slow, initial increase seen in the experimental data. The model similarly overshoots the secondary HL exposure in **G)** after a 10-minute dark period. Overall, the model is able to reproduce the rapid switch on/off with the transitions between light/dark and vice versa. 95% confidence intervals are represented by error bars (n=3). The black boxes at the bottom of each plot represent the dark periods while the white boxes represent HL exposure.

In Figure 2-6 we show the response and fits to irregular light/dark sequences for HL-grown algae. The difference in the initial response when the first light period is short (Figures 2-6A and 2-6B vs. Figures 2-5A and 2-5B) is striking. In contrast, the rapid decrease in NPQ_τ on transition to the dark and the presence of a slow decay in NPQ_τ following longer HL exposures (e.g. Figures 2-5B and 2-6B) is quite similar in two treatments. Clearly at least some of the additional Z in the HL-grown cells is available for quenching on the 1-minute timescale. Interestingly, maximum NPQ_τ values reached in both datasets are the same; they are clearly limited by something other than total [Z]. Overall, the model performs equally well for the two data sets.

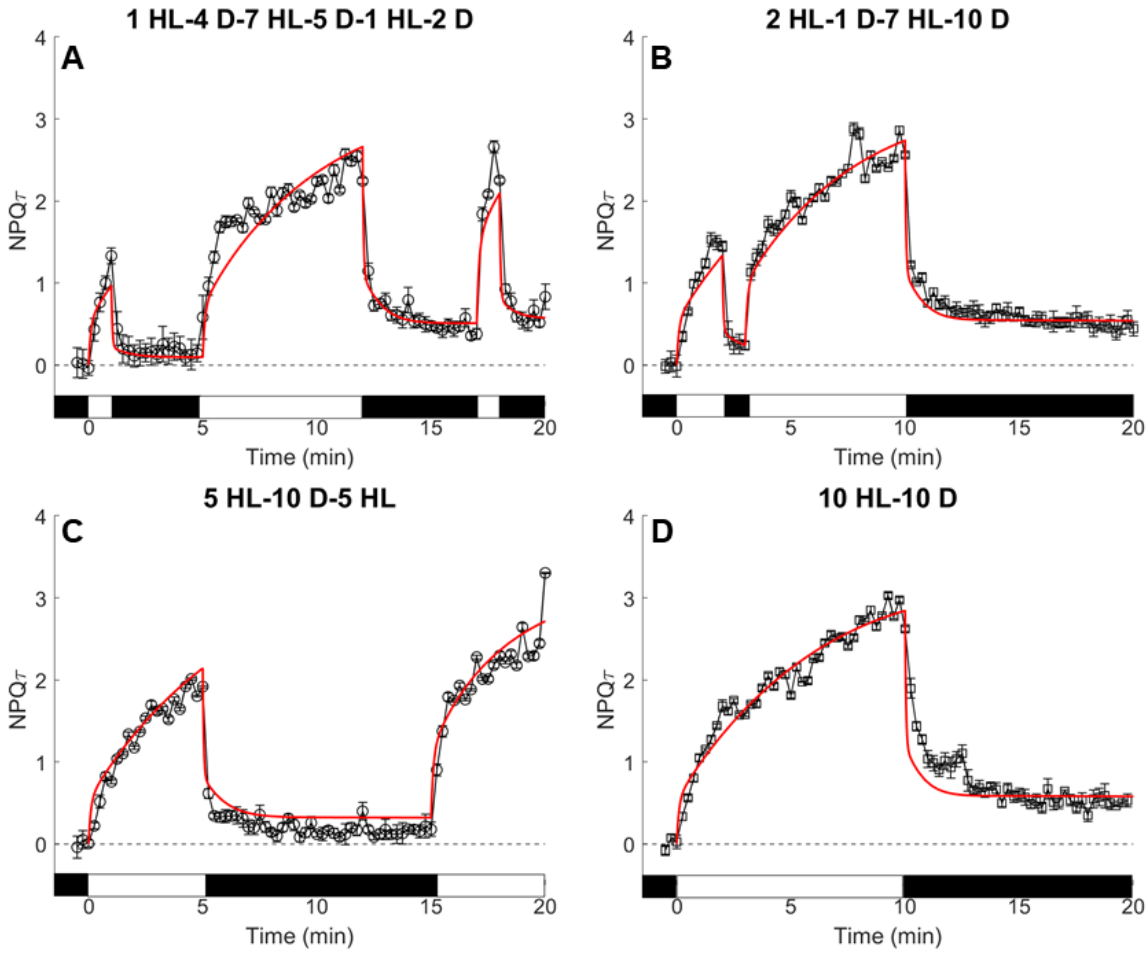

Figure 2-6. Comparison of the model (red line) to the experimental data (black squares) for the HL-grown cells. This treatment causes the algal cells to accumulate a higher [Z]. The change in kinetics can be seen in the concave curves present in all the HL exposure periods during the experimental run. Experimental NPQ_τ and predicted NPQ_τ curve for HL-grown cells for sequences **A)** 1 min HL- 4 min dark- 7 min HL- 5 min dark- 1 min HL- 2 min dark, **B)** 2 min HL- 1 min dark- 7 min HL- 10 min dark, **C)** 5 min HL- 10 min dark- 5 min HL, **D)** 10 min HL- 10 min dark. The black boxes at the bottom of each plot represent the dark duration while the white boxes represent HL exposure. 95% confidence intervals are represented by error bars (n=3). The black boxes at the bottom of each plot represent the dark periods while the white boxes represent HL exposure.

In Tables 2-1 through 2-3 we present the model parameters obtained from fitting the model to the experimental NPQ_τ datasets, all of which are given in the reduced units described above. The full set of rate constants in Table 2-1, plus $[V]_0$ and $[P]_{tot}$, were fitted directly, which were then used to obtain the other parameters listed in Tables 2-2 and 2-3. Model parameters for the two LL-grown datasets largely agree (to within 2 standard deviations), with the exception of $[P]_{tot}$, while there are more significant differences between the model parameters for the LL-grown and HL-grown algae, in particular in the values of k_Z, k_V, $[X]_{tot}$, $[P]_{tot}$, and the other parameters that depend strongly on these. In the following sections we will highlight some of the points of interest regarding the model parameters and discuss what physical insight into xanthophyll-based NPQ can be gleaned from their values.

2.4.4 *Origin of sigmoidal growth of NPQ_τ*

One intriguing feature of the NPQ_τ signals is the remarkable difference in the responses of LL- and HL-grown algae. In the former case a sigmoidal-like growth, $NPQ_\tau \propto 1/(ae^{-kt}+1)$, is observed, whereas in the latter case a much simpler $NPQ_\tau \propto 1-e^{-kt}$ response is seen. In the former case the growth rate of NPQ_τ increases then decreases, but in the latter case the NPQ_τ growth rate is decreasing at all times during the light phases.

To explain this in qualitative terms, we note there are two main factors that contribute to the growth of PZ and subsequently NPQ_τ. First, the availability of free P to which Z can bind, and second the availability of Z. Assuming V and P binding and unbinding is rapid, free P is created by the removal of V, pulling the PV binding equilibrium towards the unbound species. If there is a large excess of Z initially as in the HL-grown algae, then free P is able to bind to Z as soon as it is produced, and no sigmoidal-like growth is observed. If there is a low initial concentration of Z as in the LL-grown algae, then P and Z build up significantly before binding to form PZ, and the rate at which PZ is formed will therefore go through a maximum.

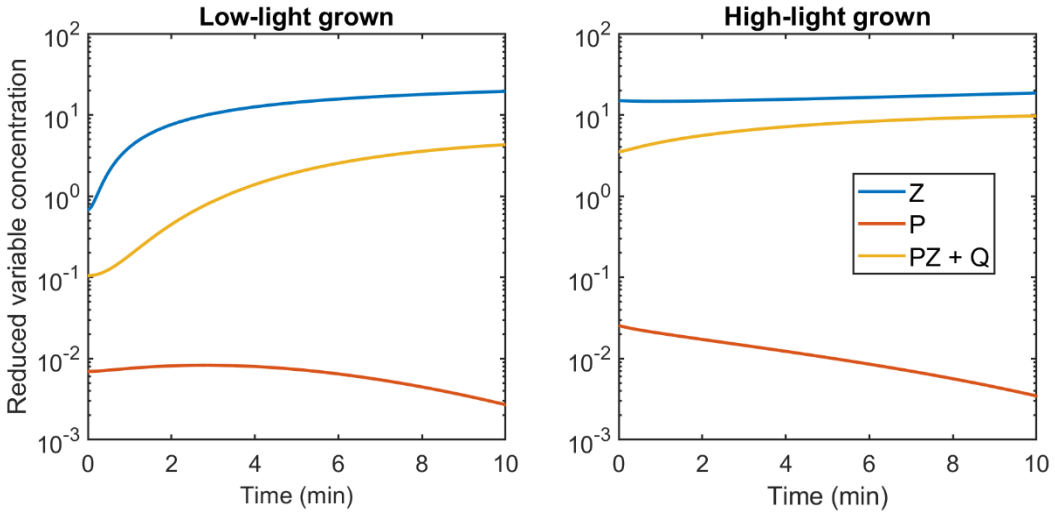

Figure 2-7. Model predictions for the concentrations of Z, P, and PZ+Q for LL- and HL-grown algae during 10 minutes of light exposure.

This is illustrated in Figure 2-7, where we show the concentrations of Z, P and PZ+Q for LL- and HL-grown models during 10 minutes of light exposure. In the LL-grown case, [P] passes through a maximum, and [Z] increases significantly, resulting in the total PZ concentration exhibiting sigmoidal-like growth. In the HL-grown case, however, the initial Z concentration is much larger, and as a result neither Z nor P build up during the light exposure, so the total PZ concentration does not exhibit sigmoidal-like growth.

Under quasi-equilibrium assumptions, detailed in Appendix 2, we find the following criterion for observing sigmoidal-like NPQ growth in our model,

$$\tau_V < \frac{K_{PV}[V]_0}{k_{PZ,f}[Z]_0}, \quad (5)$$

where $\tau_V^{-1} = k_V[\mathrm{VDEa}]_{\mathrm{light}}^{\mathrm{eq}}$ is the time-scale on which V is converted to Z in the light phases. When there is a large excess of V initially, as in the LL-grown algae, the right-hand side of Eq. 4 is large and the inequality is satisfied, and we observe sigmoidal growth. When more Z is present initially, as in the HL-grown algae, we do not see sigmoidal-like growth.

2.4.5 *Comparison of model concentration predictions to HPLC*

The model produces the time-dependent xanthophyll concentrations, which can be independently compared with HPLC data for the various illumination sequences. Figure 2-8 compares experimental plots of normalized [Z](t) ([Z]/ [V] + [A] + [Z]) with the model prediction for [Z](t) for the 5-10-5 sequence. The shape of the plot of the conventional[3] de-epoxidized quantity (([A]/2 + [Z])/ [V] + [A] + [Z]) is very similar for both HL-grown and LL-grown algae to those shown in Figure 2-8A.

One clear difference between the measurements and the model (Figure 2-8B) is in the initial value of [Z]. However, in LL-grown algae the NPQ_τ data strongly suggest that this pool of Z is not rapidly accessible to produce quenching in the first few minutes of HL exposure. If a constant [Z](0) is added to the model's LL prediction, the qualitative agreement with either model of de-epoxidized xanthophylls is good. In particular, the slow decrease in [Z] in the dark period is captured by the model, along with the steep increase in the second light period. However, we do not know when, or if, this initial pool of Z becomes active. We note that Jahns et al.[24] have shown that only a fraction of the total pool of V is accessible to VDE in plant thylakoid membranes even on a 120-minute timescale as a result of V binding to specific light-harvesting proteins. In studies of understory leaves subject to rapid high intensity sun flecks Adams et al found that high levels of Z and A were maintained between sun flecks, even though the dissipation was minimal during the low light periods[25]. The degree to which the full [Z] is available for quenching complicates the comparison of the predicted and measured [Z(t)]. In the case of LL grown cells, equating the model [Z(t)] with ΔZ, i.e. subtracting the initial [Z] from the HPLC results, seems a reasonable approach because none of the initial [Z] is immediately available for NPQ (Figure 2-2). For the HL-grown cells, however, at least some of the $[Z]_0$ is immediately available for NPQ, which suggests that this fraction may be free in the membrane rather than bound to specific pigment-protein complexes. To quantify the initial [Z] availability, we plan in future work to collect an extensive set of HPLC xanthophyll data for the light/dark sequences used in this work.

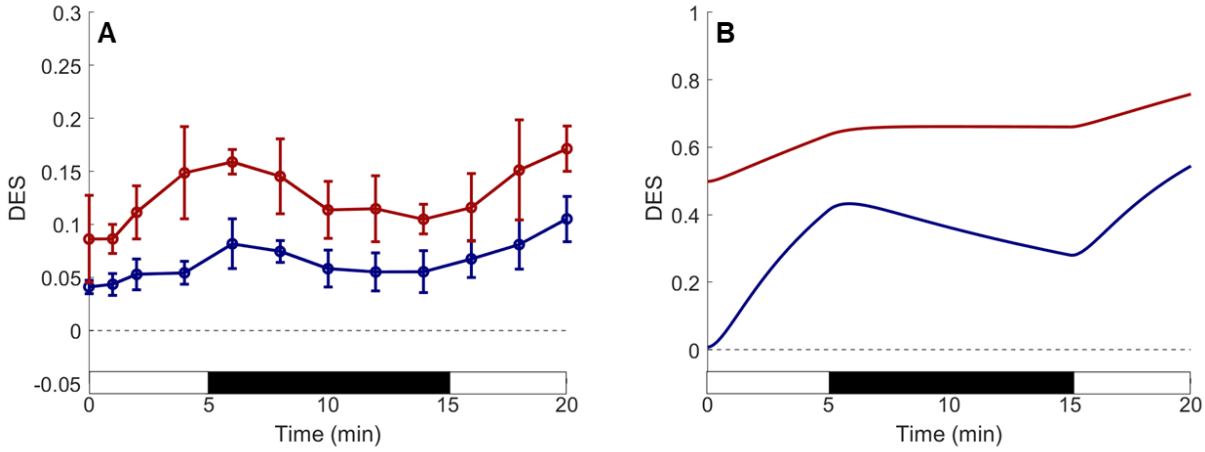

Figure 2-8. De-epoxidation states (DES) taken at various timepoints throughout the 5 min HL-10 min dark-5 min HL sequence compared to the predicted DES. Results for HL-grown cells are shown in red, and the LL-grown results are depicted in blue. **A)** The DES equation was modified to only include [Z] in the numerator since the model does not account for A contributing to the quenching state. **B)** The model's predicted DES calculated using the predicted total [Z] /([V] + [Z]). 95% confidence intervals are represented by error bars (n=3). The black boxes at the bottom of each plot represent the dark periods while the white boxes represent HL exposure.

2.5 Discussion

We now turn to the features of the model that underlie its description of the response of *N, oceanica* to excess light. We also comment on the numerical values of the fitting parameters and go on to explore whether the model can predict experimentally accessible quantities such as xanthophyll concentrations during our light/dark sequences.

The model correctly captures the change in NPQ response from accelerating (roughly exponential) to decelerating (roughly sigmoidal) with the cross over depending on the relative concentrations of V and Z, on a timescale dictated by the maximum de-epoxidation rate. The model allows us to ascertain timescales for the activation and deactivation of the quenching mechanism within the hypothetical LHCX1-Z complex. Under dark conditions the deactivation rate ($k_{\mathrm{Q},f,\mathrm{dark}} + k_{\mathrm{Q},b,\mathrm{dark}}$) is found in the range 4 – 9 min^{-1}, which is very close to the light phase activation rate of the quenching ($k_{\mathrm{Q},f,\mathrm{light}} + k_{\mathrm{Q},b,\mathrm{light}}$), which is in the 7 – 11 min^{-1} range. The faster activation/de-activation timescale of PZ could reflect the time taken for protonation/deprotonation of LHCX1. However, given the relatively small variation between light and dark phases of the forward rate (roughly a 3 – 6 fold increase), where the lumen [H^+] changes by much more, this seems unlikely. In our view this rate reflects the timescale of a conformational change of the LHCX1 protein, which is triggered by a much more rapid protonation/deprotonation[23] or unbinding of LHCX1 from an antenna protein. A slower component of the NPQ_τ decay in the dark phases is likely due to the slower unbinding of Z from LHCX1 during the dark phases, the rate of which, $k_{\mathrm{PZ},b}$, is found to be roughly 0.5 min^{-1}.

Similarly, we find a rate for activation/deactivation of the VDE enzyme $k_{\mathrm{VDE}} = k_{\mathrm{VDE},f} + k_{\mathrm{VDE},b}$ of 0.5 – 1.5 min^{-1} in the dark phases and 1.5 – 4 min^{-1} in the light phases. The relatively small

variation between light and dark phases suggests this does not directly reflect the protonation/deprotonation rate of VDE. Instead, this rate of activation could reflect a protonation-state dependent conformational change, or alternatively the rate at which the ascorbate substrate binds and unbinds from the enzyme, or unbinding VDE from the membrane.

The irregular sequence fits to LL-grown algae are used as a basis for fitting the HL-grown data. These fits captured the very different initial responses of HL- and LL-grown cells (Figure 2-6). Comparing the HL fitted parameters to the LL fitted parameters, we find the most significant difference between the rate constants to be in the rates of de-epoxidation of V and epoxidation of Z (see Table 2-1). The de-epoxidation rate k_{V} increases by a factor of ~3 in the dark phase and ~6 in the light phases between the HL- and LL-grown samples, while the epoxidation rate k_{Z} decreases by a factor of ~60 in the HL sample relative to the LL sample. These changes lead to the large observed difference in the initial Z concentration between the HL- and LL-grown samples, which leads to the very different NPQ responses to fluctuating light. One possible explanation for these changes is different levels of expression of the VDE and ZEP enzymes when the algae are grown under HL and LL conditions[26,27]. HL and LL growth could also change the availability of other substrates involved in the (de-) epoxidation, as well as the average lumen pH and stroma pH, which are known to affect the activity of these enzymes[28].

The other most significant differences between the HL- and LL-grown algae are the total concentrations of xanthophylls and LHCX1, with the xanthophyll pool being ~ 25% larger and the LHCX1 pool being around twice as large in in the HL-grown algae[12]. Increasing the sizes of both pools increases the extent of quenching in the cells and the rate at which the quenching mechanism activates in response to HL. There are other small differences in the rate constants and equilibrium constants for the various processes between the HL- and LL-grown cells. These can likely be attributed to other changes between cells grown in different light conditions, for example differences in the average dark and light phase lumen pH, and possible changes to the thylakoid membrane, stroma, and lumen compositions[29]. The maximum NPQ_{τ} values are the same in the HL- and LL-grown cells, though, which may indicate photoinhibition is occurring in HL-grown algae. However, measurements of periodic responses to different HL intensities and of gene expression levels under diverse illumination conditions should help to characterize the origin of this rather surprising result.

The success in fitting the experimental data encouraged us to see if the model could predict quantities that could be subsequently measured. For example, the equilibrium constants listed in Table 2-3 can be related to binding free energies of various complexes and how they change under protonation. Our model also allows us to examine the relative binding constants for V and Z to the LHCX1 complex. For the Z binding, we must account for the two states of the PZ complex, so we compare K_{PV} with $K_{\mathrm{PZ,eff}} = \left(1 + K_{\mathrm{Q}}\right)K_{\mathrm{PZ}}$. Under dark conditions, the model predicts that V and Z bind similarly to the protein, with binding constants (in reduced units) of around 20. However, under HL conditions Z binds about 200 – 400 times more strongly than V to LHCX1. Temperature dependent studies should enable us to directly probe the binding free energies.

2.5.1 *Model extensions*

Although the simple xanthophyll cycle-based model of NPQ presented here provides a good foundation for understanding the kinetics of NPQ and its changes with fluctuating light, it still clearly has its limitations. For example, currently the model cannot account for changes in light intensity beyond the simple binary fluctuations in light intensity. This could be accounted for by treating the light intensity-dependent rate constants phenomenological modeled, such as

$$k(I(t)) = \frac{k_{\text{light}} - k_{\text{dark}}}{1 + \left(\frac{I(t)}{I_{\text{act}}}\right)^{-n}} + k_{\text{dark}}. \quad (6)$$

which would reduce to the Eq. 1 in the limit that n is large and the activation intensity I_{act} is similar to that used under the HL condition.

An alternative approach would be to incorporate this model with an extended model for the photosynthetic reaction network, which incorporates the variables that would directly affect the light-dependent rate constants, primarily the lumen pH. This approach could also allow the incorporation of feedback effects between the quenching of chlorophyll excitations and the lumen pH (which affects the activation of quenching).

Another potential extension of the minimal model we have employed here is to incorporate more steps in the xanthophyll cycle and the quenching process itself. For example, our model makes no distinction between membrane-bound or protein-bound xanthophylls. This may be particularly important because ZEP is believed to reside in the stroma, whereas VDE is in the thylakoid lumen[30].

Furthermore, in this model we have excluded the A intermediate in the xanthophyll cycle, primarily to simplify the model and reduce the number of free parameters. Work from Arnoux et al. supports this decision as it indicates that V can be directly converted to Z without the A intermediate[31]. However, our preliminary HPLC results reveal that A is present in a significant amount. It may therefore be necessary to incorporate A and PA species into our current model to reconcile the differences between theory and experiment for the time dependence of Z concentration in HL-grown algae.

One aspect not explicitly included in our model is potential restructuring of the PSII light-harvesting complexes. State transitions (transfer of light-harvesting complexes from PSII to PSI) are not thought to occur in *N. oceanica*[16], though they will likely contribute in other species[18]. Detachment of light-harvesting complexes from the PSII reaction center and subsequent quenching as a consequence of aggregation[32,33] may occur, but without time-dependent structural data at the membrane level, incorporation of such a phenomenon in a bottom-up model is not possible.

Additionally, the rapid regular sequences do not allow full recovery between HL periods, which do not fully recovery during the dark periods. This led us to the possibility of longer timescale NPQ effects, which led us to fit the regular and irregular sequence data independently. The consistency of the best fit parameters (Tables 2-1,2-2) within the error bounds, however, give confidence in the overall self-consistency of the model. In developing and refining the model we found that fitting the irregular sequence data provided a more rigorous test of the model than

simply fitting the regular sequence data, due to the larger variability in NPQ response. We therefore suggest that irregular sequences of HL and dark or LL should be key measurements for organisms with more complex rapid photoprotection responses than *N. oceanica*.

2.6 Concluding Comments

The fits in Figures 2-4, 2-5, 2-6 demonstrate that a model containing only the pH-dependent interconversion of V and Z via the actions of enzymes VDE and ZEP together with the formation of a quenching complex, Q, can quantitatively describe the rapid response of *N. oceanica* to various sequences of alternating HL illumination and dark. For the sake of specificity, we associate Q with Z bound to the protonated LHCX1 protein, although our model does not require this. Thus *N. oceanica* appears to have a particularly simple, rapid system to dissipate excess absorbed light. Our model may provide a starting point to understand the more complex responses of land plants, with their additional dissipative pathways.

The hierarchy of timescales from seconds to minutes seen here will certainly be present in organisms with more complex, multi-component photoprotection responses, as these timescales relate to fundamental biochemical processes. In our previous analysis of regular periodic illumination of *A. thaliana* and a range of NPQ mutants, we used a purely mathematical model to fit the data and then drew mechanistic conclusions from the responses of the various mutants in comparison to the wild type[34]. In contrast, the model described here is bottom-up and, therefore, can make much more specific (and quantitative) predictions than our earlier work. Building on the work of Zaks et al.[35] and of Bennett et al.[36], it should be a possible, if complex, undertaking to build on the approach to create a bottom-up model for plant rapidly reversible photoprotection.

2.7 Appendix 1: Further details of model simulation and fitting

The model parameters, θ, are fitted by performing a least-squares fit to the experimental NPQ_τ data. The function that is minimized is the sum of square residuals for the different high-light/dark sequences S,

$$\delta^2(\theta) = \sum_{i=1}^{N_{\text{data}}} \left(\text{NPQ}_\tau^{\text{exp}}(t_i, S_i) - \text{NPQ}_\tau^{\text{model}}(t_i, S_i, \theta)\right)^2 .$$

The covariance matrix of the fitted parameters, from which uncertainties in various model parameters are derived, is obtained from the Jacobian matrix of the residuals,

$$J_{i,n} = \frac{\partial}{\partial \theta_n}\left(\text{NPQ}_\tau^{\text{exp}}(t_i, S_i) - \text{NPQ}_\tau^{\text{model}}(t_i, S_i, \theta)\right).$$

The covariance of any two functions of the parameters, f and g, can be approximated as

$$\Sigma_{f\,g} \approx \frac{\delta^2(\theta)}{N_{\text{data}} - N_\theta} (\nabla_\theta f)^{\mathsf{T}} [\mathbf{J}^{\mathsf{T}}\mathbf{J}]^{-1} (\nabla_\theta g)$$

where N_θ is the number of parameters in the model.

The model kinetic equations are solved using the ode23s solver in Matlab. The optimization is performed using Matlab's fmincon starting from ~300 randomly chosen initial guesses for the parameter set. The models with the lowest least squares fit value are then chosen as the final models

for each dataset. The Jacobian is evaluated using a second order central finite difference scheme with a step size of $\delta\theta_n = 10^{-3}\theta_n$.

2.8 Appendix 2: The sigmoidal growth criterion

Here we take a more mathematical approach to describing the sigmoidal-like growth. We note that the binding and unbinding of P and V occurs very rapidly, which enables us to apply the quasi-equilibrium/pre-equilibrium approximation to this step. With this we can obtain [P], as a function of the other concentrations,

$$[\mathrm{P}] = \frac{[\mathrm{PV}]}{K_{\mathrm{PV}}[\mathrm{V}]} = \frac{[\mathrm{P}]_{\mathrm{tot}} - [\mathrm{PZ}]_{\mathrm{tot}}}{K_{\mathrm{PV}}[\mathrm{V}] + 1}$$

Assuming $K_{\mathrm{PV}}[\mathrm{P}] \ll 1$, and neglecting the back reverse step on the xanthophyll cycle where Z is converted back to V, and assuming the VDE activity adjusts rapidly, we can also obtain [V] as $[\mathrm{V}] = [\mathrm{V}]_0 e^{-t/\tau_{\mathrm{V}}}$, where $\tau_{\mathrm{V}}^{-1} = k_{\mathrm{V}}[\mathrm{VDEa}]^{\mathrm{eq}}_{\mathrm{light}}$.

The kinetic equation for the total concentration of PZ, $[\mathrm{PZ}]_{\mathrm{tot}} = [\mathrm{Q}] + [\mathrm{PZ}]$, rate of assuming the unbinding of Z from PZ is negligible, can then be obtained as

$$\frac{\mathrm{d}}{\mathrm{d}t}[\mathrm{PZ}]_{\mathrm{tot}} \approx \frac{k_{\mathrm{PZ},f}\,[\mathrm{Z}]}{K_{\mathrm{PV}}[\mathrm{V}]_0}\left(\frac{1}{e^{-t/\tau_{\mathrm{V}}} + (K_{\mathrm{PV}}[\mathrm{V}]_0)^{-1}}\right)([\mathrm{P}]_{\mathrm{tot}} - [\mathrm{PZ}]_{\mathrm{tot}})$$

We see that the growth rate of PZ, and thus the NPQ_τ, has a sigmoidal component within these approximations. If the sigmoidal growth time-scale, τ_{V}, is shorter than the timescale on which PZ initially grows, $\tau_{\mathrm{PZ},0} = K_{\mathrm{PV}}[\mathrm{V}]_0/k_{\mathrm{PZ},f}[\mathrm{Z}]_0$ (assuming $K_{\mathrm{PV}}[\mathrm{V}]_0 \gg 1$), then the total concentration of PZ initially grows at an increasing rate. This gives the criterion for sigmoidal-like growth given above.

In order to obtain the sigmoidal-like growth criterion more carefully, we first solve the above kinetic equation. This can be done by assuming $[\mathrm{Z}] \approx [\mathrm{Z}]_0$, and then re-writing the differential equation as

$$\frac{\mathrm{d}y}{\mathrm{d}t} = -\frac{ay}{be^{-t/\tau_{\mathrm{V}}} + 1}$$

with $y = [\mathrm{PZ}]_{\mathrm{tot}} - [\mathrm{P}]_{\mathrm{tot}}$, $a = k_{\mathrm{PZ},f}[\mathrm{Z}]_0$ and $b = K_{\mathrm{PV}}[\mathrm{V}]_0$. This can be solved to give

$$y = y_0\left(\frac{b+1}{b + e^{t/\tau_{\mathrm{V}}}}\right)^{\tau_{\mathrm{V}}a}.$$

Sigmoidal-like growth will be observed when the derivative of this passes through a maximum at $t > 0$. The stationary point on this curve is found to be

$$t^* = \tau_{\mathrm{V}}\ln\left(\frac{b}{\tau_{\mathrm{V}}a}\right) = \tau_{\mathrm{V}}\ln\left(\frac{K_{\mathrm{PV}}[\mathrm{V}]_0}{\tau_{\mathrm{V}}k_{\mathrm{PZ},f}\,[\mathrm{Z}]_0}\right),$$

This time is positive, and sigmoidal-like growth is observed when the inequality in Eq. (5) is satisfied. It should be noted that these approximations do not capture the true kinetics quantitatively, in particular the approximation of constant [Z] is somewhat weak, but these approximations do give insight into the origin of the sigmoidal-like growth in NPQ.

2.9 Appendix 3: Xanthophyll concentration for low light and high light cells for one fluctuating light sequence

The concentration of V in LL-grown *N. oceanica* decreases throughout the first HL-period as it is converted into A and Z, which simultaneously increase in concentration. The [V] stabilizes during the dark period while [Z] decreases more noticeably than [A]. In HL-grown cells, the [V] decrease more rapidly. The [A] and [Z] are also higher in HL-grown cells. Similar to the LL-grown cells, the [Z] is more responsive to the changes in illumination (Figure 2-9).

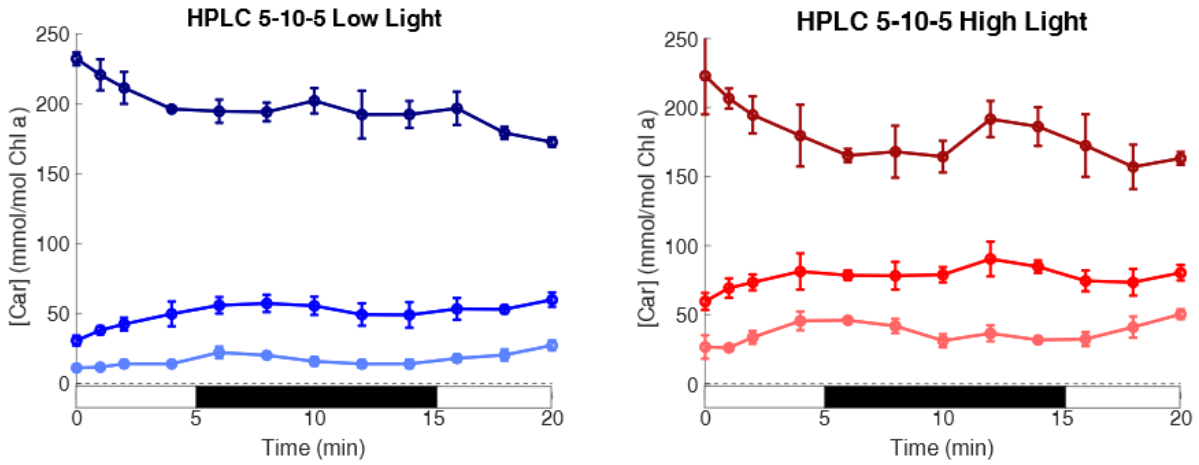

Figure 2-9. Concentration of V, A, Z for LL- (blue shades) and HL-grown (red shades) cells for 5-10-5 fluctuating light sequence. **Left)** [V] (dark blue) decreases through the sequence while [A] (blue) and [Z] (light blue) decrease and increase as a function of HL exposure. **Right)** The trends for V, A, and Z are similar in HL-grown *N. oceanica*. [V] (dark red) is lower while [A] (red) and [Z] (pink) are higher than the concentration in LL-grown plants. 95% confidence intervals are represented by error bars (n=3). The black boxes at the bottom of each plot represent the dark periods while the white boxes represent HL exposure.

As stated in the main text and seen in Appendix 3 Figure 2-1, while there is some amount of Z present before cells are exposed to HL in LL-grown cells, this is not readily available to contribute to quenching mechanisms. Since the model equates [Z(t)] with ΔZ, the initial [Z] available to incorporate was subtracted from [Z] in both the HL and LL-grown cells to produce ΔZ, which is normalized to the total VAZ value. The $[Z]_0$ in LL-grown cells was used to solve for the accessible Z as HL- grown cells have a higher initial [Z] and it appears that at least some is available for NPQ, suggesting a fraction of Z is free in the membrane to rapidly interact with the quenching complex (Figure 2-10).

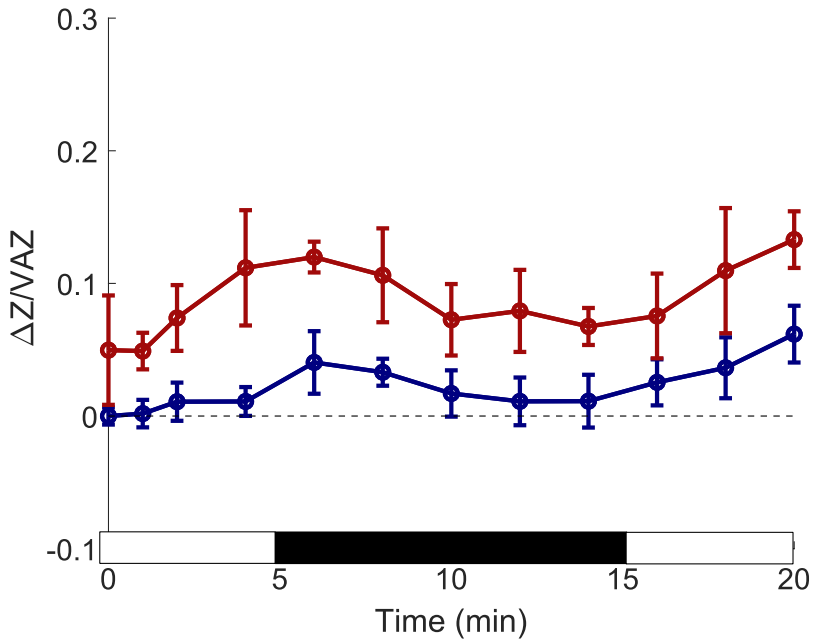

Figure 2-10. ΔZ for LL-grown (blue) and HL-grown (red) normalized by the total VAZ concentration. The initial [Z], taken after 30 minutes of dark adaptation, was subtracted from LL-grown Z values. The initial [Z] for LL-grown cells was also subtracted from the HL-grown [Z].

2.10 References

1. Blankenship, R. E. *Molecular Mechanisms of Photosynthesis*. (John Wiley & Sons, 2021).
2. Eskling, M., Emanuelsson, A. & Åkerlund, H.-E. Regulation of Photosynthesis. *Adv Photosynth Respir* 433–452 (2004) doi:10.1007/0-306-48148-0_25.
3. Demmig-Adams, B. & III, W. W. A. Photoprotection and Other Responses of Plants to High Light Stress. *Annu Rev Plant Phys* **43**, 599–626 (1992).
4. Li, Z., Wakao, S., Fischer, B. B. & Niyogi, K. K. Sensing and Responding to Excess Light. *Annu Rev Plant Biol* **60**, 239–260 (2009).
5. Ruban, A. V. Crops on the fast track for light. *Nature* **541**, 36–37 (2017).
6. Kaiser, E., Morales, A. & Harbinson, J. Fluctuating Light Takes Crop Photosynthesis on a Rollercoaster Ride. *Plant Physiol* **176**, 977–989 (2018).
7. Kulheim, C., Agren, J. & Jansson, S. Rapid Regulation of Light Harvesting and Plant Fitness in the Field. *Science* **297**, (2002).
8. Kromdijk, J. *et al.* Improving photosynthesis and crop productivity by accelerating recovery from photoprotection. *Science* **354**, 857-861 (2016).
9. Ma, Y., Wang, Z., Yu, C., Yin, Y. & Zhou, G. Evaluation of the potential of 9 Nannochloropsis strains for biodiesel production. *Bioresource Technol* **167**, 503–509 (2014).
10. Gouveia, L. & Oliveira, A. C. Microalgae as a raw material for biofuels production. *J Ind Microbiol Biot* **36**, 269–274 (2009).

11. Park, S. *et al.* Chlorophyll–carotenoid excitation energy transfer and charge transfer in *Nannochloropsis oceanica* for the regulation of photosynthesis. *Proc National Acad Sci* **116**, 3385--3390 (2019).
12. Chukhutsina, V. U., Fristedt, R., Morosinotto, T. & Croce, R. Photoprotection strategies of the alga N*annochloropsis gaditana*. *Biochimica Et Biophysica Acta Bba - Bioenergetics* **1858**, 544-552 (2017).
13. Vieler, A. *et al.* Genome, Functional Gene Annotation, and Nuclear Transformation of the Heterokont Oleaginous Alga *Nannochloropsis oceanica* CCMP1779. *Plos Genet* **8**, e1003064 (2012).
14. Litvin, R., Bina, D., Herbstova, M. & Gardian, Z. Architecture of the light-harvesting apparatus of the eustigmatophyte alga *Nannochloropsis oceanica*. *Photosynth Res* **130**, 137--150 (2016).
15. Demmig-Adams, B., Stewart, J. J., López-Pozo, M., Polutchko, S. K. & Adams, W. W. Zeaxanthin, a Molecule for Photoprotection in Many Different Environments. *Molecules* **25**, 5825 (2020).
16. Alboresi, A. *et al.* Conservation of core complex subunits shaped the structure and function of photosystem I in the secondary endosymbiont alga *Nannochloropsis gaditana*. *New Phytol* **213**, 714–726 (2017).
17. Büchel, C. Evolution and function of light harvesting proteins. *J Plant Physiol* **172**, 62–75 (2015).
18. Steen, C. J., Burlacot, A., Short, A. H., Niyogi, K. K. & Fleming, G. R. Interplay between LHCSR proteins and state transitions governs the NPQ response in intact cells of *Chlamydomonas* during light fluctuations. *Biorxiv* 2021.12.31.474662 (2022) doi:10.1101/2021.12.31.474662.
19. Kilian, O., Benemann, C. S. E., Niyogi, K. K. & Vick, B. High-efficiency homologous recombination in the oil-producing alga *Nannochloropsis* sp. *Proc National Acad Sci* **108**, 21265–21269 (2011).
20. Sylak-Glassman, E. J., Zaks, J., Amarnath, K., Leuenberger, M. & Fleming, G. R. Characterizing non-photochemical quenching in leaves through fluorescence lifetime snapshots. *Photosynth Res* **127**, 69--76 (2016).
21. Porra, R. J., Thompson, W. A. & Kriedemann, P. E. Determination of accurate extinction coefficients and simultaneous equations for assaying chlorophylls a and b extracted with four different solvents: verification of the concentration of chlorophyll standards by atomic absorption spectroscopy. *Biochimica Et Biophysica Acta Bba - Bioenergetics* **975**, 384–394 (1989).
22. García-Plazaola, J. I. & Becerril, J. M. A rapid high-performance liquid chromatography method to measure lipophilic antioxidants in stressed plants: simultaneous determination of carotenoids and tocopherols. *Phytochem Analysis* **10**, 307–313 (1999).
23. Zhang, R. & Sharkey, T. D. Photosynthetic electron transport and proton flux under moderate heat stress. *Photosynth Res* **100**, 29–43 (2009).
24. Jahns, P., Latowski, D. & Strzalka, K. Mechanism and regulation of the violaxanthin cycle: The role of antenna proteins and membrane lipids. *Biochimica Et Biophysica Acta Bba - Bioenergetics* **1787**, 3–14 (2009).
25. III, W. W. A., Demmig-Adams, B., Logan, B. A., Barker, D. H. & Osmond, C. B. Rapid changes in xanthophyll cycle-dependent energy dissipation and photosystem II efficiency in

two vines*, Stephania japonica* and *Smilax australis*, growing in the understory of an open Eucalyptus forest. *Plant Cell Environ* **22**, 125–136 (1999).
26. Bugos, R. C., Chang, S.-H. & Yamamoto, H. Y. Developmental Expression of Violaxanthin De-Epoxidase in Leaves of Tobacco Growing under High and Low Light. *Plant Physiol* **121**, 207–214 (1999).
27. Eskling, M. & Åkerlund, H.-E. Changes in the quantities of violaxanthin de-epoxidase, xanthophylls and ascorbate in spinach upon shift from low to high light. *Photosynth Res* **57**, 41–50 (1998).
28. Bratt, C. E., Arvidsson, P.-O., Carlsson, M. & Åkerlund, H.-E. Regulation of violaxanthin de-epoxidase activity by pH and ascorbate concentration. *Photosynth Res* **45**, 169–175 (1995).
29. Meneghesso, A. *et al.* Photoacclimation of photosynthesis in the Eustigmatophycean *Nannochloropsis gaditana*. *Photosynth Res* **129**, 291–305 (2016).
30. Reinhold, C., Niczyporuk, S., Beran, K. C. & Jahns, P. Short-term down-regulation of zeaxanthin epoxidation in *Arabidopsis thaliana* in response to photo-oxidative stress conditions. *Biochimica Et Biophysica Acta Bba - Bioenergetics* **1777**, 462–469 (2008).
31. Arnoux, P., Morosinotto, T., Saga, G., Bassi, R. & Pignol, D. A structural basis for the ph-dependent xanthophyll cycle in *Arabidopsis thaliana*. *Plant Cell* **21**, 2036--2044 (2009).
32. Ruban, A. V. & Saccon, F. Chlorophyll a de-excitation pathways in the LHCII antenna. *J Chem Phys* **156**, 070902 (2022).
33. Horton, P., Ruban, A. V. & Walters, R. G. Regulation of Light Harvesting in Green Plants (Indication by Nonphotochemical Quenching of Chlorophyll Fluorescence). *Plant Physiol* **106**, 415–420 (1994).
34. Steen, C. J., Morris, J. M., Short, A. H., Niyogi, K. K. & Fleming, G. R. Complex Roles of PsbS and Xanthophylls in the Regulation of Nonphotochemical Quenching in *Arabidopsis thaliana* under Fluctuating Light. *J Phys Chem B* **124**, 10311–10325 (2020).
35. Zaks, J., Amarnath, K., Kramer, D. M., Niyogi, K. K. & Fleming, G. R. A kinetic model of rapidly reversible nonphotochemical quenching. *Proc National Acad Sci* **109**, 15757–15762 (2012).
36. Bennett, D. I. G., Fleming, G. R. & Amarnath, K. Energy-dependent quenching adjusts the excitation diffusion length to regulate photosynthetic light harvesting. *Proc National Acad Sci* **115**, 201806597 (2018).

Chapter 3

The Kinetics of a Three-State Xanthophyll Cycle and its Impact on Photoprotective Memory

This chapter is reproduced with permission from

Audrey Short, Thomas P. Fay, Thien Crisanto, Ratul Mangal, Krishna K. Niyogi, David T. Limmer, and Graham R. Fleming

"Kinetics of the xanthophyll cycle and its role in photoprotective memory and response"
Nat. Commun. (2023) 14, 6621
DOI:10.1038/s41467-023-42281-8. Copyright © 2023 Authors

3.1 Abstract

Efficiently balancing photochemistry and photoprotection is crucial for survival and productivity of photosynthetic organisms in the rapidly fluctuating light levels found in natural environments. The ability to respond quickly to sudden changes in light level is clearly advantageous. In the alga Nannochloropsis oceanica we observed an ability to respond rapidly to sudden increases in light level which occur soon after a previous high-light exposure. This ability implies a kind of memory. In this work, we explore the xanthophyll cycle in *N. oceanica* as a short-term photoprotective memory system. By combining snapshot fluorescence lifetime measurements with a biochemistry-based quantitative model, we show that short-term "memory" arises from the xanthophyll cycle. In addition, the model enables us to characterize the relative quenching abilities of the three xanthophyll cycle components. Given the ubiquity of the xanthophyll cycle in photosynthetic organisms the model described here will be of utility in improving our understanding of vascular plant and algal photoprotection with important implications for crop productivity.

3.2 Introduction

In high-intensity light photosynthetic organisms are unable to utilize all available energy for photochemistry. In order to minimize the formation of damaging reactive oxygen species, the excess energy is dissipated as heat through non-photochemical quenching (NPQ) pathways[1,2]. The eustigmatophyte alga *Nannochloropsis oceanica* has a relatively simple NPQ system[3,4] in comparison to vascular land plants. It consists of two main components: a pH-sensing protein, potentially LHCX1, and the xanthophyll cycle. The xanthophyll cycle in *N. oceanica* is a shared feature with higher plants, but this alga lacks additional features like state transitions or pigments like lutein and chlorophyll-*b*[5–7]. This simplistic nature makes *N. oceanica* an ideal model organism for studying the essential components of NPQ.

The xanthophyll cycle in N. oceanica consists of the same de-epoxidation steps, from violaxanthin (V) to antheraxanthin (A) to zeaxanthin (Z), and reverse epoxidation steps, as seen in green algae and plants[6,8]. The enzyme violaxanthin de-epoxidase (VDE), located in the thylakoid lumen, converts V to A to Z upon protonation under high-light (HL) stress. Simultaneously, zeaxanthin epoxidase (ZEP), which is found in the stroma and thought to be constitutively active, reverses the VAZ cycle by epoxidizing Z to A to V[9–11] (Figure 3-1). It is now well-established that the VAZ cycle correlates with activation of energy-dependent quenching, "qE", in both *N. oceanica*[3,4] and more complex organisms[12–14]. The fast activating, pH-dependent quenching, qE, in *N. oceanica* also depends on the protein LHCX1[4]. The mechanism of sensing changes in the thylakoid membrane pH-gradient and whether or not LHCX1 can bind pigments is still under investigation[4,15–19], however the vital role of Z together with a pH-sensing protein in qE is widely achknowledged[8,14]. The accumulation of A and Z has been observed to correlate with an increase in NPQ throughout a diurnal cycle in plants[10,11], and it has been proposed that an additional, slower activating and slow deactivating Z-dependent quenching process also operates in the absence of a pH-gradient sensing protein, termed "qZ"[12,13]. However the precise roles of the three xanthophylls and the kinetics of their interconversion in NPQ is not well understood, which is surprising given the prevalence of this widespread three-state photoprotective system in photosynthetic organisms.

In previous work[20], we utilized a simplified kinetic model of the VAZ cycle that did not include the intermediate A to understand NPQ in *N. oceanica*. Despite this simplification, the model gave useful insights into the time scales of processes involved in NPQ activation, and it could quantitatively predict the quenching response, as well as qualitatively predict changes in V and Z concentrations, in response to a variety of regular and irregular light/dark illumination sequences. However, when exploring how the response changed when the dark period was progressively lengthened, it became clear that *N. oceanica* has short-term "memory" of previous HL exposure which could not be captured by the simplified two-xanthophyll model. This type of memory of previous exposure to stressor events, wherein some organisms remain primed for an extended period to quickly respond to further stress, has been observed for other stressors such as in drought conditions[21]. Various plant species, including *Smilax australis*, *Monstera deliciosa*, *Vinca minor*, and *Vinca major*, have been shown to possess a long-term memory of growth light conditions, which is strongly species dependent. This long-term memory manifests in xanthophyll pool size and composition as well as maximum NPQ levels[8,22], an effect we also found evidence for previously in N. oceanica[20]. It has also been shown that in phytoplankton and algae possessing a simpler two-state xanthophyll cycle, the xanthophylls can act as a long-term memory of growth

light conditions[23–25]. In this work we aim to explore the details of short-term photoprotective memory (operating on time scales $\lesssim$ 1 hour), complementing existing studies on connections between longer-term light exposure memory and the xanthophyll cycle.

We hypothesize that in response to light stress, the VAZ cycle, and the kinetics of the different de-epoxidation/epoxidation steps, may act as a memory of previous HL exposure[26]. Specifically, we propose that the presence of A in a system could keep plants and algae primed to respond to further HL stress, due to the slow rates of transforming A back to V. The role of the partially de-epoxidized xanthophyll A in photoprotection has been difficult to investigate directly, however, work on plants has suggested that both A and Z correlate with NPQ in plants[22,27], but in this work, we also aim to further elucidate its role in photoprotection. Previous work has shown the ratio of the rates from A $\rightarrow$ Z to V $\rightarrow$ A ranges from 4.5–6.3 times faster in various plant species[28–30], and the rate of epoxidation has been measured to be 1.4 times faster for Z than A[11]. However precise measurements of these rates in *N. oceanica* and their functional significance in NPQ and short-term memory of light stress have not been fully explored.

In this work, we aim to fully understand the role of xanthophyll cycle kinetics in photoprotective memory by considering the full VAZ cycle in modeling NPQ, and we show that differential rates of interconversion between the three xanthophylls are responsible for the multiple timescales of photoprotective memory. In a further step towards a comprehensive understanding of NPQ in *N. oceanica*, the full VAZ model allows us to assess the relative quenching abilities of the three xanthophylls in the qE process, estimate the relative abundance of quenchers in the thylakoid membrane, and also quantify the relative contributions of LHCX1-dependent qE quenching and zeaxanthin-dependent qZ quenching in NPQ. In what follows, we start by briefly presenting our expanded model, then show how it accurately describes the HL stress responses of *N. oceanica*, and how it encodes the functional role of the VAZ cycle in photoprotection.

3.3 Methods

3.3.1 *Algal Growth Conditions*

N. oceanica CCMP17796 was obtained from the National Center for Marine Algae and Microbiota (https://ncma.bigelow.org/) and cultivated in F2N medium[40]. Liquid cultures were grown to 2–5 × 10^7 cells/mL in continuous light at a photon flux density of 60 μmol photons $m^{-2}s^{-1}$ at 22 °C or room temperature. The knock-out mutants *vde* and *lhcx1* (Ref. 4) were generated using homologous recombination of a hygromycin resistance cassette, with the addition of Cas9 RNP for *lhcx1*. Further details of how the mutants were generated will be presented in a separate manuscript.

3.3.2 *Time-Correlated Single Photon Counting*

Time-correlated single photon counting results in a histogram of Chl-*a* fluorescence decay, which is then fit to a biexponential decay function yielding an average lifetime ($\bar{\tau}$). Fluorescence lifetime measurements were taken every 15 seconds to capture the change in fluorescence lifetimes as a function of HL exposure. The amplitude-weighted average lifetime of the Chl-a fluorescence decay is converted into a unitless form, like that measured in the conventional pulse-amplitude

modulation technique using the following equation: where $\bar{\tau}(0)$ and $\bar{\tau}(t)$ are the average lifetimes in the dark and at any time point *t*, respectively, during the experiment.

$$\mathrm{NPQ}_{\tau} = \frac{(\bar{\tau}(0) - \bar{\tau}(t))}{\bar{\tau}(t)}$$

An ultrafast Ti:sapphire coherent Mira 900 oscillator was pumped using a diode laser (Coherent Verdi G10, 532 nm). The center wavelength of the oscillator was 808 nm with a full width at half maximum of 9 nm. After frequency doubling the wavelength to 404 nm with a β-barium borate crystal, the beam was split between the sample and a sync photodiode, which was used as a reference for snapshot measurements. Three synchronized shutters controlled the exposure of actinic light and the laser to the sample as well as to the microchannel plate-photomultiplier tube detector (Hamamatsu106 R3809U). The shutters were controlled by a LABVIEW software sequence. The detector was set to 680 nm to measure Chl-a emission. During each snapshot, the laser and detection shutters were opened, allowing an excitation pulse with a power of 1.7 mW to saturate the reaction center for 1 second while the emission was recorded. During HL periods, samples were exposed to white light with an intensity of 885 μmol photons $m^{-2}s^{-1}$ (Leica KL 1500 LCD, peak 648 nm, FWHM 220 nm) by opening the actinic light shutter. The N. oceanica sample was concentrated at 40 μg Chl mL^{-1}. To do this, 1 mL of N. oceanica culture was pelleted for 5 minutes at room temperature at max speed, flash frozen in liquid nitrogen, thawed at room temperature, and broken using FastPrep-24 (MP Biomedicals LLC) at 6.5 m/s for 60 seconds. The pellet was flash-frozen and broken two more times. Chlorophyll was extracted from the broken cells using 1 mL of 80% acetone, and total chlorophyll in the culture was quantified according to Porra et al.[41]. The culture was then concentrated by centrifuging for 5 minutes at room temperature at 3320 g. Samples were dark-acclimated for 30 minutes prior to the experiment and placed in the custom-built sample holder on a sample stage. The LABVIEW sequence was altered for each regular, irregular, and dark duration sequence run to control exposure to light fluctuations. For the NPQτ experiments, three technical replicates were performed for the WT and three for each mutant. Two experimental replicates were performed for the 5 HL-*T* D-5 HL experiments and the training data for the model. Only one experimental replicate was performed for the mutants.

3.3.3 *High-Performance Liquid Chromatography*

Aliquots of *N. oceanica* in F2N media were taken at various time points during several regular and irregular HL/dark duration actinic light sequences. Samples were then flash-frozen in liquid nitrogen. After thawing, the samples were pelleted for 5 minutes at 4°C at maximum speed to reach a cell count of ~45–60 × 10^6. The cells were washed twice with dH2O and pelleted at maximum speed for 5 minutes. The cells were again flash-frozen and thawed at room temperature followed by breaking the cells using FastPrep-24 (MP Biomedicals LLC) at 6.5 m/s for 60 seconds. The bead beating step was repeated once before adding 200 μL of 100% cold acetone. The samples were centrifuged for 10 minutes (maximum speed, 4°C), and the supernatant was filtered (0.2 μm nylon filter) into HPLC vials. The supernatant was separated on a Spherisorb S5 ODS1 4.6- × 250 mm cartridge column (Waters, Milford, MA) at 30°C. Analysis was completed using a modification of García-Plazaola and Becerril[42]. Pigments were extracted with a linear gradient from 14% solvent A (0.1M Tris-HCl pH 8.0 ddH20), 84% (v/v) solvent B (acetonitrile), 2.0% solvent C (methanol) for 15 minutes, to 68% solvent C and 32% solvent D (ethyl acetate) for 33

min, and then to 14% solvent A (0.1M Tris-HCl pH 8.0 ddH2O), 84% (v/v) solvent B (acetonitrile), 2.0% solvent C (methanol) for 19 min. The solvent flow rate was 1.2 mL min^{-1}. Pigments were detected by A445 with reference at 550 nm by a diode array detector. Standard curves were prepared from isolated pigments. The HPLC peaks were normalized to the total Chl-*a* concentration.

3.3.4 *Model Details*

Each step of the model given in Figure 3-1 is treated as an elementary reaction step in the 12 species model. As described in our previous work[20], we cannot determine from these experiments the absolute concentration of VDE, so we replace the VDE species with a dynamical quantity $\alpha_{\mathrm{VDE}}(t)$ representing the activity of VDE at a time *t* relative to its maximum possible value. We also work in a reduced unit system defined for species B by $[\widetilde{\mathrm{B}}] = \tau_{\mathrm{F}}(0)k_{\mathrm{qE}}[\mathrm{B}]$, where $\tau_{\mathrm{F}}(0)$ is the fluorescence lifetime at t = 0. With these reduced variables $\mathrm{NPQ}_{\tau}(t) = \Delta[\widetilde{\mathrm{QV}}](t) + \Delta[\widetilde{\mathrm{QA}}](t) + \Delta[\widetilde{\mathrm{QZ}}](t) + (k_{\mathrm{qZ}}/k_{\mathrm{qE}})\Delta[\tilde{\mathrm{Z}}](t)$, where $\Delta[\mathrm{QX}](t)$ is the change in reduced concentration of QX relative to the t = 0 value, and likewise for $\Delta[\tilde{\mathrm{Z}}](t)$.

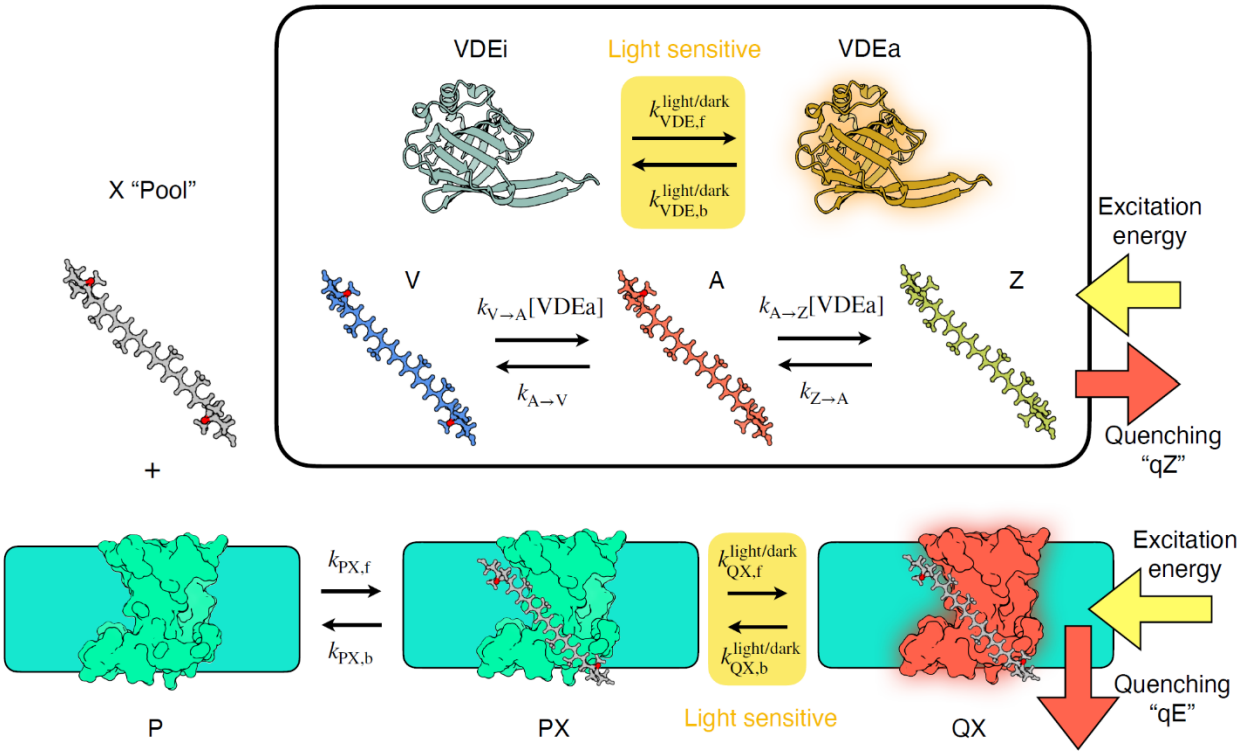

Figure 3-1. Illustration showing the processes included in the xanthophyll cycle-based model. The xanthophyll (X) binds to the protein (P) reversibly to form a protein-xanthophyll complex (PX). In response to light this can convert into an active quencher form (QX). When not bound to the protein, the xanthophylls interconvert between violaxanthin (V), antheraxanthin (A) and zeaxanthin (Z). The activation of the VDE enzyme, which controls the V → A → Z processes, is dependent on light conditions, which alter the ratio of the active VDE enzyme (VDEa) and its inactive from (VDEi). The light-sensitive steps in the model are highlighted in yellow. The species responsible for quenching, the QX complexes in qE and pool Z in qZ, are also indicated by red arrows.

The model parameters were fitted by minimizing the sum of square differences between the model NPQτ and the experimental NPQτ for the 5 HL-9 D-5 HL, 5 HL-15 D-5 HL, 3 HL-1 D-1 HL-3 D-9 HL-3 D, 1 HL-2 D-7 HL-5 D-1 HL-2 D, 2 HL-2 D sequences. Parameters for the VAZ interconversion steps were estimated from a least squares fit of a reduced model, which is a simple first-order kinetic model with activation of the VDE enzyme, to the HPLC data (this is detailed in the SI). In the rest of the parameter fitting these parameters were constrained to only vary by 50%. Additionally, to reduce the number of free parameters, the forward and backward binding rate constants $k_{\mathrm{PX.f}}$ and $k_{\mathrm{PX,b}}$, and the activation rate to form QX, $k_{\mathrm{QX}}^{\mathrm{light/dark}} = k_{\mathrm{QX,f}}^{\mathrm{light/dark}} + k_{\mathrm{QX,b}}^{\mathrm{light/dark}}$, were set to be independent of the species X. This way the equilibrium constant KQX is the only parameter in the model controlling the quenching capacity of each xanthophyll. The remaining parameters were fitted first using Matlab's "globalsearch" function from an initial guess based on our previous model. This was then refined using the "patternsearch" algorithm. Errors in the fitted parameters were estimated by bootstrapping the experimental time series 1000 times. The conversion factor from reduced units to the mmol/mol Chl units the HPLC data are reported in was found using a simple least squares fit between the experimental HPLC and model $\Delta[\mathrm{X}]_{\mathrm{tot}}$ values shown in Figure 3-2. Full details of the model kinetic equations and the full parameter set are given in the SI.

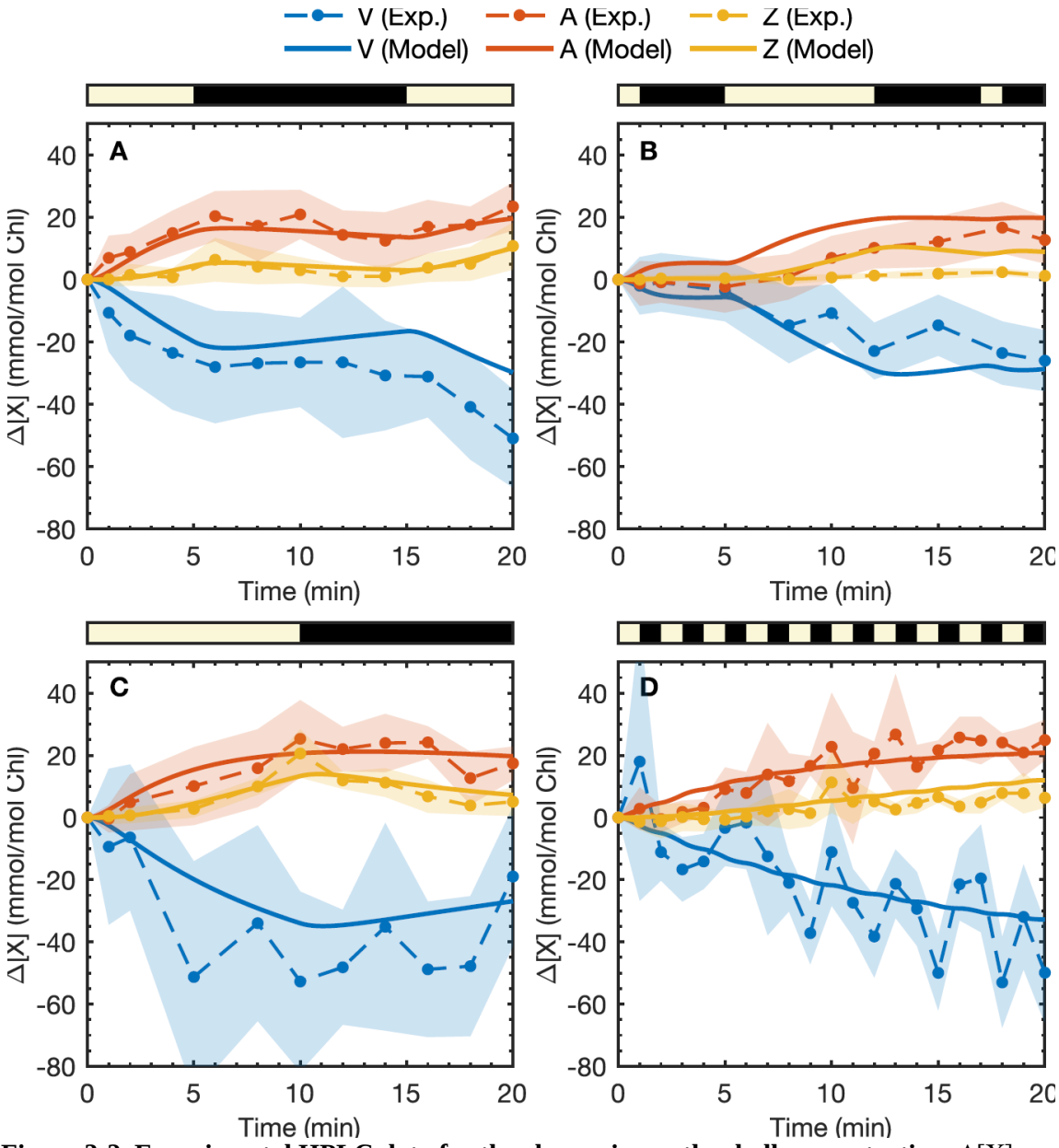

Figure 3-2. Experimental HPLC data for the change in xanthophyll concentration. Δ[X] as a function of time for four HL exposure sequences: **A** 5 HL- 10 D- 5 HL, **B** 1 HL- 4 D- 7 HL- 5 D- 1 HL- 2 D, **C** 10 HL- 10 D, **D** 1 HL-1 D (yellow shaded regions indicate the HL phases). Experimental results are shown as points and model predictions are shown as solid lines. Predictions correspond to the total xanthophyll concentrations, $\Delta[X]_{tot} = \Delta[X] + \Delta[PX] + \Delta[QX]$. Experimental error bars (shaded regions) correspond to two standard errors of the mean (from n = 3 technical replicates). RMSD (root mean square deviations) in the fits are **A** $RMSD_V$ = 11.2, $RMSD_A$ = 8.6, $RMSD_Z$ = 11.5 **B** $RMSD_V$ = 6.8, $RMSD_A$ = 11.5, $RMSD_Z$ = 3.1 **C** $RMSD_V$ = 14.6, $RMSD_A$ = 9.5, $RMSD_Z$ = 8.4, and **D** $RMSD_V$ = 11.7, $RMSD_A$ = 11.6, RMSDZ = 10.7 all in mmol/ mol Chl a.

3.4 Results

3.4.1 *Kinetic model of xanthophyll-mediated photoprotection*

Motivated by measurements of xanthophyll concentrations and NPQ in response to light exposure (as presented in the next section), we have developed a new model for the coupled LHCX1-xanthophyll cycle photoprotection system in *N. oceanica*, as is summarized schematically in Figure 3-1. Before presenting any results, we briefly summarize the features of the model (details of the kinetic equations are given in the SI). In the predecessor to this model[20], we neglected several important features that are included in the new model presented here, such as the intermediate A, which we will show plays an essential role in photoprotective memory, and the capability of each xanthophyll to act as a quencher, facilitated by LHCX1, which will be important for understanding the immediate response of *N. oceanica* to light stress. Furthermore, we will show that the new model can quantitatively describe xanthophyll concentrations in cells, enabling us to estimate the absolute abundance of quenching sites in *N. oceanica* and estimate its absolute quenching rate.

Overall the model involves 12 chemical species: the protein P, the three "pool" xanthophylls X = V, A, and Z, three xanthophyll-bound complexes PX in the non-quenching state and three in the quenching state QX, and the active (protonated) VDEa and inactive (unprotonated) VDEi forms of the VDE enzyme. Within the model, the protein P, binds the xanthophylls, X = V, A, Z, reversibly to form a complex PX. For simplicity, we assume a single labile xanthophyll binding site per P, which we have found is sufficient to interpret the available experimental data. This PX complex is activated under HL conditions to reversibly form an active quencher, establishing the PX⇌QX equilibrium, which we assume arises due to protonation and conformational changes. Previous work has identified LHCX1 as an essential component in activating the protein P, in the "qE" quenching mechanism[4,11,20], although the actual active quencher PX/QX could involve other proteins, especially since it is not known if LHCX1 binds pigments, and alternatively, LHCX1 may just induce the conformational changes in P to activate quenching. Thus the precise identity of PX/QX is open to interpretation. The total fluorescence decay rate $\tau_{\mathrm{F}}(t)^{-1}$ of chlorophylls in the membrane at a given time in the experiment t is assumed to be related linearly to the concentration of the QX species,

$$\frac{1}{\tau_{\mathrm{F}}(t)} = \frac{1}{\tau_{\mathrm{F},0}} + k_{\mathrm{qE}}\big([QV](t) + [QA](t) + [QZ](t)\big) + k_{\mathrm{qZ}}[Z](t),$$

where $1/\tau_{\mathrm{F},0}$ is the intrinsic fluorescence decay rate of chlorophyll (arising from both the dominant non-radiative and minor radiative pathways), and k_{qE} is the quenching rate constant for the QX complexes that mediate the LHCX1 and ΔpH-dependent qE quenching. We also incorporate zeaxanthin-dependent quenching, qZ, into the model by adding a quenching contribution that solely depends on the concentration of zeaxanthin in the "pool". The quenching rate constant for Z is denoted k_{qZ}. We assume that qE and qZ mechanisms are non-radiative, dissipating chlorophyll excitation energy as heat into the environment. From this we can obtain the experimentally measured $\mathrm{NPQ}_{\tau} = (\tau_{\mathrm{F}}(0) - \tau_{\mathrm{F}}(t))/\tau_{\mathrm{F}}(t)$. We assume that whilst the extent to which PX converts to QX under HL conditions is dependent on X, the quenching rate of each complex in the chloroplast is the same. With the available NPQτ data, we found that it is not possible to ascertain whether the differences in total quenching capacity of the different QX species arise due to

differences in quenching rate, or the positions of the PX $\rightleftharpoons$ QX equilibrium under HL conditions. Therefore, for simplicity, we treat the quenching rate k_{qE} as being identical for all QX, and we also assume that the equilibrium constant for this process is zero in the dark.

The interconversion of the xanthophylls is assumed to occur after unbinding of X from P, PX $\rightleftharpoons$ P + X. The X species in the model should be regarded as X in the pool of xanthophylls not bound to P. For example, X could be bound to other light-harvesting proteins from which it can unbind rapidly and reversibly. The xanthophylls in the pool can be de-epoxidized sequentially, from $V \longrightarrow A$ and then $A \longrightarrow Z$, by VDEa, where the maximum turnover rate for the VDE enzyme is different for the two de-epoxidation steps. VDE is assumed to interconvert between VDEa and VDEi forms depending on light conditions. We model this as a simple two-state equilibrium with first-order rate laws for the activation and deactivation. We also treat the epoxidation steps as sequential, first from $Z \longrightarrow A$ then from $A \longrightarrow V$, and we assume that each epoxidation by the ZEP enzyme can be treated as a first-order rate process, with different epoxidation rates for Z and A.

3.4.2 *Dynamical response of xanthophyll concentrations to light stress*

In order to investigate the response of the xanthophyll cycle to fluctuating light conditions, we have measured the changes in concentrations of these pigments in *N. oceanica* in response to four sequences of high-intensity light exposure: 5 HL- 10 D- 5 HL, 1 HL- 4 D- 7 HL- 5 D- 1 HL- 2 D, 10 HL- 10 D, and 1 HL-1 D, where HL denotes high light, D denotes darkness, and numbers indicate the duration of the exposure in minutes. The HPLC data showed a significant fraction of xanthophylls, particularly V, that remained constant over the time scale of the experiment, which we believe corresponds to xanthophylls strongly bound to proteins other than LHCX1. The samples were dark-acclimated for 30 min prior to HL exposure to ensure minimal initial amounts of A and Z. Figure 3-2 shows the change in VAZ cycle carotenoids relative to their initial dark-acclimated values (at t = 0), i.e. $\Delta[\mathrm{X}] = [\mathrm{X}](t) - [\mathrm{X}](0)$ and $[\mathrm{X}](t)$ is the total concentration of X at *t*. The experimental data show that Δ[A] was greater than Δ[Z] during HL exposures; Δ[A] remained relatively constant during dark periods (Figure 3-2), which shows a more rapid dynamical response to reduction in light exposure. In the 5 HL- 10 D- 5 HL sequence (Figure 3-2A), during the 10-minute dark period Δ[Z] decreased almost entirely back to its dark-acclimated value whilst Δ[A] remained constant for the first five minutes of darkness before it began to diminish. Both Δ[A] and Δ[Z] increased in response to the second HL exposure, and the rate of Z accumulation was greater than during the first HL period. Similarly in the 10 HL-10 D sequence (Figure 3-2C), Δ[A] remained at a constant level compared to Δ[Z], which decreased more rapidly back to its dark-acclimated concentration. In the 5 HL- 10 D - 5 HL and 10 HL-10 D sequences, there was a small amount of continued accumulation of A and Z in the first dark phase for ~1 min, indicating a delayed deactivation of the de-epoxidation process, as we found previously in modeling the NPQτ response of *N. oceanica*[20].

Rate constants for xanthophyll interconversion in the model were parameterized based on a reduced form of the full model, fitted to the experimental HPLC data, as detailed in the Supplementary Information (Sec. 2). The full model predictions for the HPLC data are also shown in Figure 3-2, where we see the model mostly predicts the HPLC data within the experimental fluctuations, although in the 1 HL- 4 D- 7 HL- 5 D- 1 HL- 2 D sequence the model slightly overestimates Δ[A] and Δ[Z] after 1 min of light exposure (it should be noted that the fluctuations

in xanthophyll concentrations in Figure 3-2D do not correlate with the periodicity of light exposure on close inspection). In Table 1 we summarize the maximum rates for the de-epoxidation processes, defined as $k_{\mathrm{X}\to\mathrm{X}'}[\mathrm{VDEa}]_{\max}^{\mathrm{light/dark}}$, and the epoxidation rates in the light and dark phases, and the rate constant for activation/deactivation (i.e. formation of VDEa from VDEi). We see that VDE activity increases by a factor of around 1000 in HL conditions, and that the VDE de-epoxidizes A slightly faster than V, although the difference is small. Conversely for the epoxidation we see that Z is epoxidized nearly twice as fast as A. In our model, we find that the VDE enzyme takes just over 1 min to activate and deactivate in both the light and dark phases, which is consistent with the continuing increase in A and Z concentrations observed at the start of the dark phases in the HPLC experiments.

Table 1. Rate constants for xanthophyll interconversion steps for the full VAZ model

Rate Constants (min^{-1})	HL Conditions	Dark Conditions
$k_{\mathrm{V}\to\mathrm{A,max}}$	0.092 ± 0.02	$(9.1 \pm 6.2) \times 10^{-5}$
$k_{\mathrm{A}\to\mathrm{Z,max}}$	0.14 ± 0.05	$(1.4 \pm 1.0) \times 10^{-4}$
$k_{\mathrm{Z}\to\mathrm{A}}$	$(8.5 \pm 3.0) \times 10^{-2}$	$(8.5 \pm 3.0) \times 10^{-2}$
$k_{\mathrm{A}\to\mathrm{V}}$	$(5.1 \pm 2.8) \times 10^{-2}$	$(5.1 \pm 2.8) \times 10^{-2}$
k_{VDE}	1.3 ± 0.8	1.0 ± 0.75

$k_{\mathrm{X}\to\mathrm{X}',\max}$ is defined as $k_{\mathrm{X}\to\mathrm{X}'}[\mathrm{VDEa}]_{\max}^{\mathrm{light/dark}}$, where $[\mathrm{VDEa}]_{\max}^{\mathrm{light/dark}}$ is the maximum concentration of VDEa light/dark conditions. $k_{\mathrm{VDE}} = k_{\mathrm{VDE,f}} + k_{\mathrm{VDE,b}}$ is the rate constant for activation/deactivation of VDE, such that in a light/dark phase [VDEa] changes according to $[\mathrm{VDEa}](t) - [\mathrm{VDEa}](t_0) = ([\mathrm{VDEa}]_{\max} - [\mathrm{VDEa}](t_0))\mathrm{e}^{-k_{\mathrm{VDE}}(t-t_0)}$. Errors given are two standard errors in the mean from bootstrapping.

3.4.3 *Modeling NPQ response of* N. oceanica *to light exposure*

Time-correlated single photon counting (TCSPC) experiments were also performed on *N. oceanica* to measure NPQτ in response to sequences of HL/dark exposure. In addition to 20-minute regular and irregular light sequences that were utilized in previous work[20], seven new HL/dark cycles were utilized to ascertain how long algae retain their "photoprotective memory" of previous HL exposure. The sequences had increasing dark durations (T = 1, 5, 9, 10, 12, 15, 20 min) between two five-minute HL periods. The model was employed to describe NPQτ dynamics of N. oceanica in response to various HL/dark exposure sequences, with parameters determined by fitting a subset of the NPQτ sequences, namely the 5 HL-9 D-5 HL, 5 HL-15 D-5 HL, 3 HL-1 D-1 HL-3 D-9 HL-3 D, 1 HL-2 D-7 HL-5 D-1 HL-2 D, 2 HL-2 D sequences [Figure 3-3C, F, H, J]. Further details of this fitting procedure are given in the Methods section and Supplementary Information (Sec. 1).

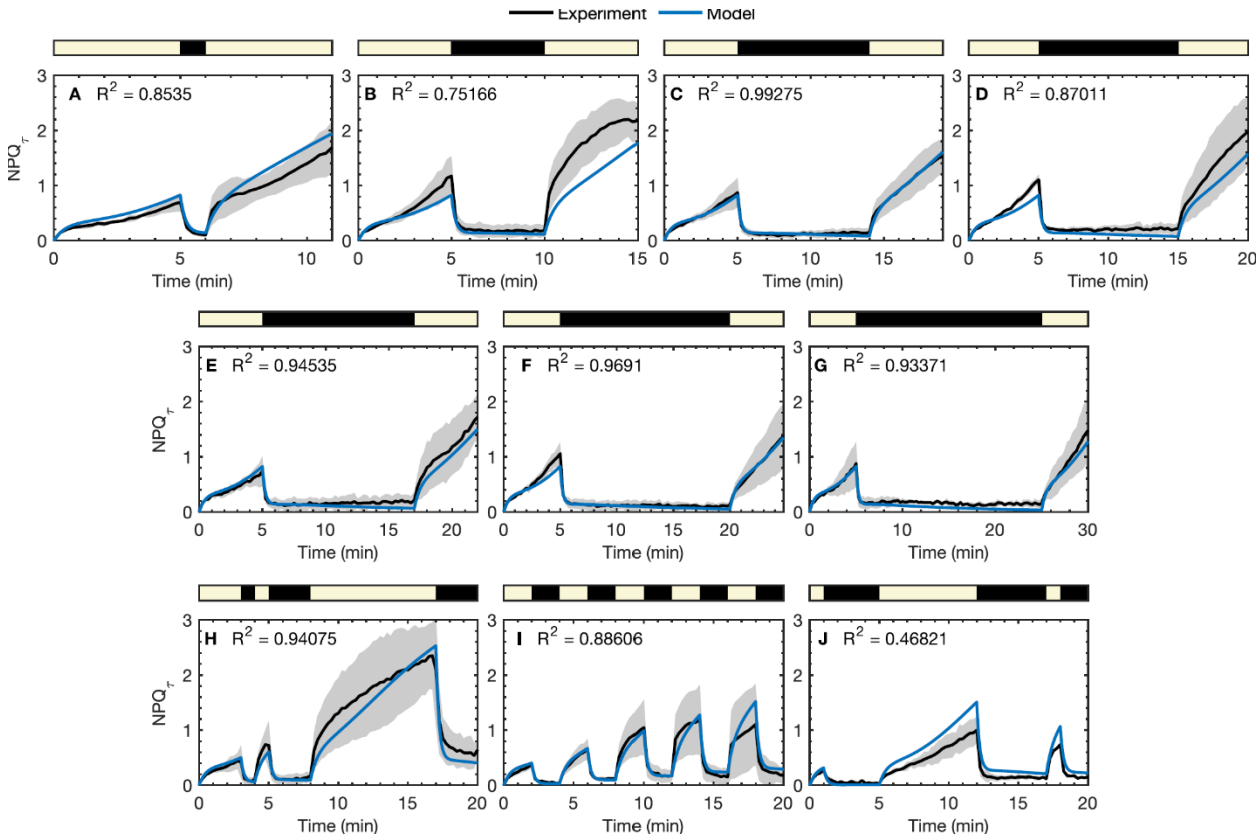

Figure 3-3. Experimental NPQτ data (black) together with the model predictions for the NPQτ (blue) for various sequences of HL exposure/darkness for *N. oceanica*. Yellow regions indicate HL phases of the experiments. Error bars correspond to two standard errors in the NPQτ measurements (from n = 3 technical replicates). **A–G** show data and model predictions for the 5 HL-T D- 5 HL sequences and **H–J** show three additional sequences, where HL denotes HL exposure and D denotes darkness, with number indicating the exposure time in min. RMSD values for the fits are **A** 0.174 (n = 3), **B** 0.370 (n = 3), **C** 0.036 (n = 3), **D** 0.190 (n = 3), **E** 0.099 (n = 3), **F** 0.062 (n = 3), **G** 0.081 (n = 3), **H** 0.185 (n = 3), **I** 0.121 (n = 3), **J** 0.193 (n = 3).

The experimental NPQτ data are shown in Figure 3-3. We see rapid NPQ activation and deactivation in response to changes in light levels, occurring on a timescale of <1 min, together with a slower increase in NPQτ during light exposure. The rapid component of NPQτ activation and deactivation arising from the pH-sensing protein corresponds to the equilibration rate for the PX equilibrium in the model, given by $k_{\mathrm{QX}}^{\mathrm{light/dark}} = k_{\mathrm{QX,f}}^{\mathrm{light/dark}} + k_{\mathrm{QX,b}}^{\mathrm{light/dark}}$. This equilibration rate is 2.1 min^{-1} under light conditions and 4.7 min^{-1} in the dark which gives an activation time of 29 s and a deactivation time of 13 s. Experimental data for the 5 HL-*T* D-5 HL sequences, Figure 3-3A–G, show how NPQτ recovers after various dark durations, directly probing the photoprotective memory of *N. oceanica*. The NPQτ component recovered to its value at the end of the initial light period (t = 5 min) within 1 min upon secondary light exposure when dark durations were up to T = 5 min, and even with a 20 min dark duration, the NPQτ recovered within 3 min.

In addition to the HPLC $\Delta[\mathrm{X}]_{\mathrm{tot}}$ data in Figure 3-2, the model is able to predict the average NPQτ levels for all the sequences as shown in Figure 3-3, including sequences other than those in the training datasets. Differences between the model predictions and experiments were generally

comparable to the variability between experimental runs. For example, at the end of the first five minutes of light exposure, NPQτ in the 5 HL- *T* D- 5 HL sequences (Figure 3-3A–G) the experimental NPQτ varies between around 0.8 and 1.4, although some discrepancies may be attributed to shortcomings of the model. Specifically the over-prediction of NPQτ for the 1 HL-2 D-7 HL-5 D-1 HL-2 D, 2 HL-2 D sequence [Figure 3-3J] in the second light phase could be attributed to VDE activating too fast, as is seen in both the HPLC data and modeling [Figure 3-2B].

In the model, the position of the PX ⇌ QX equilibrium under HL conditions determines how well each of the xanthophylls can act as a quencher in qE. The maximum fraction of P-bound X that can exist in the QX state under HL conditions, denoted q_X, determines the quenching capacity of each xanthophyll within our model. This can be expressed as

$$q_{\mathrm{X}} = \frac{K_{\mathrm{QX}}^{\mathrm{light}}}{1 + K_{\mathrm{QX}}^{\mathrm{light}}}$$

Where $K_{\mathrm{QX}}^{\mathrm{light}}$ is the equilibrium constant for the PX ⇌ QX process under HL conditions determined from fitting the model to the experimental data. In Table 2 we list these values for our model under light and dark conditions, obtained from fitting the model to the experimental NPQτ curves. From the q_{X} values we find that A is approximately three times more effective as a quencher than V, and Z is nearly 10 times more effective than V. From the model we can also quantify the relative contributions of qE and qZ to the overall quenching, by the ratio of k_{qZ} to k_{qE}, which is found to be$k_{\mathrm{qZ}}/k_{\mathrm{qE}} = 0.026 \pm 0.005$.

Table 2. Quenching capacity, q_{X}, for each of the xanthophylls

X	Violaxanthin	Antheraxanthin	Zeaxanthin
q_{X}	0.10 ± 0.02	0.28 ± 0.08	0.92 ± 0.05

Errors given are two standard errors in the mean.

3.4.4 *NPQ in* N. oceanica *mutants*

To further test the model, we have modified the wild type (WT) *N. oceanica* parameterized model to predict the NPQτ response of two *N. oceanica* mutants: the *vde* and *lhcx1* mutants. The NPQτ response of the *vde* mutant, which has VDE knocked out preventing the accumulation of Z, was modeled utilizing parameters obtained from the WT model with $k_{\mathrm{V}\to\mathrm{A}}$ and $k_{\mathrm{A}\to\mathrm{Z}}$ to zero. The NPQτ response was measured for three HL/D sequences, shown in Figure 3-4A–C together with model predictions. Even in the absence of A and Z, NPQτ increases near-instantaneously to around 0.3 in response to light, demonstrating the relevant role of LHCX1 in the *vde* mutant. However, because of V's low quenching capacity, the NPQτ response is significantly smaller than that seen in WT, and there is no steady increase of NPQτ over the duration of the experiment, unlike in the WT *N. oceanica*. The model captures the NPQτ response of the *vde* mutant remarkably well, despite not being parameterized with these data.

We have also modeled the NPQτ response of the *lhcx1* mutant, in which LHCX1 is not expressed and only zeaxanthin-mediated qZ quenching operates. This was modeled by simply setting

$[P]_{tot} = 0$, removing the qE quenching process, while holding the total xanthophyll concentration constant. The experimental NPQτ data and model predictions are shown in Figure 3-4D–F, where we see the model accurately captures the slow rise of NPQτ in the light phases, arising from the build-up of Z during light exposure, and the slower decay in the dark phases due to slow epoxidation of Z. The success of the model in predicting the NPQ response of the *lhcx1* mutant strongly supports the interpretation of the kinetic model species "P" as involving or at least requiring LHCX1 to function.

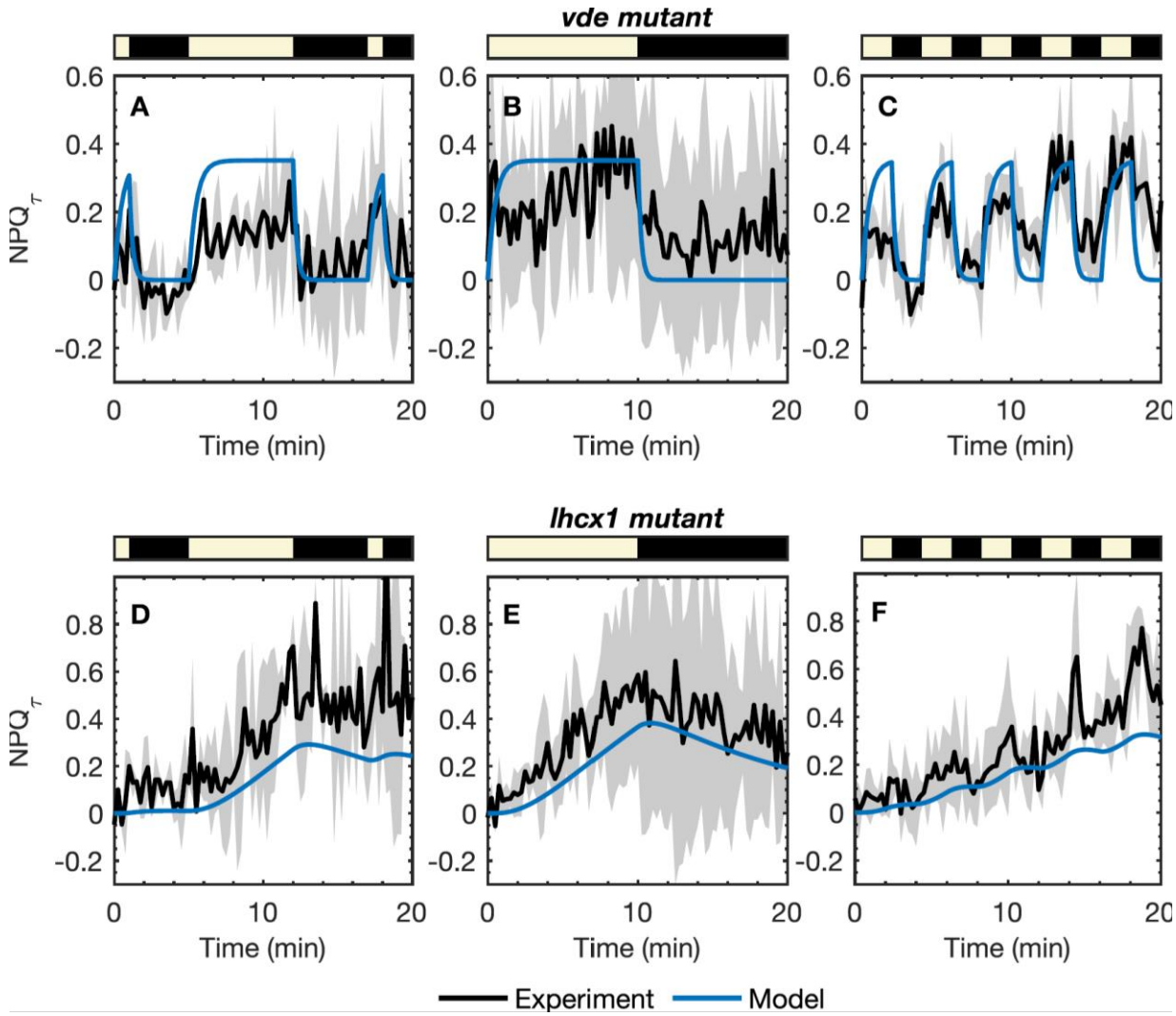

Figure 3-4. NPQτ responses measured for the *vde* mutant (black) together with model predictions (blue) for three sequences of light/dark exposure. Error bars correspond to two standard errors in the NPQτ measurements (from n = 3 technical replicates). Light/dark sequences: A 1 HL-2 D-7 HL-5 D-1 HL-2 D (n = 2), B 10 HL-10 D (n = 2), and C 2 HL-2 D (n = 3) × 5**. D–F** NPQτ responses were measured for the *lhcx1* mutant (black) together with model predictions (blue) for three sequences of light/dark exposure. Light/dark sequences: A 1 HL-2 D-7 HL-5 D-1 HL-2 D (n = 2), B 10 HL- 10 D (n = 3), and C) 2 HL-2 (n = 3) D × 5. RMSD for the model predictions are **A** 0.134, **B** 0.136, **C** 0.118, **D** 0.227, **E** 0.139, **F** 0.142.

3.5 Discussion

Our combined experimental and kinetic model results suggest that photoprotective memory in *N. oceanica* can be explained qualitatively with a simple three-state model. The three-state system should consist of a poor quencher (V), a modest quencher (A), and a good quencher (Z). After a sample has sufficiently accumulated the good quencher, during brief dark/low-light periods, Z remains before being converted back to the modest quencher (A), acting as short-term memory. However, during extended dark durations, Z will be converted almost entirely to A. Whilst A is also converted back to V, the A → V transition occurs at a slower rate such that during another HL exposure occurs, the Z pool can form more rapidly from the reservoir of A. We can also see this dynamic represented in the HPLC data (Figure 3-2). By adding the intermediate step in the VAZ cycle, the model not only more accurately reflects the biochemical processes but also allows for the short-term photoprotective memory, over time scales between 1 min to ~30 min, to be modeled and understood.

From our experiments and modeling, we have also been able to determine the relative quenching capacities of the different xanthophylls. We find that V facilitates a weak but rapid response to changes in HL. The *vde* mutant demonstrates that even without an effective quencher like Z, there is still an NPQτ response to fluctuating light. In very short bursts of HL, V may act as the main quencher where the switch between its roles in photochemistry and photoprotection is determined by the pH gradient, as suggested previously[31].

As the intermediate step in the VAZ cycle, A's role as a potential quencher in qE is often overlooked. With a quenching capacity of around 30%, it is 3.5 times less efficient than Z (95%) at dissipating excess energy. However, it plays a crucial role in photoprotection in facilitating NPQ recovery after long dark durations. In Figure 3-5 we show a breakdown of the NPQτ response predicted by the model for the 5 HL-10 D-5 HL sequence, where we see at short times the main quencher in qE is actually V complexed with LHCX1, with contributions from A emerging at t = 1 min and Z at t = 2 min. After light exposures of more than 2 min, Z functions as the primary quencher, with small, but not insignificant, contributions from V and A. Whilst LHCX1-dependent qE makes the largest contribution to NPQτ, qZ also makes a small contribution, and within the model, this is the sole contributor to the long-lived NPQτ response in the dark. Even for very long-time light exposure, the model predicts that LHCX1-dependent qE dominates over qZ, with qZ making up only ~23% of the total NPQτ in this limit, whilst the LHCX1-Zeaxanthin qE accounts for the majority (~75%) of the limiting NPQτ. It should be noted that this limit is based on extrapolating the model to light exposure times beyond those that we have investigated, which may not be reliable, and we also expect the relative contributions of qE and qZ to depend strongly on species and growth conditions, as has been found in studies of plants[22,32,33]. We have not suggested a microscopic model for the qZ process, although in the SI, Sec. 4, we show how a quenching process depending on some other zeaxanthin binding protein (or protein complex) P' would be consistent with our simple model. Zeaxanthin binding to some other protein could activate qZ by directly quenching excitation energy, potentially via charge transfer, or inducing conformational changes in the protein that promote other quenching mechanisms[34–36].

An essential element of the three-state photoprotective memory system observed in N. oceanica is the kinetics of xanthophyll cycle, which together with the quenching capacities of the xanthophylls creates an effective photoprotective system. Upon the first exposure to light, NPQ activation is

limited by moving through two steps before Z, the primary quencher, is accumulated, where VDE activation and the V → A step (with a half-life of ~7 min) control the initial rate of NPQ activation. Z may still function as a moderate quencher in the dark through qZ, so fast conversion of Z → A by ZEP (half-life ~8 min) in the dark is necessary to facilitate efficient photosynthesis under low-light conditions. The slower kinetics of A → V in the dark (with a half-life ~20 min) enables A to function as a buffer, facilitating rapid NPQ reactivation if light levels fluctuate again to damaging levels. The fast A → Z conversion by VDE on light exposure (with a half-life of ~4 min) also plays an essential role in photoprotective memory by enabling the buffer of A to be rapidly converted to an active quencher. Previous work in plants found the rate of de-epoxidation of A to be about 4 times faster than that of V[28–30], which is a much larger difference compared to the de-epoxidation rates that we have found, with de-epoxidation of A being only about 1.5 times faster than that of V. However, VDE activity is influenced by the thylakoid lumen acidity, availability of ascorbate, and potentially unique species-specific differences, any of which could explain this discrepancy. Furthermore, because VDE is not active in the dark, the relative activity of ZEP on Z and A is far more relevant to photoprotective memory than the relative activity of VDE on V and A. On top of the slower time scale kinetics of the VAZ cycle, which control the maximum quenching capacity of the system, very rapid responses to light fluctuations, on time scales of around 1 min or less, are facilitated by protonation and subsequent conformational changes of the quenching protein which binds the xanthophylls.

From the model, we can directly probe how the total A and Z concentrations vary during the 5 HL-*T* D- 5 HL sequences to demonstrate the functional role of xanthophyll cycle kinetics in photoprotective memory. Here we show in Figure 3-5 the model NPQτ and the total A and Z concentrations normalized by their values at t = 5 min. For very short dark phase (T = 1 min, Figure 3-5B) Z continues to accumulate (due to the finite deactivation time of VDE in our model), acting as short-term light exposure memory and the NPQτ recovers very rapidly upon re-illumination. For intermediate and longer lengths of dark duration (T = 10 min, Figure 3-5C and T = 20 min, Figure 3-5D), the quencher Z decreases but A remains steady, presumably acting as a buffer, and thus as a short-term memory for excess light exposure and facilitating a fast response to HL in the second light phase. In these cases, the NPQτ response in the second HL phase correlates most strongly with the A concentration, and not the Z concentration. In the Supplementary Information, Figure 3-S2, we show the experimental and model NPQτ recovery, averaged over the first minute of HL, in the second light phase for the 5 HL-*T* D- 5 HL sequences, as a function of dark duration *T*. From this we have extracted (see Supplementary Information Sec. 2 for details) an NPQτ memory time scale of ~22 min, which matches the model A → V time scale given by $1/k_{\mathrm{A}\to\mathrm{V}} = 19.9$ min. This strongly suggests that antheraxanthin acts as a short-term memory for light exposure, with the A → V step of the xanthophyll cycle controlling the effective memory time scale. It has previously been observed that xanthophyll composition correlates with photoprotection, long- and medium-term light-exposure memory, and light levels during growth in plants[8,33], phytoplankton[23,24] and algae[25]. We can now however add to this picture that the kinetics of the xanthophyll cycle also plays an important role in short-term photoprotective memory.

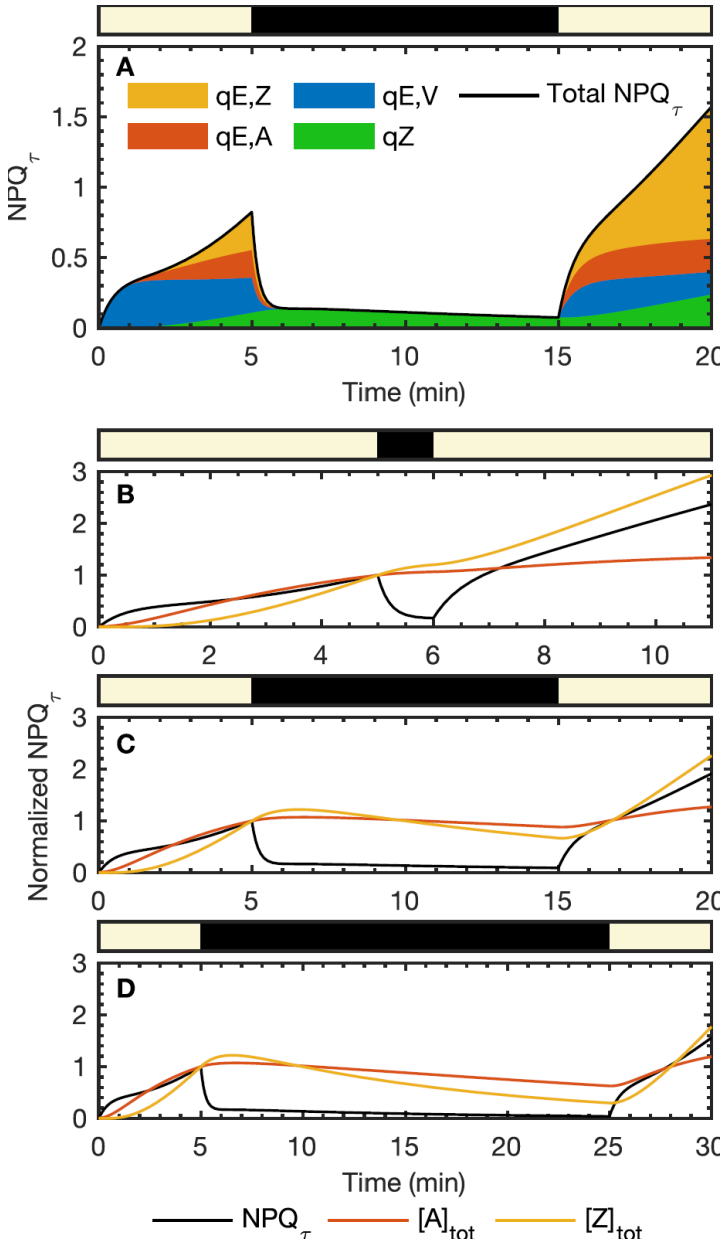

Figure 3-5. Contributions of each xanthophyll to the total NPQτ. A Contributions of each xanthophyll to the total NPQτ as predicted by the model as a function of time for the 5 HL- 10 D-5 HL sequence. **B–D** NPQτ, $[A]_{tot}$ = [A] + [PA] + [QA], and $[Z]_{tot}$ = [Z] + [PZ] + [QZ], predicted by the model for three 5 HL-T D-5 HL sequences of light/dark exposure: **B** T = 1 min, **C** T = 10 min and **D** T = 20 min.

One important quantity we can estimate from this study is the lifetime of Chl-*a* excitations on the active quenching complexes QX. Firstly from the HPLC data and model we obtain an estimate of the total concentration of P (possibly LHCX1 or LHCX1 in a complex with other proteins) in the system as ~0.6 mmol/mol Chl. Assuming roughly ten Chl-*a* molecules per light-harvesting protein, this means the species P makes up ~1 in 30 light-harvesting proteins in *N. oceanica*. Using this ratio of P to the other light-harvesting proteins and assuming excitation energy diffusion between proteins is faster than quenching, we can estimate the lifetime of Chl-*a** on the active quenchers

to be less than ~10 ps (further details of this calculation are given in the SI, Sec. 4). This approximate time scale is roughly consistent with the quenching time scale in HL acclimated *N. oceanica* observed in transient-absorption experiments of ~8 ps[4] (especially given the simplifying assumptions we use to deduce our estimate). Recent work has suggested that quenching can be limited by excitation energy redistribution within and between light-harvesting proteins[35,37,38], so the actual quenching process (likely either excitation energy transfer or charge transfer quenching[4]) may need to occur on an even shorter time scale than this estimate.

Overall in this work, we have presented a model of xanthophyll cycle mediated non-photochemical quenching in *N. oceanica*, which can both accurately describe the short and intermediate timescale NPQτ responses of N. oceanica to HL stress and the accompanying changes in xanthophyll concentrations. Employing a combination of experiments and modeling we have developed a deeper understanding of the photoprotective roles of the xanthophylls together with LHCX1. From this, we have suggested a three-state model for short time scale photoprotection in *N. oceanica*, where the zeaxanthin-LHCX1 system acts as the primary quencher, with antheraxanthin acting as a short-term "memory" of HL stress capable of facilitating rapid response to fluctuations in light levels, and V deactivating quenching under low-light conditions. This adds to the established picture of xanthophyll composition correlating with long-term memory of light-exposure[22]. Although we cannot conclusively identify the qE quencher, PX/QX, we can say that LHCX1 is an essential component of this system. We have also been able to estimate the chlorophyll excitation lifetime on active quenching proteins as less than ~10 ps, as well as the relative abundance of quenchers in the thylakoid membrane. Evidence for zeaxanthin-dependent but LHCX1-independent "qZ" quenching has also been found, although its contribution to NPQ appears to be much smaller than that of LHCX1-dependent "qE" quenching. However, the proportion of qE or qZ contributions is going to vary depending on the species[39]. In order to implement a similar model of NPQ for use in vascular plants, more components need to be incorporated such as quenching due to lutein and state transitions[5–7], which are not present in N. oceanica. However, we believe the model presented here provides a basis for building a quantitative model of NPQ responses for plants and other photosynthetic organisms, which are mediated by the same xanthophyll cycle.

3.6 Supplementary Information

I. Further Model Details

The kinetic scheme for our VAZ cycle based model of non photochemical quenching in Nanno is given explicitly here

$$\mathrm{P} + \mathrm{V} \underset{k_{\mathrm{PV,b}}}{\overset{k_{\mathrm{PV,f}}}{\rightleftharpoons}} \mathrm{PV} \underset{k_{\mathrm{QV,b}}^{\mathrm{light/dark}}}{\overset{k_{\mathrm{QV,f}}^{\mathrm{light/dark}}}{\rightleftharpoons}} \mathrm{QV} \tag{1}$$

$$\mathrm{P} + \mathrm{A} \underset{k_{\mathrm{PA,b}}}{\overset{k_{\mathrm{PA,f}}}{\rightleftharpoons}} \mathrm{PV} \underset{k_{\mathrm{QA,b}}^{\mathrm{light/dark}}}{\overset{k_{\mathrm{QA,f}}^{\mathrm{light/dark}}}{\rightleftharpoons}} \mathrm{QA} \tag{2}$$

$$\mathrm{P} + \mathrm{Z} \underset{k_{\mathrm{PZ,b}}}{\overset{k_{\mathrm{PZ,f}}}{\rightleftharpoons}} \mathrm{PV} \underset{k_{\mathrm{QZ,b}}^{\mathrm{light/dark}}}{\overset{k_{\mathrm{QZ,f}}^{\mathrm{light/dark}}}{\rightleftharpoons}} \mathrm{QZ} \tag{3}$$

$$\mathrm{V} + \mathrm{VDEa} \underset{k_{\mathrm{A}\to\mathrm{V}}}{\overset{k_{\mathrm{V}\to\mathrm{A}}}{\rightleftharpoons}} \mathrm{A} + \mathrm{VDEa} \underset{k_{\mathrm{Z}\to\mathrm{A}}}{\overset{k_{\mathrm{A}\to\mathrm{Z}}}{\rightleftharpoons}} \mathrm{Z} + \mathrm{VDEa} \tag{4}$$

$$\mathrm{VDEi} \underset{k_{\mathrm{VDE,b}}^{\mathrm{light/dark}}}{\overset{k_{\mathrm{VDE,f}}^{\mathrm{light/dark}}}{\rightleftharpoons}} \mathrm{VDEa}. \tag{5}$$

Each step is treated as an elementary rate process in constructing kinetic equations for the chemical species. The full set of kinetic equations is therefore

$$\frac{\mathrm{d}}{\mathrm{d}t}[\mathrm{X}] = -k_{\mathrm{PX,F,eff}}[\mathrm{X}][\mathrm{P}] + k_{\mathrm{PX,b}}[\mathrm{PX}], \text{for } \mathrm{X} = \mathrm{V}, \mathrm{A}, \mathrm{Z} \tag{6}$$

$$\frac{\mathrm{d}}{\mathrm{d}t}[\mathrm{PX}] = k_{\mathrm{PX,F,eff}}[\mathrm{X}][\mathrm{P}] - k_{\mathrm{PX,b}}[\mathrm{PX}] - k_{\mathrm{QX,F,eff}}^{\frac{\mathrm{light}}{\mathrm{dark}}}[\mathrm{PX}] + k_{\mathrm{QX,b}}^{\frac{\mathrm{light}}{\mathrm{dark}}}[\mathrm{QX}], \text{for } \mathrm{X} = \mathrm{V}, \mathrm{A}, \mathrm{Z} \tag{7}$$

$$\frac{\mathrm{d}}{\mathrm{d}t}[\mathrm{QX}] = k_{\mathrm{QX,F,eff}}^{\frac{\mathrm{light}}{\mathrm{dark}}}[\mathrm{PX}] - k_{\mathrm{QX,b}}^{\frac{\mathrm{light}}{\mathrm{dark}}}[\mathrm{QX}], \text{for } \mathrm{X} = \mathrm{V}, \mathrm{A}, \mathrm{Z} \tag{8}$$

$$\frac{\mathrm{d}}{\mathrm{d}t}[\mathrm{P}] = -\sum_{\mathrm{X=V,A,Z}} k_{\mathrm{PX,F,eff}}[\mathrm{X}][\mathrm{P}] + \sum_{\mathrm{X=V,A,Z}} k_{\mathrm{PX,b}}[\mathrm{PX}] \tag{9}$$

$$\frac{\mathrm{d}}{\mathrm{d}t}[\mathrm{V}] = -k_{\mathrm{V}\to\mathrm{A}}[\mathrm{VDEa}][\mathrm{V}] + k_{\mathrm{A}\to\mathrm{V}}[\mathrm{A}] \tag{10}$$

$$\frac{\mathrm{d}}{\mathrm{d}t}[\mathrm{A}] = k_{\mathrm{V}\to\mathrm{A}}[\mathrm{VDEa}][\mathrm{V}] - k_{\mathrm{A}\to\mathrm{V}}[\mathrm{A}] - k_{\mathrm{A}\to\mathrm{Z}}[\mathrm{VDEa}][\mathrm{A}] + k_{\mathrm{Z}\to\mathrm{A}}[\mathrm{Z}] \tag{11}$$

$$\frac{\mathrm{d}}{\mathrm{d}t}[\mathrm{Z}] = k_{\mathrm{A}\to\mathrm{Z}}[\mathrm{VDEa}][\mathrm{A}] + k_{\mathrm{Z}\to\mathrm{A}}[\mathrm{Z}] \tag{12}$$

$$\frac{\mathrm{d}}{\mathrm{d}t}[\mathrm{VDEa}] = -\frac{\mathrm{d}}{\mathrm{d}t}[\mathrm{VDEi}] = k_{\mathrm{VDE,F,eff}}^{\frac{\mathrm{light}}{\mathrm{dark}}}[\mathrm{VDEi}] - k_{\mathrm{VDE,b}}^{\frac{\mathrm{light}}{\mathrm{dark}}}[\mathrm{VDEa}] \tag{13}$$

The light/dark labeled rate constants take different values depending on the light conditions at a time t in a given sequence of HL/D exposures i.e.

$$k^{\frac{\mathrm{light}}{\mathrm{dark}}} \equiv k^{\frac{\mathrm{light}}{\mathrm{dark}}}(t) = \begin{cases} k^{\mathrm{light}}, \text{if HL at time } t \\ k^{\mathrm{dark}}, \text{if D at time } t. \end{cases} \tag{14}$$

There is some parametric redundancy in fitting the model to NPQτ and HPLC data, specifically the model is independent of scaling $[\mathrm{VDE}]_{\mathrm{tot}} \to \gamma[\mathrm{VDE}]_{\mathrm{tot}}, k_{\mathrm{V}\to\mathrm{A}} \to (1/\gamma)k_{\mathrm{V}\to\mathrm{A}}$ and $k_{\mathrm{A}\to\mathrm{Z}} \to (1/\gamma)k_{\mathrm{A}\to\mathrm{Z}}$. As such we only work explicitly with the activity of VDE as a dynamical variable,

$$\alpha_{\mathrm{VDE}}(t) = \frac{[\mathrm{VDEa}]}{[\mathrm{VDEa}]_{\mathrm{eq}}^{\mathrm{light}}}, \tag{15}$$

2here $[\mathrm{VDEa}]_{\mathrm{eq}}^{\mathrm{light}}$ is the equilibrium concentration of VDEa under light conditions, and we fit the maximum de-epoxidation rates, $k_{\mathrm{V}\to\mathrm{A,max}} = k_{\mathrm{V}\to\mathrm{A}}[\mathrm{VDEa}]_{\mathrm{eq}}^{\mathrm{light}}$ and $k_{\mathrm{A}\to\mathrm{Z,max}} = k_{\mathrm{A}\to\mathrm{Z}}[\mathrm{VDEa}]_{\mathrm{eq}}^{\mathrm{light}}$, and the response rate $k_{\mathrm{VDE}}^{\frac{\mathrm{light}}{\mathrm{dark}}} = k_{\mathrm{VDE,f}}^{\frac{\mathrm{light}}{\mathrm{dark}}} + k_{\mathrm{VDE,b}}^{\frac{\mathrm{light}}{\mathrm{dark}}}$. Overall the equation for $\alpha_{\mathrm{VDE}}(t)$ is

$$\frac{\mathrm{d}}{\mathrm{d}t}\alpha_{\mathrm{VDE}}(t) = k_{\mathrm{VDE,eq}}^{\frac{\mathrm{light}}{\mathrm{dark}}} - k_{\mathrm{VDE,eq}}^{\frac{\mathrm{light}}{\mathrm{dark}}}\left(\alpha_{\mathrm{VDE}}(t) - \alpha_{\mathrm{VDE,eq}}^{\frac{\mathrm{light}}{\mathrm{dark}}}\right) \tag{16}$$

where $\alpha_{\mathrm{VDE,eq}}^{\mathrm{light}} = 1$ and $\alpha_{\mathrm{VDE,eq}}^{\mathrm{dark}} = [\mathrm{VDEa}]_{\mathrm{eq}}^{\mathrm{dark}}/[\mathrm{VDEa}]_{\mathrm{eq}}^{\mathrm{light}}$.

As stated in the methods section, we work in reduced variables given by $\left[\widetilde{\mathrm{B}}\right] = \tau_F(0)k_{\mathrm{qE}}[\mathrm{B}]$, where $\tau_F(0)$ is the fluorescence lifetime at $t = 0$ and k_{qE} is the quenching rate associated with the QX species. With this total NPQτ is given by

$$\mathrm{NPQ}_\tau(t) = \frac{\tau_F(0) - \tau_F(t)}{\tau_F(t)} = \tau_F(0)(\tau_F(t)^{-1} - \tau_F(0)^{-1}) \tag{17}$$

$$\mathrm{NPQ}_\tau(t) = \tau_F(0)k_{\mathrm{qE}}\left(\Delta[\mathrm{QV}](t) + \Delta[\mathrm{QA}](t) + \Delta[\mathrm{QZ}](t) + \frac{k_{\mathrm{qZ}}}{k_{\mathrm{qE}}}\Delta[\mathrm{Z}](t)\right) \tag{18}$$

$$\mathrm{NPQ}_\tau(t) = \Delta\left[\widetilde{\mathrm{QV}}\right](t) + \Delta\left[\widetilde{\mathrm{QA}}\right](t) + \Delta\left[\widetilde{\mathrm{QZ}}\right](t) + \frac{k_{\mathrm{qZ}}}{k_{\mathrm{qE}}}\Delta[\tilde{\mathrm{Z}}](t) \tag{19}$$

In order the model the Vde mutant NPQτ we account for the fact that the model predicts different fluorescence lifetimes for the WT and *vde* mutant,

$$\mathrm{NPQ}_\tau^{vde}(t) = \frac{1}{1 - \left[\widetilde{\mathrm{QV}}\right]^{vde}(0) + \sum_{\mathrm{X}}\left[\widetilde{\mathrm{QX}}\right]^{\mathrm{WT}}(0) + \left(k_{\mathrm{qZ}}/k_{\mathrm{qE}}\right)[\tilde{\mathrm{Z}}]^{\mathrm{WT}}(0)}\Delta\left[\widetilde{\mathrm{QV}}\right]^{vde}(t). \tag{20}$$

We find the correction factor to be almost exactly 1 (1.000006), which agrees with the very similar fluorescence lifetimes of *vde* and WT species in the initial dark period of the experiments.

In fitting the model parameters we set the rate constants for the P+X binding and unbinding to be independent of the xanthophyll, and we also set the $k_{\mathrm{QX}}^{\mathrm{light/dark}} = k_{\mathrm{QX,f}}^{\mathrm{light/dark}} + k_{\mathrm{QX,b}}^{\mathrm{light/dark}}$ to be the same for all three xanthophylls. This reduces the number of free parameters and ensures that the only parameter controlling the efficacy of the xanthophylls as quencher is the equilibrium constant

for the PX ⇌ QX of a given xanthophyll. The parameters treated explicitly as free parameters are those given in Table I. The kinetic equations for the model were solved using the "ode23s" solver in Matlab. Model parameters were fit to minimize the least squares difference between the model and experimental NPQτ

$$\mathcal{L} = \sum_{s,i} \left(NPQ_{\tau}^{\text{model}}(t_i; s) - \text{NPQ}_{\tau}^{\text{exp}}(t_i; s) \right)^2 \tag{21}$$

Where *s* labels the sequences used in the fitting procedure: the 5 HL- 9 D- 5 HL, 5 HL- 15 D- 5 HL, 3 HL- 1 D- 1 HL- 3 D- 9 HL- 3 D, 1 HL- 2 D- 7 HL- 5 D- 1 HL- 2 D, 2 HL- 2 D sequences. The parameters were fitted first using Matlab's "global search" function from an initial guess based on our previous model and HPLC data fits (described below). This was then refined using the "patternsearch" algorithm. Errors in the fitted parameters were estimated by bootstrapping the experimental data 1000 times and all reported errors are two standard deviations in the mean of the bootstrapped parameter distributions.

II. Reduced Model for HPLC Data

In order to obtain first estimates of the xanthophyll epoxidation/de-epoxidation rates, we fitted the HPLC data directly to a reduced version of the full. We obtain this reduced model by assuming the binding/unbinding time-scales and PX ⇌ QX time-scales are fast compared to the xanthophyll interconversion. With this we can invoke a quasi-equilibrium approximation for the P,X,PX and QX species.

$$[\text{QX}] \approx K_{\text{QX}}^{\frac{\text{light}}{\text{dark}}} [\text{PX}] \tag{22}$$

$$[\text{PX}] \approx K_{\text{PX}} [\text{P}][\text{X}]. \tag{23}$$

With this we find the pool X concentration is

$$[\text{X}] \approx \frac{1}{1 + K_{\text{PX,eff}}[\text{P}]} [\text{X}]_{\text{tot}} \tag{24}$$

$$K_{\text{PX,eff}} = \left(1 + K_{\text{QX}}^{\frac{\text{light}}{\text{dark}}} \right) K_{\text{PX}}, \tag{25}$$

And therefore the rate of xanthophyll interconversion is given by

$$\frac{\text{d}}{\text{d}t}[\text{V}]_{\text{tot}} = -\alpha_{\text{VDE}}(t) \frac{k_{V \to A,max}}{1 + K_{\text{PV,eff}}[\text{P}]} [\text{V}]_{\text{tot}} + \frac{k_{A \to V}}{1 + K_{\text{PA,eff}}[\text{P}]} [\text{A}]_{\text{tot}} \tag{26}$$

$$\frac{\text{d}}{\text{d}t}[\text{V}]_{\text{tot}} = \alpha_{\text{VDE}}(t) \frac{k_{\text{V} \to \text{A,max}}}{1 + K_{\text{PV,eff}}[\text{P}]} [\text{V}]_{\text{tot}} + \frac{k_{\text{A} \to \text{V}}}{1 + K_{\text{PA,eff}}[\text{P}]} [\text{A}]_{\text{tot}} - \alpha_{\text{VDE}}(t) \frac{k_{\text{A} \to \text{Z,max}}}{1 + K_{\text{PA,eff}}[\text{P}]} [\text{A}]_{\text{tot}} + \frac{k_{\text{Z} \to \text{A}}}{1 + K_{\text{PZ,eff}}[\text{P}]} [\text{Z}]_{\text{tot}} \tag{27}$$

$$\frac{\text{d}}{\text{d}t}[\text{Z}]_{\text{tot}} = \alpha_{\text{VDE}}(t) \frac{k_{\text{A} \to \text{Z,max}}}{1 + K_{\text{PA,eff}}[\text{P}]} [\text{A}]_{\text{tot}} + \frac{k_{\text{Z} \to \text{A}}}{1 + K_{\text{PZ,eff}}[\text{P}]} [\text{Z}]_{\text{tot}}. \tag{28}$$

Because the "pool" xanthophylls are in excess [P] is very small so it can be treated as being in steady state, so we assume that $K_{PX}[P]$ can be treated as constant. This means estimates of the xanthophyll interconversion rates can be obtained using a first order kinetic model with light-phase dependent rate constants, and the VDE activation as treated in the full model.

III. Model Parameters

The final set of fitted model parameters are given in Table I, obtained from least squares fitting of a subset of the NPQτdata with xanthophyll interconversion rate constants constrained to be within 50% of values obtained from the reduced model fitting. The reduced model fitting produced rate constants of $k_{V\to A,max} = 0.1307\ \text{min}^{-1}, k_{A\to Z,max} = 0.1245\ \text{min}^{-1}, k_{A\to V,max} = 0.0458\ \text{min}^{-1}, \alpha_{VDE,eq}^{dark} = 0.0013, k_{VDE}^{light} = 1.285\ \text{min}^{-1}$, and $k_{VDE}^{dark} = 1.019\ \text{min}^{-1}$.

In comparing the model HPLC data to the experimental HPLC data, we found a scaling constant of 0.98 mmol/mol Chl between the reduced units of the model and the concentration relative the Chl by least squares fitting the full model HPLC predictions to the experimental values. From this we can estimate the total concentration of LHCX1 (P in the model) to be about 3.5 mmol/mol Chl.

Table 3-S1. Best fit parameters obtained for the full model. Confidence intervals obtained by bootstrapping experimental NPQ runs and estimating 95% confidence intervals from the approximate parameter distribution. All parameters are given in reduced units of the model, therefore all rate constants are in min^{-1} and all other parameters are unitless.

Parameter	Value	Lower Bound (95% CI)	Upper Bound (95% CI)
$k_{A\to Z,max}$	0.1361	0.0935	0.1951
$k_{V\to A,max}$	0.0918	0.0688	0.1181
$k_{Z\to A}$	0.0854	0.0832	0.1414
$k_{A\to V}$	0.0509	0.0307	0.0685
k_{VDE}^{light}	1.2846	1.1954	1.2962
k_{VDE}^{dark}	1.0193	0.5732	76.4352
$\alpha_{VDE,eq}^{dark}$	0.001	0.0009	0.0019
$k_{PV,b}$	3.4187	1.6648	10.8108
$k_{PA,b}$	3.4187	1.6648	10.8108
$k_{PZ,b}$	3.4187	1.6648	10.8108
k_{QZ}^{light}	2.0744	1.9304	2.3957
k_{QZ}^{dark}	4.6913	4.3656	8.3424
K_{PV}	0.24	0.2079	1623.424
K_{PA}	0.24	0.2079	1623.424
K_{PZ}	0.24	0.2079	1623.424
K_{QZ}^{light}	10.9158	3.4519	14.5586
K_{QZ}^{dark}	0	--	--
$[\tilde{V}]_0$	67.9332	67.6284	69.1663
$[\tilde{P}]_{tot}$	3.5324	3.5245	3.5326

K_{QA}^{light}	0.3872	0.0353	0.5163
K_{QA}^{dark}	0	--	--
k_{QA}^{light}	2.0744	1.9304	2.3957
k_{QA}^{dark}	4.6913	4.3656	8.3424
K_{QV}^{light}	0.1173	0.0879	0.1175
K_{QV}^{dark}	0	--	--
k_{QV}^{light}	2.0744	1.9304	2.3957
k_{QV}^{dark}	4.6913	4.3656	8.3424
k_{qZ}/k_{qE}	0.0259	0.0234	0.0343

IV. Mechanism of qZ

In our model we treat the qZ quenching process as an additional first order quenching process just proportional to the concentration of "pool" Zeaxanthin. We can arrive at this model using a simple model similar to our LHCX1 based quenching model. We consider adding a second protein or complex to our model denoted P′, which binds xanthophylls to form complexes PX′ =PV′, PA′, PZ′. We assume the quenching of chlorophyll excitations is proportional to the concentration of PZ′, such that the change in fluorescence decay rate is $\Delta k_{F,qZ} = k_{Q,PZ'}[PZ']$. Assuming that P' binding X can be treated with the pre-equilibrium/quasi-equilibrium approximation, we find that

$$[PX'] = \frac{K_{PX'[P]}[X]_{pool}}{K_{PX'}[P]+1}. \quad (29)$$

Where $[X]_{pool}$ is the xanthophyll concentration in the pool including the bound to P', and K_{PX} is the equilibrium constant for P' binding X. Assuming that P' is in a steady state, where $\frac{d}{dt}[P](t) \approx 0$, and thus $[P](t) \approx [P]_0$, the change in quenching rate due to qZ is simply proportional to $[Z]_{pool}$, as is assumed in the model.

V. Estimating Quenching Rates

We can construct a simple model for excitation quenching as follows. We assume that the excited chlorophylls, Chl*, can exist either on an active quenching complex, QX, which we label Chl_Q^*, or on the other light-harvesting complexes, which we label Chl_{Pool}^*. We treat the population of Chl* in these two environment with a simple first order kinetic model, with a diffusion rate onto QX of $\eta_Q k_D$ and a diffusion rate off the QX site given by k_D. η_Q is the ratio of the number of Chl on QX to the number of Chl in the whole system, which we estimate to be approximately the ratio of QX to the all of the light harvesting proteins. We further assume that the rate of decay of the Chl* down to its ground state is dependent on the site, occurring at a rate $k_{F,eff,0}$ (Chl* decay is dominated by non-radiative decay, but this rate constant should be understood as including a small radiative contribution) in the pool and at a rate $k_{F,eff,Q}$ on the quenching sites. Putting these ingredients together we arrive at the following kinetic equations for Chl_Q^* and Chl_{Pool}^*

$$\frac{\mathrm{d}}{\mathrm{d}t}\left[\mathrm{Chl}_{\mathrm{Q}}^{*}\right] = -\left(k_{\mathrm{F,eff,Q}} + k_{\mathrm{D}}\right)\left[\mathrm{Chl}_{\mathrm{Q}}^{*}\right] + \eta_{\mathrm{Q}} k_{\mathrm{D}}[\mathrm{Chl}_{\mathrm{Pool}}^{*}] \tag{30}$$

$$\frac{\mathrm{d}}{\mathrm{d}t}[\mathrm{Chl}_{\mathrm{Pool}}^{*}] = -\left(k_{\mathrm{F,eff,0}} + \eta_{\mathrm{Q}} k_{\mathrm{D}}\right)[\mathrm{Chl}_{\mathrm{Pool}}^{*}] + k_{\mathrm{D}}\left[\mathrm{Chl}_{\mathrm{Q}}^{*}\right]. \tag{31}$$

Applying the steady state approximation to $[\mathrm{Chl}_{\mathrm{Pool}}^{*}]$, we obtain the following equation for the decay of the pool Chl*,

$$\frac{\mathrm{d}}{\mathrm{d}t}[\mathrm{Chl}_{\mathrm{Pool}}^{*}] \approx -\left(k_{\mathrm{F,eff,0}} + \eta_{\mathrm{Q}} k_{\mathrm{D}} \frac{k_{\mathrm{F,eff,Q}}}{k_{\mathrm{F,eff,Q}} + k_{\mathrm{D}}}\right)[\mathrm{Chl}_{\mathrm{Pool}}^{*}], \tag{32}$$

From which we obtain the fluorescence lifetime as

$$\frac{1}{\tau_{\mathrm{F,eff}}} = k_{\mathrm{F,eff,0}} + \eta_{\mathrm{Q}} k_{\mathrm{D}} \frac{k_{\mathrm{F,eff,Q}}}{k_{\mathrm{F,eff,Q}} + k_{\mathrm{D}}}, \tag{33}$$

Recalling that $\eta_{\mathrm{Q}} \propto \sum_{\mathrm{X}}[\mathrm{QX}]$, the expression we find is consistent wit the assumption of our NPQ model (excluding qZ). Assuming $\eta_{\mathrm{Q}} \approx 0$ before light exposure, we find the NPQτ as

$$\mathrm{NPQ}_{\tau} = \eta_{\mathrm{Q}} \frac{k_{\mathrm{D}}}{k_{\mathrm{F,eff,0}}} \frac{k_{\mathrm{F,eff,Q}}}{k_{\mathrm{F,eff,Q}} + k_{\mathrm{D}}}. \tag{34}$$

If we assume excitation energy diffusion is very fast between proteins compared to the other time-scales in the model, we find that NPQτ is given by approximately

$$\mathrm{NPQ}_{\tau} = \eta_{\mathrm{Q}} \frac{k_{\mathrm{F,eff,Q}}}{k_{\mathrm{F,eff,0}}}. \tag{35}$$

From the time-correlated photon counting experiments used to obtain the NPQτ we know $k_{\mathrm{F,eff,0}} \approx 1\ \mathrm{ns}^{-1}$. The maximum NPQ$\tau$ within our model is limited by the total concentration of P (in reduced units), $[\widetilde{\mathrm{P}}]_{\mathrm{tot}} \sim 3.5$. From the HPLC experiments we have deduced that P is present at a concentration of around 3.5 mmol/mol Chl. Assuming ~10 Chl per light-harvesting protein, this means about 1 in 30 proteins in the chloroplast would be P, which puts an upper bound on η_{Q} of ~ 1/30. From this we can estimate a lower bound on $k_{\mathrm{F,eff,Q}}$ to be $k_{\mathrm{F,eff,Q}} \sim 100\ \mathrm{ns}^{-1}$, i.e. the lifetime of Chl* on the quencher must be ~ 10 ps. If we instead use (1/7.7) ps^{-1} as an estimate for $k_{\mathrm{F,eff,Q}}$, as obtained in Ref. 1, we deduce that roughly 1 in 43 light-harvesting proteins in the chloroplast are P. Given the large simplifications and the uncertainty in the abundance of P deduced from HPLC data and the model (due to the large uncertainty in the conversion factor from model concentration to abundance in the thylakoid membrane), we consider these estimates of the proportion of P and the quenching lifetimes as being in excellent agreement.

VI. Raw HPLC Data

In Figure 3-S1 we show the raw HPLC data for each of the HL/D sequences shown in the main text. A certain fraction of each xanthophyll does not change over the course of the experiment. Since our model only includes xanthophylls that are free to bind/unbind from proteins on the time-scale of our experiments, we only examine the changes in xanthophyll concentration, and use these changes in fitting the model.

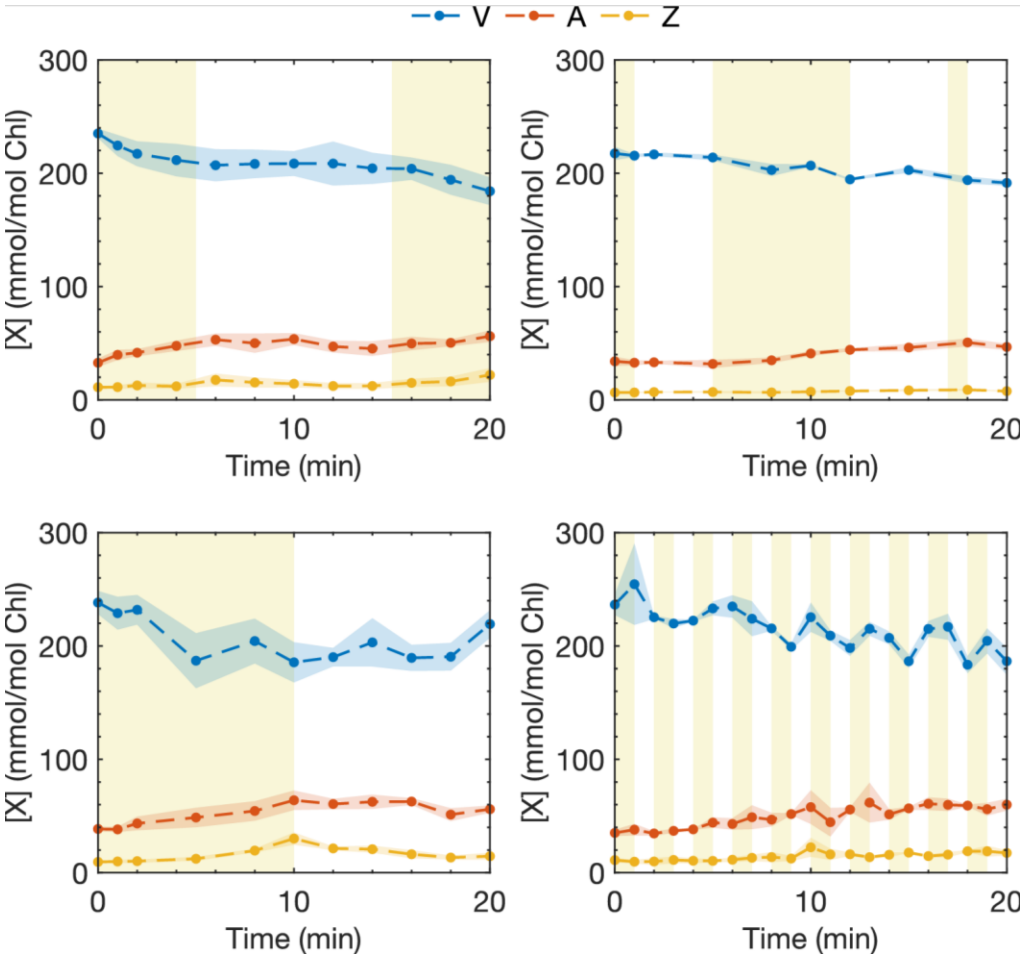

Figure 3-S1. Raw HPLC data for concentrations of each xanthophyll normalized by the total Chl concentration for four HL/D sequences: 5 HL – 10 D – 5 HL(top left), 1 HL – 4 D – 7 HL – 5 D – 1 HL – 2 D (top right), 10 HL – 10 D (bottom left), 1 HL –1 D (bottom right).

VII. NPQ Recovery in 5 HL-*T* D- 5 HL Sequences

In Figure 3-S2 we show window averaged NPQτ in the second light phase for the 5 HL-*T* D-5 HL sequences, normalized by the NPQτ value at t = 5 min. This window averaging is defined as

$$\overline{\mathrm{NPQ}}_\tau = \frac{1}{t_f - t_i}\int_{t_i}^{t_f} \mathrm{NPQ}_\tau(t)\mathrm{d}t\,. \tag{36}$$

The experimental window averaging is estimated using the trapezoidal rule. Fitting the averaged normalized NPQτ in the first minute to an exponential decay as a function of T, i.e. $\overline{\mathrm{NPQ}}_\tau = \overline{\mathrm{NPQ}_\tau}(0)e^{-k_{\mathrm{mem}}T}$, we obtain an effective recovery rate constant of k_{mem} = 0.0464 (lower CI (95%): 0.0064, upper CI (95%): 0.0861) min^{-1}, which matches the model $k_{\mathrm{A}\to\mathrm{V}}$ rate constant of 0.0509 min^{-1}.

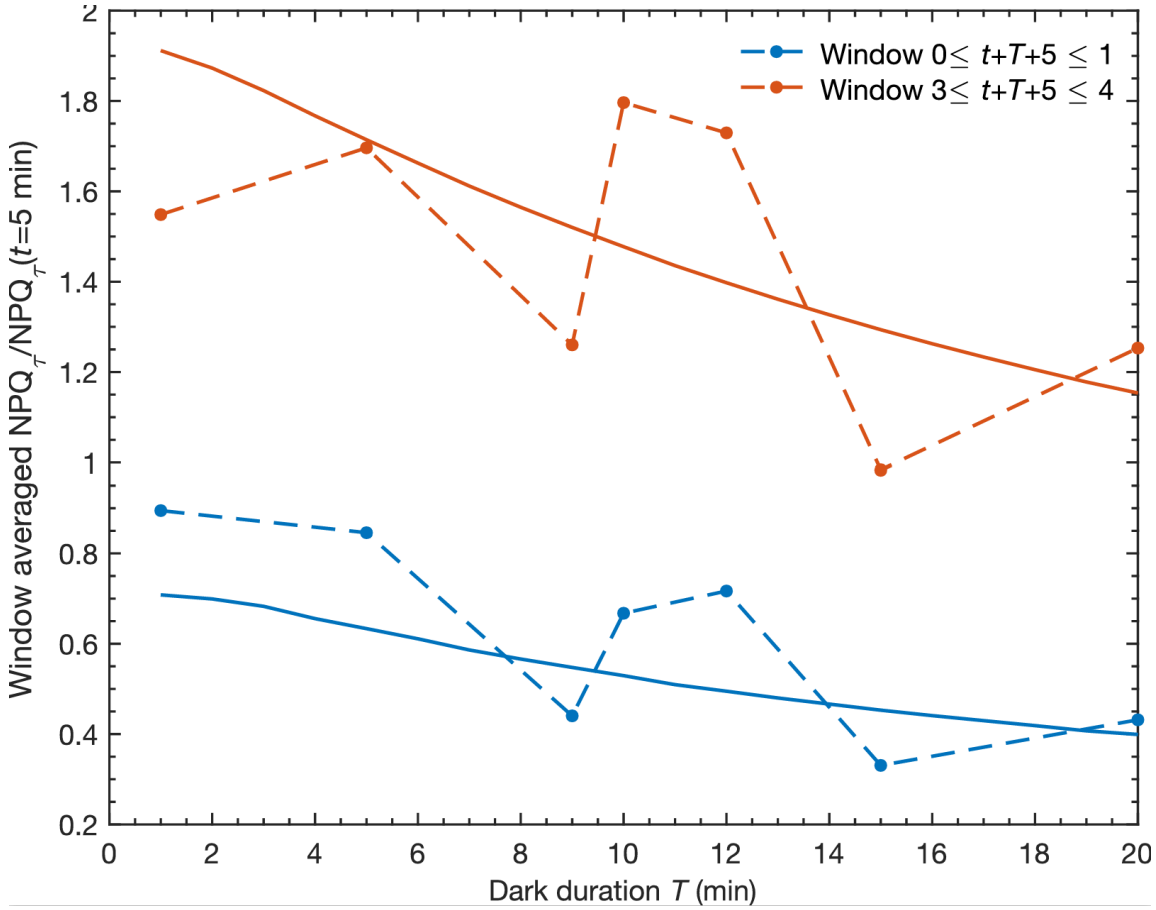

Figure 3-S2. Window averaged NPQτ in the second light phase for the 5 HL–T D–5 HL sequences, normalized by the NPQτ value at t = 5 min, for the first minute (blue) and fourth minute (red) of the second light phase, from the experiment (dashed lines and circles) and model (solid line). Error bars correspond to two standard errors in the mean. The data collection/number of replicates is described in the methods section of the main text.

3.7 Reference

1. Demmig-Adams, B. & Adams, W. W. Photoprotection in an ecological context: the remarkable complexity of thermal energy dissipation. *New Phytol* **172**, 11–21 (2006).
2. Ledford, H. K. & Niyogi, K. K. Singlet oxygen and photo-oxidative stress management in plants and algae. *Plant Cell Environ* **28**, 1037–1045 (2005).
3. Chukhutsina, V. U., Fristedt, R., Morosinotto, T. & Croce, R. Photoprotection strategies of the alga Nannochloropsis gaditana. *Biochimica Et Biophysica Acta Bba - Bioenergetics* **1858**, 544-552 (2017).
4. Park, S. *et al.* Chlorophyll–carotenoid excitation energy transfer and charge transfer in *Nannochloropsis oceanica* for the regulation of photosynthesis. *Proc National Acad Sci* **116**, 3385-3390 (2019).
5. Litvin, R., Bina, D., Herbstova, M. & Gardian, Z. Architecture of the light-harvesting apparatus of the eustigmatophyte alga *Nannochloropsis oceanica*. *Photosynth Res* **130**, 137-150 (2016).
6. Vieler, A. *et al.* Genome, Functional Gene Annotation, and Nuclear Transformation of the Heterokont Oleaginous Alga *Nannochloropsis oceanica* CCMP1779. *Plos Genet* **8**, e1003064 (2012).
7. Llansola-Portoles, M. J. *et al.* Pigment structure in the violaxanthin–chlorophyll-a-binding protein VCP. *Photosynth Res* **134**, 51–58 (2017).
8. Demmig-Adams, B., Stewart, J. J., López-Pozo, M., Polutchko, S. K. & Adams, W. W. Zeaxanthin, a Molecule for Photoprotection in Many Different Environments. *Molecules* **25**, 5825 (2020).
9. Yamamoto, H. Y. Biochemistry of the violaxanthin cycle in higher plants. *Pure Applied Chemistry* 639–648 (1979) doi:10.1016/b978-0-08-022359-9.50017-5.
10. Demmig-Adams, B. & Adams, W. W. Carotenoids in Photosynthesis. 206–251 (1993) doi:10.1007/978-94-011-2124-8_7.
11. Goss, R., Lepetit, B. & Wilhelm, C. Evidence for a rebinding of antheraxanthin to the light-harvesting complex during the epoxidation reaction of the violaxanthin cycle. *J Plant Physiol* **163**, 585–590 (2006).
12. Nilkens, M. *et al.* Identification of a slowly inducible zeaxanthin-dependent component of non-photochemical quenching of chlorophyll fluorescence generated under steady-state conditions in Arabidopsisi. *Biochimicia et Biophysica Acta* **1797**, 466–475 (2010).
13. Goss, R. & Lepetit, B. Biodiversity of NPQ. *J Plant Physiol* **176**, 13–32 (2014).
14. Perin, G., Bellan, A., Lyska, D., Niyogi, K. K. & Morosinotto, T. Modulation of xanthophyll cycle impacts biomass productivity in the marine microalga *Nannochloropsis*. *Biorxiv* 2022.08.16.504082 (2022) doi:10.1101/2022.08.16.504082.
15. Buck, J. M. *et al.* Lhcx proteins provide photoprotection via thermal dissipation of absorbed light in the diatom *Phaeodactylum tricornutum*. *Nat Commun* **10**, 4167 (2019).
16. Giovagnetti, V. *et al.* Biochemical and molecular properties of LHCX1, the essential regulator of dynamic photoprotection in diatoms. *Plant Physiol* (2021) doi:10.1093/plphys/kiab425.
17. Taddei, L. *et al.* Dynamic Changes between Two LHCX-Related Energy Quenching Sites Control Diatom Photoacclimation. *Plant Physiol.* **177**, 953–965 (2018).
18. Lacour, T., Babin, M. & Lavaud, J. Diversity in Xanthophyll Cycle Pigments Content and Related Nonphotochemical Quenching (NPQ) Among Microalgae: Implications for Growth Strategy and Ecology. *J. Phycol.* **56**, 245–263 (2020).

19. Buck, J. M., Kroth, P. G. & Lepetit, B. Identification of sequence motifs in Lhcx proteins that confer qE-based photoprotection in the diatom *Phaeodactylum tricornutum*. *Plant J.* **108**, 1721–1734 (2021).
20. Short, A. H. *et al.* Xanthophyll-cycle based model of the rapid photoprotection of *Nannochloropsis* in response to regular and irregular light/dark sequences. *J Chem Phys* (2022) doi:10.1063/5.0089335.
21. Sadhukhan, A. *et al.* How do plants remember drought? *Planta* **256**, 7 (2022).
22. Demmig-Adams, B., Polutchko, S. K., Stewart, J. J. & Adams, W. W. History of excess-light exposure modulates extent and kinetics of fast-acting non-photochemical energy dissipation. *Plant Physiol. Rep.* **27**, 560–572 (2022).
23. Polimene, L. *et al.* Modelling xanthophyll photoprotective activity in phytoplankton. *J. Plankton Res.* **34**, 196–207 (2012).
24. Bidigare, R. R. *et al.* Evaluation of the utility of xanthophyll cycle pigment dynamics for assessing upper ocean mixing processes at Station ALOHA. *J. Plankton Res.* **36**, 1423–1433 (2014).
25. Galindo, V. *et al.* Pigment composition and photoprotection of Arctic sea ice algae during spring. *Marine Ecology Progress Series* **585**, 49–69 (2017).
26. Esteban, R., Moran, J. F., Becerril, J. M. & García-Plazaola, J. I. Versatility of carotenoids: An integrated view on diversity, evolution, functional roles and environmental interactions. *Environ Exp Bot* **119**, 63–75 (2015).
27. Demmig-Adams, B. & Adams, W. W. Xanthophyll cycle and light stress in nature: uniform response to excess direct sunlight among higher plant species. *Planta* **198**, 460–470 (1996).
28. Hartel, H., Lokstein, H., Grimm, B. & Rank, B. Kinetic Studies on the Xanthophyll Cycle in Barley Leaves (Influence of Antenna Size and Relations to Nonphotochemical Chlorophyll Fluorescence Quenching). *Plant Physiol* **110**, 471–482 (1996).
29. Siefermann, D. Photosynthesis, two centuries after its discovery by Joseph Priestley, Proceedings of the IInd International Congress on Photosynthesis Research Volume I Primary reactions and electron transport. 629–635 (1972) doi:10.1007/978-94-010-2935-3_65.
30. Yamamoto, H. Y. & Higashi, R. M. Violaxanthin de-epoxidase Lipid composition and substrate specificity. *Arch Biochem Biophys* **190**, 514–522 (1978).
31. Horton, P. & Ruban, A. Molecular design of the photosystem II light-harvesting antenna: photosynthesis and photoprotection. *J Exp Bot* **56**, 365–373 (2005).
32. Havaux, M. & Niyogi, K. K. The violaxanthin cycle protects plants from photooxidative damage by more than one mechanism. *Proc. Natl. Acad. Sci.* **96**, 8762–8767 (1999).
33. Demmig-Adams, B., Cohu, C. M., Muller, O. & Adams, W. W. Modulation of photosynthetic energy conversion efficiency in nature: from seconds to seasons. *Photosynth Res* **113**, 75–88 (2012).
34. Lapillo, M., Cignoni, E., Cupellini, L. & Mennucci, B. The energy transfer model of nonphotochemical quenching: Lessons from the minor CP29 antenna complex of plants. *Biochim. Biophys. Acta (BBA) - Bioenerg.* **1861**, 148282 (2020).
35. Cupellini, L., Calvani, D., Jacquemin, D. & Mennucci, B. Charge transfer from the carotenoid can quench chlorophyll excitation in antenna complexes of plants. *Nat. Commun.* **11**, 662 (2020).
36. Cignoni, E. *et al.* A different perspective for nonphotochemical quenching in plant antenna complexes. *Nat. Commun.* **12**, 7152 (2021).

37. Bennett, D. I. G., Fleming, G. R. & Amarnath, K. Energy-dependent quenching adjusts the excitation diffusion length to regulate photosynthetic light harvesting. *Proc National Acad Sci* **115**, 201806597 (2018).
38. Fay, T. P. & Limmer, D. T. Coupled charge and energy transfer dynamics in light harvesting complexes from a hybrid hierarchical equations of motion approach. *J. Chem. Phys.* **157**, 174104 (2022).
39. López-Pozo, M., Adams, W. W., Polutchko, S. K. & Demmig-Adams, B. Terrestrial and Floating Aquatic Plants Differ in Acclimation to Light Environment. *Plants* **12**, 1928 (2023).
40. Kilian, O., Benemann, C. S. E., Niyogi, K. K. & Vick, B. High-efficiency homologous recombination in the oil-producing alga *Nannochloropsis* sp. *Proc National Acad Sci* **108**, 21265–21269 (2011).
41. Porra, R. J., Thompson, W. A. & Kriedemann, P. E. Determination of accurate extinction coefficients and simultaneous equations for assaying chlorophylls a and b extracted with four different solvents: verification of the concentration of chlorophyll standards by atomic absorption spectroscopy. *Biochimica Et Biophysica Acta Bba - Bioenergetics* **975**, 384–394 (1989).
42. García-Plazaola, J. I. & Becerril, J. M. A rapid high-performance liquid chromatography method to measure lipophilic antioxidants in stressed plants: simultaneous determination of carotenoids and tocopherols. *Phytochem Analysis* **10**, 307–313 (1999).

Chapter 4

The effect of a two-state xanthophyll cycle on photoprotective memory in the diatom *Thalassiosira pseudonana*

This chapter is based on work performed by A.H. Short in collaboration with S. Wakao, R. Mangal, R. Lee, K. K. Niyogi, and G.R. Fleming

4.1 Abstract

In high light (HL) conditions, plants and algae are exposed to excess energy, which cannot be utilized in photochemistry and is instead dissipated through non-photochemical quenching (NPQ) as heat, minimizing damage. In most photosynthetic organisms, the VAZ cycle, which is a type of xanthophyll cycle, is integral to NPQ. In *Nannochloropsis* algae, the xanthophyll cycle imparts a memory of previous stressor events, allowing cells to attenuate their relaxation rate, improving responsiveness to successive stressors. This photoprotective memory arises due to the three-state nature of the VAZ cycle. Antheraxanthin, which is the intermediate pigment, acts as a buffer allowing the system to reset back to a light harvesting state while being able to immediately convert back into a photoprotective state upon HL exposure. A two-state xanthophyll cycle does not have this ability. In the diatom species, *Thalassiosira pseudonana,* the diadinoxanthin-diatoxanthin cycle is the main xanthophyll cycle. The differences that arise between the two systems could be due to 1) Dt have a higher quenching efficiency than Z, 2) the Dd to Dt de-epoxidation is faster or the epoxidation step in Dd-Dt is slower than in the VAZ cycle, or 3) a higher initial concentration of Dt than Z even after dark adaption. With the aid of modeling, we speculate that there is more Dt present even after long incubations in the dark compared to Z, and that Dt is a more effective quencher than Z. Further work needs to be done to confirm the modeling predictions.

4.2 Introduction

In nature, plants and algae are exposed to rapidly fluctuating light environments that can range from limiting to excessive light conditions[1]. In low light conditions, chlorophylls (Chl) absorb energy and transfer it to the reaction centers of photosystem (PS) I or II where it will eventually be utilized to reduce NADP+ and form ATP for the Calvin-Benson cycle[2]. However, during high light (HL) exposure, reaction centers reach a saturation level and are unable to process all energy captured by the photosynthetic antennae. Plants and algae have therefore developed non-photochemical quenching (NPQ) pathways to dissipate the excess energy as heat, preventing the accumulation of reactive oxygen species[3–6]. Understanding how NPQ pathways are activated and regulated can be important for improving photosynthetic efficiencies in fluctuating light conditions[7,8]. Research by Souza et al. has shown that altering gene expression of NPQ-related proteins can improve soybean yields by ~25%[9]. It is unknown if this is the maximum increase in yield that can be achieved by modifying NPQ.

In attempt to model NPQ behaviors to theoretically test for optimal balance between NPQ expression and the light-harvesting state, we created a model based on the xanthophyll cycle and pH-sensing protein, which are the main molecular actors involved in photoprotection, in the simplified model organism, *Nannochloropsis oceanica*[10,11]. In *N. oceanica* and vascular plants, the xanthophyll cycle refers to the conversion of violaxanthin (V) to zeaxanthin (Z) through the intermediate antheraxanthin (A), known as the VAZ cycle[3,12]. A key aspect of antheraxanthin is that it acts as a buffer because of its slow conversion back to V[11]. This dynamic occurs specifically because the VAZ cycle is a three-state system, where the conversion between each carotenoid is its own individual step. Because A is able to accumulate, it facilitates a 'photoprotective memory' for *N. oceanica*, allowing the algae to transition back to a light-harvesting state while being able to rapidly respond to subsequent stressor events[11,13,14]. To further understand the role of the xanthophyll cycle, this chapter will explore how a two-state xanthophyll cycle differs in its photoprotective responses compared to a three-state xanthophyll cycle like the VAZ cycle.

Diatoms are an incredibly diverse species of unicellular, photosynthetic eukaryotes found in all types of aquatic environments that are responsible for about 40% of oceanic carbon fixation[15–17]. There are two types of diatoms: pennates like *Phaedactylum tricornutum* and centrics like *Thalassiosira pseudonana*[18]. Diatoms contain a two-state xanthophyll cycle known as the diadinoxanthin- diatoxanthin (Dd-Dt) cycle. Diatoms contain the VAZ cycle and utilize the same enzyme that converts V to A to Z—violaxanthin de-epoxidase (VDE)— to transform Dd to Dt because V is a precursor to Dd[19]. A and Z can accumulate in diatoms, but the VAZ cycle does not typically contribute to NPQ unless exposed to extreme HL[20,21]. When the lumen is acidified, Dd is converted to Dt with a VDE enzyme, referred to here as Dd epoxidase (DDE) for clarity [22,23]. DDE is very similar to plant VDE; though, the optimal pH for DDE is slight shifted towards a more neutral pH[23,24]. Zeaxanthin epoxidase (ZEP), which is utilized by the VAZ cycle to add epoxy groups back to the pigments, epoxidizes Dt, here referred to as Dt epoxidase (DEP). DDE and DEP have similar structures and are encoded by the same genes as their plant counterparts[4]. The diatom xanthophyll enzymes have faster conversions rates comparitively[23,25].

In this study, we utilized *T. pseudonana* to explore the effects of a two-state xanthophyll cycle on photoprotective dynamics and memory. The photoprotective pathways in *T. pseudonana* are relatively simple like *Nannochloropsis* since diatoms do not accumulate lutein[23]. *T. pseudonana* has a pH-sensing protein, which is in the LHCX protein family, though the identity is still being

researched as to if it is LHCX1, LHCX4, LHCX6, or some combination of multiple proteins[18,26]. For these reasons, *T. pseudonana* also provides a good model system to extend our model to test its flexibility in predicting NPQ responses in other species.

4.3 Methods

4.3.1 Cell Culturing

Thalassiosira pseudonana was cultivated in ASW medium. Liquid cultures were grown to 2–5 × 10^6 cells/mL in diurnal light (12 hr night- 12 hr day) at a photon flux density of 100 µmol photons $m^{-2}s^{-1}$ at 18 °C. Two cultures of *T. pseudonana* were grown—a static culture and a shaken culture—to see if this resulted in a difference. Shaking the culture allows for more CO_2 to be circulated throughout the cells, which leads to greater relaxation of NPQ during darkness (Figure 4-1). Because of this, all experiments are done with shaken cultures.

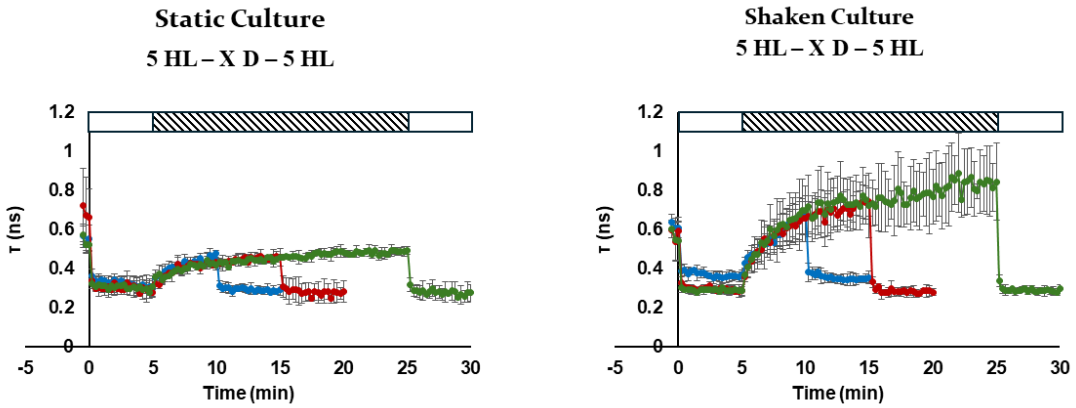

Figure 4-1. Comparison of static and shaken *T. pseudonana* cultures grown in diurnal light. On the left are the fluorescence lifetime measurements of the static culture. The initial dark-adapted lifetimes for each actinic light sequence are spread over a range from ~0.6 to 0.75 ns. On the right are the fluorescence lifetime measurements for the shaken culture. The dark-adapted lifetime measurements are more consistent between the different actinic light sequences averaging at 0.6 ns. The white boxes represent HL periods while the striped boxes represent the varying dark durations of the memory series.

4.3.2 Time Correlated Single Photon Counting

The data collection method for this investigation was Time Correlated Single Photon Counting, or TCSPC. TCSPC is a process by which the average time taken for an electron to absorb and emit singular photons can be measured. The photons were fed into the sample by pumping a diode laser (Coherent Verdi G10, 532nm) with a Ti:sapphire coherent Mira 900 oscillator. After frequency doubling the wavelength to 404nm, with a β-barium borate crystal, the beam was split between the sample and a sync photodiode, which was used as a reference for snapshot measurements. Three synchronized shutters controlled the exposure of actinic light, the laser to the sample and to the microchannel plate-photomultiplier tube detector (Hamamatsu106 R3809U). The shutters were controlled using a LABVIEW software sequence. The detector was set to 680nm to detect Chl-a emission. During each snapshot, the laser and detection shutters were opened, allowing an excitation pulse of 1.2mW to saturate the reaction center for one second while the emission was recorded. Emissions were recorded in 15 second intervals. During high light periods, the species was exposed to white light with an intensity of 850uE. The detection times for photon emission

were plotted on a histogram. These data were analyzed, first using a MatLab file, then using PicoQuant FluoFit to find a best fit estimate bi-exponential function for the histogram. The average lifetime ($\bar{\tau}$) values from this function were then used to calculate NPQ values using the following formula:

$$NPQ_\tau = \frac{\left(\bar{\tau}(0) - \bar{\tau}(t)\right)}{\bar{\tau}(t)} \quad (1)$$

$\bar{\tau}(0)$ is the average lifetime in the dark and $\bar{\tau}(t)$ is the average lifetimes at some time point *t* during the experiment.

The samples were concentrated to 80ug/mL of chlorophyll by centrifugation. To do so, two tubes each containing 2mL of cell culture were centrifuged for 5 min at 14,000rpm. The supernatant was removed and discarded, after which 1mL of 80% acetone was added to each tube. Tubes were centrifuged again for 5 min at 14,000rpm. The supernatant from each was added to cuvettes and spectrophotometer readings taken to determine chlorophyll concentration according to Porra *et al*[27]. The culture was then concentrated by centrifuging an appropriate volume for 6 min at 1300G. Supernatant was discarded, and the pellet was suspended in vitamin rich ASW media to bring up to volume.

4.4 Results and Discussion

4.4.1 NPQ Dynamics in Response to Short High Light Exposures

We tested to see how an initial, short (< 2 min) HL period would affect NPQ dynamics as well as subsequent aperiodic light exposures (Figure 4-2). Within 1 min, NPQ is fully induced and steady state levels of NPQτ are reached and maintained in all subsequent HL exposures. At the light to dark transitions, the NPQτ value drops instantaneously before more gradually relaxing back towards its dark-adapted state, indicating a fast and slow component to the relaxation dynamics.

When compared to *Nannochloropsis* for the same irregular light fluctuations (Figure 4-2 and see ref.[10]), the HL-adapted *Nannochloropsis*, which has a higher [Z] accumulated than LL-adapted *Nannochloropsis*, response more closely resembles the diatom phenotype. There are notable differences, though. First, *T. pseudonana* has a much sharper increase in its initial response to HL that is only seen in *Nannochloropsis* with subsequent HL exposures. This could be explained by three possibilities:

1. *T. pseudonana* either does not need to accumulate Dt like *Nannochloropsis* needs to accumulate Z for a significant NPQ response. Previous work in diatoms has shown that the ΔpH gradient alone cannot induce a significant NPQ response[28]. However, it may be that a lower concentration of Dt is necessary to induce photoprotection. This could be due to a number of factors such as the quenching efficiency Dt/Dd or the ability for LHCX1 to bind pigment, making it the quenching cite. Though, Z is thought to have a higher quenching efficiency, but Dd has a stronger involvement than V[4,21].
2. *T. pseudonana* has a significantly faster de-epoxidation cycle to accumulate Dt or slower epoxidation step. Interestingly, even though DDE and DEP are homologues of VDE and ZEP found in *Nannochloropsis*, both diatom enzymes are suspected to be faster. DDE's conversion rate may be faster due to its higher affinity for the co-substrate, ascorbate [23]. DEP is regulated by the ΔpH across the thylakoid membrane such that when the pH-

gradient is established, DEP is inactivated. In the dark, when NADPH concentrations are limited, DEP is also inactivated[29].

3. After one hour of dark adaption, a significant amount of Dt remains, enabling a rapid, steady state response. While *T. pseudonana* has a rapid response to transitions from light to dark, there is a slow component that is not present in *Nannochloropsis*. In another diatom species, *Phaeodactylum tricornutum*, it too has sustained NPQ in the dark that lasts 5-10 minutes, but an hour of darkness seems to reverse the effect on fluorescence quenching, which has been linked to Dt[30]. In line with this theory, is that Dt epoxidation might be limited in the dark, allowing some Dt molecules remain after incubation in the dark[21].

The next difference in the NPQ response between *T. pseudonana* and *Nannochloropsis* is their relaxation kinetics. *Nannochloropsis* appears to only have one significant component, being related to the pH-sensing protein, i.e. the sharp decrease in NPQτ upon transition into the dark before it reaches a steady state. *Nannochloropsis*'s relaxation is independent of its [Z]. *T. pseudonana* seems to have a rapid component likely related to its pH-sensing protein(s), but it also has a slower component that may be related to the inactivation of DEP in the dark.

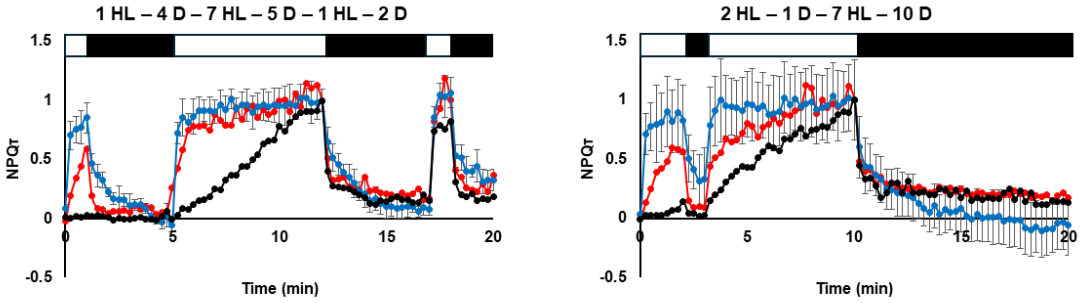

Figure 4-2. The NPQτ traces for *T. pseudonana* (blue) in irregular light fluctuations compared to *Nannochloropsis*. The error bars HL-Grown *Nannochloropsis* NPQτ (red) and LL-Grown *Nannochloropsis* (black) are omitted for clarity. *Left* graph shows the photoprotective response to 1 HL – 4 D – 7 HL – 5 D – 1 HL – 2 D. *Right* graph shows the NPQ response to 2 HL – 1 D – 7 HL – 10 D actinic light sequence. Standard deviation was used to calculate the error bars. *Nannochloropsis* data was obtained from ref [10]. The white boxes represent HL periods while the black boxes represent the dark periods.

4.4.2 Photoprotective Memory in a Two-State System

To understand how memory is affected by a two-state xanthophyll cycle, we utilized a similar approach as in Short, Fay *et al.* where an initial five-minute HL period is followed by increasing dark durations ranging from 5 minutes to 15 minutes which is then followed by a second five minutes of HL[11]. The data is normalized at t = 5 min to compare between species as well as focus on the relaxation dynamics after the first HL period.

In the first HL period, the diatom NPQτ response is immediate and significant, reaching a steady state value within 1 minute of HL exposure (Figure 4-3A). Unlike *Nannochloropsis*, which requires the entirety of the HL exposure before it reaches its peak value, *T. pseudonana* maintains the same NPQτ level (Figure 4-3B,C). This indicates *T. pseudonana* is already at a quasi-steady state.

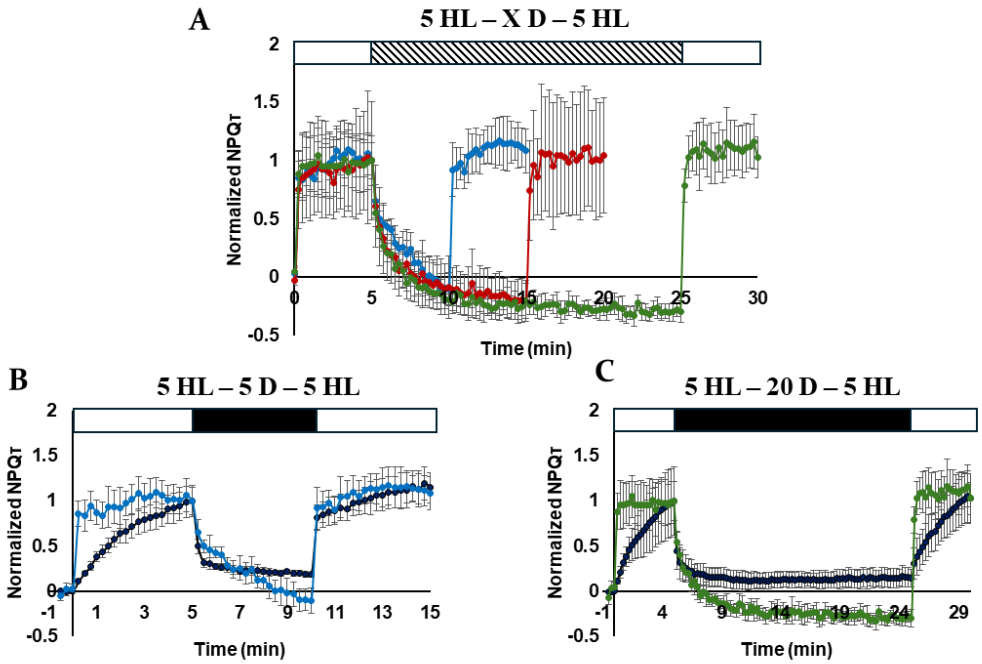

Figure 4-3. The photoprotective dynamics and memory of *T. pseudonana* in 5 min HL- X min D- 5 min HL actinic light sequence, where X= 5, 10, 20 minutes. **A** graph shows the three light sequences of 5 HL – 5 D – 5 HL (blue), 5 HL – 10 D – 5 HL (red), and 5 HL – 20 D – 5 HL (green). **B** graph shows the comparison between *N. oceanica* (black) and *T. pseudonana* (blue) for 5 HL – 5 D – 5 HL. **C** graph shows the comparison between *N. oceanica* (black) and *T. pseudonana* (green) for 5 HL – 20 D – 5 HL. *Nannochloropsis* data is taken from Short, Fay *et al. Nat. Commun.* 2023, *14*[11]. The white boxes represent HL periods, the black boxes represent the dark periods, and the striped box represents the varying dark durations of the memory series.

At the transition from HL to darkness, the diatom NPQτ level instantaneously drops before slowing down to a more moderate decline, displaying the same two-component relaxation as noted above. When the *T. pseudonana* cells are transitioned into the second HL exposure, they instantaneously respond and reach the steady state value within 30 seconds for all sequences (Figure 4-3A). In comparison, the response to secondary HL stress is vastly different in *Nannochloropsis*. For *Nannochloropsis*, as the dark duration increase, the photoprotective 'memory' of the previous HL exposure is lost. That is to say that *Nannochloropsis* begins to reset its photoprotective pathways such that it takes longer to return to the previous NPQ level after long incubations in the dark. However, for *T. pseudonana*, regardless of dark duration, its memory of stress induced by the first HL period is retained, even after 20 minutes of darkness. When the dark duration is 5 minutes, *Nannochloropsis* has an immediate response to the secondary HL period that reaches steady state within 1 minute, which resembles the response seen in *T. pseudonana* (Figure 4-3B). When considering the longer dark duration, the 20 minutes of darkness reduces the extent of the response for *Nannochloropsis*, causing a delay in reaching the steady state value (Figure 4-3C).

T. pseudonana also relaxes past the NPQτ value of zero, reaching negative values. This comes from how the NPQτ is calculated (see eq 1). The negative NPQτ values indicate the fluorescence lifetimes of the diatom cells increase past the starting fluorescence lifetime. While the diatom cells were incubated for 1 hour in the dark, the cells could be in an initially more quenched state than is

relaxed to during the experimental run. Why this happens is still unknown, but potentially *T. pseudonana* has an over-dampening effect when in fluctuating light. Longer studies of how NPQτ respond in prolonged dark periods should be run.

4.5 Modeling

We fit the diatom data using the two-state model from ref 10. In this simple model of the NPQ response in *Nannochloropsis*, only a few changes have been made to fit the *T. pseudonana* data. First, the data was all normalized to be between zero and one as the model was unable to process negative NPQτ values. Second, the quenching complex, Q, was also assumed to be zero at $t = 0$. As in the *Nannochloropsis* model, we assume DDE has an active and inactive form which is controlled by the pH gradient, which is assumed to activate/de-activate instantly at light transitions[31]. The pH-sensing protein, P, is again agnostic to the actual identity, but forms a connection with either Dd or Dt. The PDt complex converts to Q, indicating it is a quenching state upon HL exposure. As with the first iteration of modeling, only one pigment, in this case Dt, is assumed to contribute to quenching.

Figures 4-4 and 4-5 show the results of the model based on the fitted data. While the model is able to fit the data reasonably well, there are some aspects where the model cannot capture the data—particularly, the relaxation dynamics. While the model is able to capture the rapid decrease in NPQτ at the HL to dark transition, it fails to capture the slower component. This is evident in Figure 4-4 for the irregular sequences as well as the 5 HL – 20 D – 5 HL in Figure 4-5. Additionally, while the model is assumed to begin with no formed quenching complex, therefore the model starts at an NPQτ = 0, the experimental data begins at higher values between 0.1 and 0.3 depending on the sequence. This indicates that the cells are either already quenched due to damage from the growth or experimental conditions or that some concentration of the quenching complex is already present.

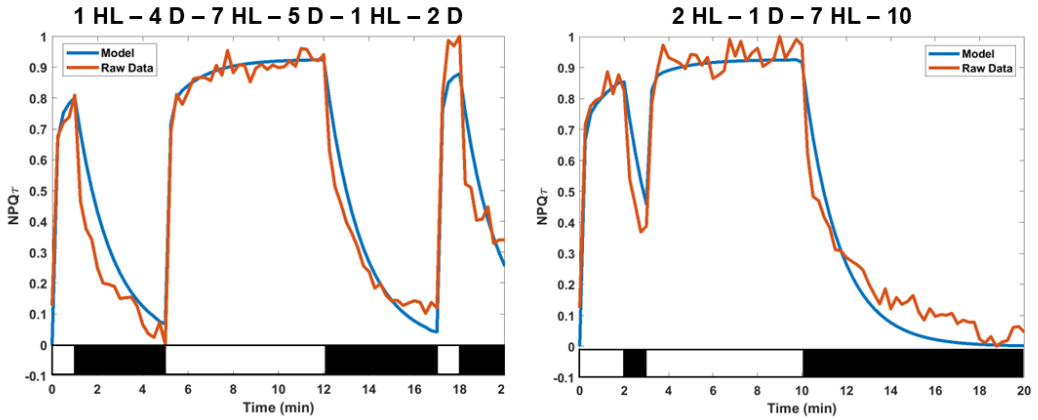

Figure 4-4. Comparison of the model to the experimental data for irregular light sequences. The model is shown in blue while the experimental data is in red. The white boxes represent HL periods while the black boxes represent the dark periods.

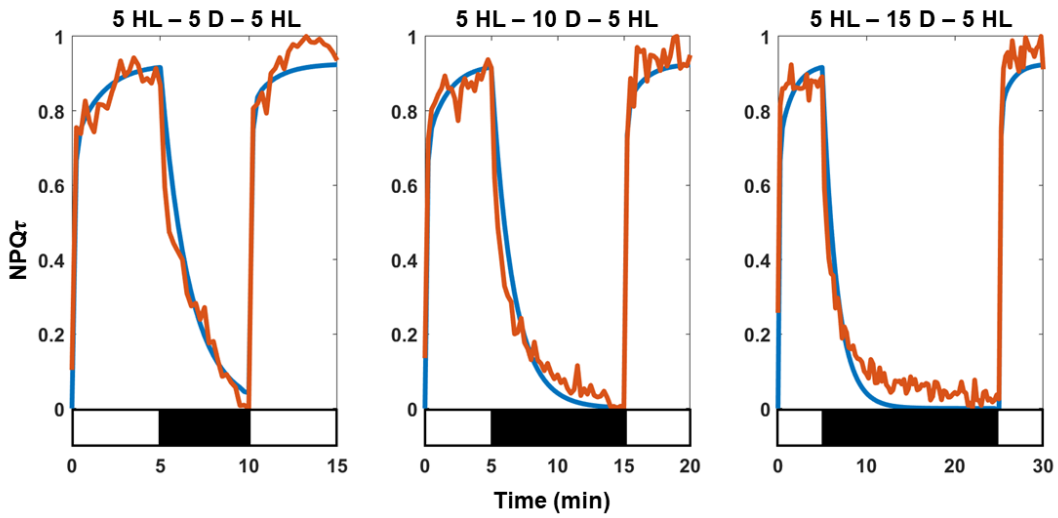

Figure 4-5. Comparison of the model to the experimental data for 5 HL – X D – 5 HL sequences. The model is shown in blue while the experimental data is in red. The white boxes represent HL periods while the black boxes represent the dark periods.

With the modeling, the initial starting concentrations can be determined (Figure 4-6). All values are given for the reduced variable model, as described in the Short *et al.* (2022)[10], and as such all concentrations are unitless. Figure 4-6 shows how these parameters change during an actinic light sequence. While the quenching complex begins at 0, the protein-Dt complex, PDt begins at 0.7785, indicating the system is primed to respond to a HL stimulus. Also, the model predicts that the Dd concentration is much greater than Dt, which is consistent with dark-adapted cells[32], but some amount of Dt is accumulated before the experiment, and the amount of Dt nearly doubles by the end of the actinic light sequence. Interestingly, instead of the [Dt] decreasing during the dark periods, it remains constant, which could account for the slow component noted during *T. pseudonana's* relaxation.

When considering the hypotheses listed above, the modeling supports that there is more Dt, which is equivalent to Z, present even after long incubations in the dark. The model also supports the notion that Dt is a more efficient quencher than Z. The [Dt] is nearly five times greater than [Z] found in LL-Grown *Nannochloropsis* initially. However, the HL-Grown *Nannochloropsis* has four times the concentration of Z compared to Dt, which may indicate that less Dt is needed as it is a more efficient quencher. Considering the starting protein-pigment complexes across the two *Nannochloropsis* growth conditions and the diatom species, we can see that HL-Grown *Nannochloropsis* and *T. pseudonana* are more similar in their relative concentrations with [PDt] being about half of [PZ] while [PDt] is nine times greater than LL-Grown *Nannochloropsis*. but in this grown condition *Nannochloropsis* has $[Q]_0 = 1.86$[10].

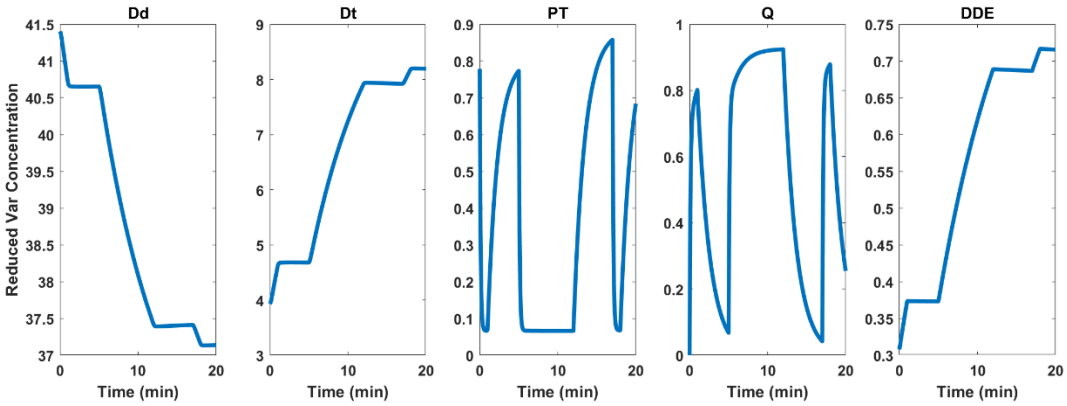

Figure 4-6. The dynamics of the Dd, Dt, PDt, and Q, and VDE during the actinic light sequence of 1 HL – 4 D – 7 HL – 5 D – 1 HL – 2 D given as reduced variables. The initial parameters are as follows $[Dd]_0 = 41.40$, $[Dt]_0 = 3.93$, $[PDt]_0 = 77.85 \times 10^{-2}$, $[Q]_0 = 0$, and $[DDE]_0 = 30.77 \times 10^{-2}$.

4.6 Future Work

Diatoms exist in turbulent waters where due to mixing they are exposed to rapid changes in light levels that they must adapt to[33]. Studying these systems can provide useful insights into enzyme dynamics that could lead to improved responsiveness of NPQ in algae and plants. For this work, we can see that *T. pseudonana* has a rapid, quasi-steady state response that does not require time to accumulate a photoprotective pigment as seen in *Nannochloropsis*. *Nannochloropsis* only has as rapid and significant of a response when [Z] is already accumulated due to growth conditions. However, *T. pseudonana* has a slower relaxation component that is absent in *Nannochloropsis*. Yet, given enough time in the dark that begins to reset the three-state xanthophyll cycle, *T. pseudonana* is able to recover to its previous NPQτ level within one minute of the secondary light exposure.

However, more work still needs to be done before the complete story of how a two-state xanthophyll cycle affects photoprotective memory can be unraveled. First, is to understand why *T. pseudonana* displays a rapid, quasi-steady state behavior. Three hypotheses were given above. Using HPLC experiments, the concentrations of Dd and Dt as a function of actinic light exposures can be determined. Not only will this inform us as to the relative starting concentrations of Dd to Dt but will also provide the rate of converse for the forward and backwards reactions. Additionally, experiments using low light instead of darkness should be run to see if *T. pseudonana* relaxes more rapidly, confirming that DEP is NADPH limited. Finally, the duration of how long it takes for Dt to convert fully back to Dd should be observed. Together all of this information can be used to improve the model and provide realistic boundaries. Additionally, using the updated model[11] modified for a two-state system will provide estimates on the quenching efficiencies.

4.7 References

1. Morales, A. & Kaiser, E. Photosynthetic Acclimation to Fluctuating Irradiance in Plants. *Front. Plant Sci.* **11**, 268 (2020).
2. Blankenship, R. E. *Molecular Mechanisms of Photosynthesis*. (John Wiley & Sons, 2021).
3. Demmig-Adams, B. Carotenoids and photoprotection in plants: A role for the xanthophyll zeaxanthin. *Biochimica Et Biophysica Acta Bba - Bioenergetics* **1020**, 1–24 (1990).
4. Goss, R. & Lepetit, B. Biodiversity of NPQ. *J Plant Physiol* **176**, 13–32 (2014).
5. Müller, P., Li, X.-P. & Niyogi, K. K. Non-Photochemical Quenching. A Response to Excess Light Energy. *Plant Physiol* **125**, 1558–1566 (2001).
6. LEDFORD, H. K. & NIYOGI, K. K. Singlet oxygen and photo-oxidative stress management in plants and algae. *Plant Cell Environ* **28**, 1037–1045 (2005).
7. Kromdijk, J. *et al.* Improving photosynthesis and crop productivity by accelerating recovery from photoprotection. *Science* **354**, 857--861 (2016).
8. Long, S. P. *et al.* Into the Shadows and Back into Sunlight: Photosynthesis in Fluctuating Light. *Annu. Rev. Plant Biol.* **73**, 617–648 (2022).
9. Souza, A. P. D. *et al.* Soybean photosynthesis and crop yield are improved by accelerating recovery from photoprotection. *Science* **377**, 851–854 (2022).
10. Short, A. H. *et al.* Xanthophyll-cycle based model of the rapid photoprotection of Nannochloropsis in response to regular and irregular light/dark sequences. *J Chem Phys* (2022) doi:10.1063/5.0089335.
11. Short, A. *et al.* Kinetics of the xanthophyll cycle and its role in photoprotective memory and response. *Nat. Commun.* **14**, 6621 (2023).
12. Yamamoto, H. Y. Biochemistry of the violaxanthin cycle in higher plants. *Pure Applied Chemistry* 639–648 (1979) doi:10.1016/b978-0-08-022359-9.50017-5.
13. Demmig-Adams, B., Polutchko, S. K., Stewart, J. J. & Adams, W. W. History of excess-light exposure modulates extent and kinetics of fast-acting non-photochemical energy dissipation. *Plant Physiol. Rep.* **27**, 560–572 (2022).
14. Hilker, M. & Schmülling, T. Stress priming, memory, and signalling in plants. *Plant Cell Environ* **42**, 753–761 (2019).
15. Smetacek, V. Diatoms and the Ocean Carbon Cycle. *Protist* **150**, 25–32 (1999).
16. Falkowski, P. G., Barber, R. T. & Smetacek, V. Biogeochemical Controls and Feedbacks on Ocean Primary Production. *Science* **281**, 200–206 (1998).
17. Bowler, C., Vardi, A. & Allen, A. E. Oceanographic and Biogeochemical Insights from Diatom Genomes. *Mar. Sci.* **2**, 333–365 (2010).
18. Büchel, C. Light harvesting complexes in chlorophyll c-containing algae. *Biochim. Biophys. Acta (BBA) - Bioenerg.* **1861**, 148027 (2020).
19. Dambek, M. *et al.* Biosynthesis of fucoxanthin and diadinoxanthin and function of initial pathway genes in Phaeodactylum tricornutum. *J. Exp. Bot.* **63**, 5607–5612 (2012).
20. Lohr, M. & Wilhelm, C. Algae displaying the diadinoxanthin cycle also possess the violaxanthin cycle. *Proc National Acad Sci* **96**, 8784–8789 (1999).
21. Lacour, T., Babin, M. & Lavaud, J. Diversity in Xanthophyll Cycle Pigments Content and Related Nonphotochemical Quenching (NPQ) Among Microalgae: Implications for Growth Strategy and Ecology. *J. Phycol.* **56**, 245–263 (2020).
22. Lepetit, B. *et al.* High Light Acclimation in the Secondary Plastids Containing Diatom Phaeodactylum tricornutum is Triggered by the Redox State of the Plastoquinone Pool . *Plant Physiol.* **161**, 853–865 (2012).

23. Bertrand, M. Carotenoid biosynthesis in diatoms. *Photosynth. Res.* **106**, 89–102 (2010).
24. Kuczynska, P. *et al.* The xanthophyll cycle in diatom Phaeodactylum tricornutum in response to light stress. *Plant Physiol. Biochem.* **152**, 125–137 (2020).
25. Goss, R., Pinto, E. A., Wilhelm, C. & Richter, M. The importance of a highly active and ΔpH-regulated diatoxanthin epoxidase for the regulation of the PS II antenna function in diadinoxanthin cycle containing algae. *J. Plant Physiol.* **163**, 1008–1021 (2006).
26. Zhu, S.-H. & Green, B. R. Photoprotection in the diatom Thalassiosira pseudonana: Role of LI818-like proteins in response to high light stress. *Biochim. Biophys. Acta (BBA) - Bioenerg.* **1797**, 1449–1457 (2010).
27. Porra, R. J., Thompson, W. A. & Kriedemann, P. E. Determination of accurate extinction coefficients and simultaneous equations for assaying chlorophylls a and b extracted with four different solvents: verification of the concentration of chlorophyll standards by atomic absorption spectroscopy. *Biochimica Et Biophysica Acta Bba - Bioenergetics* **975**, 384–394 (1989).
28. Lavaud, J., Rousseau, B. & Etienne, A.-L. In diatoms, a transthylakoid proton gradient alone is not sufficient to induce a non-photochemical fluorescence quenching. *FEBS Lett.* **523**, 163–166 (2002).
29. Blommaert, L., Chafai, L. & Bailleul, B. The fine-tuning of NPQ in diatoms relies on the regulation of both xanthophyll cycle enzymes. *Sci Rep-uk* **11**, 12750 (2021).
30. Ruban, A. *et al.* The super-excess energy dissipation in diatom algae: comparative analysis with higher plants. *Photosynth. Res.* **82**, 165 (2004).
31. Zhang, R. & Sharkey, T. D. Photosynthetic electron transport and proton flux under moderate heat stress. *Photosynth Res* **100**, 29–43 (2009).
32. Kuczynska, P. & Jemiola-Rzeminska, M. Isolation and purification of all-trans diadinoxanthin and all-trans diatoxanthin from diatom Phaeodactylum tricornutum. *J. Appl. Phycol.* **29**, 79–87 (2017).
33. Kuczynska, P., Jemiola-Rzeminska, M. & Strzalka, K. Photosynthetic Pigments in Diatoms. *Mar. Drugs* **13**, 5847–5881 (2015).

Chapter 5

Conclusions and Future Directions

5.1 Conclusions

With the work presented in this thesis, significant steps towards creating a flexible model that is based on the universal biochemical processes that occur in the majority of photosynthetic organisms—specifically, the VAZ xanthophyll cycle which is found in vascular plants and many algal species. Yet, the model is adaptable enough to also model the Dd-Dt xanthophyll cycle found in diatoms with a few modifications. This reinforces the understanding that de-epoxidated carotenoids are vital in photoprotection. The second main biochemical aspect used to create the model was the pH-gradient instantaneously activating a pH-sensing protein upon exposure to light or deactivating the photoprotective mechanisms when transitioned back to darkness. Because the model is agnostic to the identity of the pH-sensing protein, this factor does not need to be altered between species. Because the model is based on biochemical processes, mutant NPQ behavior can be described using parameters derived from WT fittings and setting the model to reflect the mutant phenotype. This is a powerful capability of our model, which can allow us to explore which molecular aspects should be tuned for optimized photoprotective responses. Looking forward, the model can be iterated and refined to guide the necessary changes to crop genomes to improve the responsiveness of NPQ to fluctuating light environments[1]. In order to achieve this goal, future work needs to (1) increase our understanding of NPQ in dynamic environments that resemble the light fluctuations in nature; (2) explore the effects of differing xanthophyll cycles on photosynthetic efficiencies; and (3) scale the model to fit other species, specifically vascular plants, by adding in the molecular components unique to each species.

5.2 Mimicking Natural Light Fluctuations to Improve Model Complexity

In our previous experiments to understand NPQ activation and deactivation rates, we subjected organisms to changes in light intensities by transitioning between HL and D to turn on and then off NPQ pathways, respectively[2–4]. In these experiments, periodic light fluctuations are used; however, in nature, light fluctuations are sporadic and random between a multitude of light levels. Plants and algae experience various levels of shading from canopies or cloud coverage or intense, brief spikes of light levels from sunflecks[5–7]. Algae can also experience rapid changes in light level from mixing experienced in aquatic environments[8,9]. To fully replicate the NPQ response plants and algae use, we need to increase the complexity of our actinic light fluctuations. In Chapter 2, we introduced irregular light sequences to replicate natural fluctuations more closely in light levels[10]. Utilizing irregular light periods allowed us to notice interesting NPQ dynamics, indicating the role antheraxanthin plays in NPQ relaxation.

Yet, within the work presented in this thesis, we have not addressed changing light intensities. Some works have conducted experiments at varying light intensities[11–13]. However, most studies focus on growing organisms in either high light or low light rather than observing changes in rapid

fluctuating light intensities[14–17]. Following similar experiments as utilized in previous chapters, changing the HL intensity during periodic and aperiodic light fluctuations would help create an intuitive understanding of how NPQ is modulated by light intensities. With this information, we could add onto the model a function to modulate the photoprotective response based on the light intensity input. Additionally, pigment data as a function of light intensity could also reveal how the xanthophyll cycle rates are affected.

Finally, to simulate more accurately what occurs in nature, the effect of transitions between HL and low light (LL) conditions should be observed. Transitions between excessive light and limiting light conditions may affect the rates of NPQ activation/deactivation. Some work has shown that relaxation of NPQ mechanisms is faster as carbon sink pathways are activated to more rapidly de-acidify the lumen[18,19]. However, pathways that are not as rapidly reversible as qE such slower relaxing pathways of state transitions and qZ might have a greater effect on NPQ levels in natural light conditions than previously considered. By testing several low light conditions, we can determine a potential light intensity threshold needed to maintain NPQ mechanisms even in seemingly ideal light environments. Understanding how photoprotection works in more natural light environments will help improve modeling NPQ systems and our understanding of NPQ's effect on crop yields. Some preliminary work has been conducted for these experiments, but more work needs to be done to completely understand the effect of lower light levels between HL periods.

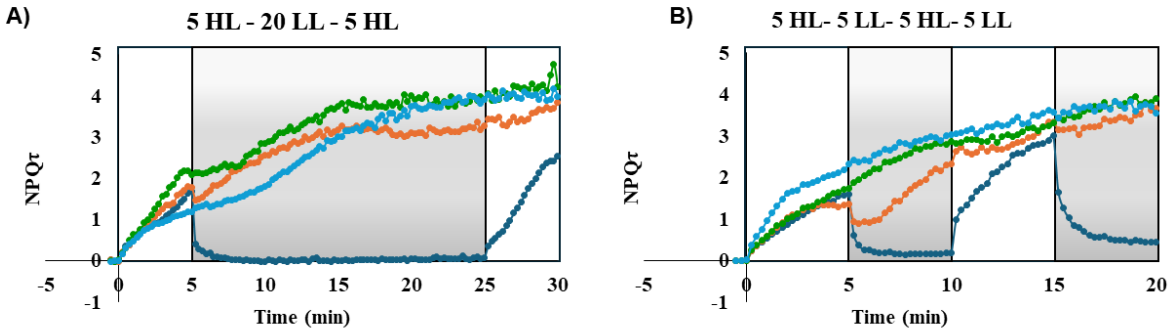

Figure 5-1. Preliminary data of WT *N. oceanica* exposed to HL-LL sequences. WT *N. oceanica* cells subjected to fluctuating light sequences of **A)** 5 min HL- 20 min LL- 5 min HL and **B)** 5 min HL- 5 min LL- 5 min HL- 5 min LL. The LL values are 0 µE (dark blue), 50 µE (orange), 200 µE (green), and 400 µE (light blue). The gray to white gradient box depicts the low light actinic light exposures while the white boxes represent 750 µE HL.

The preliminary work shown in Figure 5-1 shows two light sequences of two 5 min of HL exposure with 20 minutes of LL ranging from 0 µE to 400 µE separating the two HL periods. The second sequence is of two repeating cycles of 5 min of HL followed by 5 minutes of LL. Unfortunately, there is an issue of biological noise that arises from how the *N. oceanica* was cultured, but several interesting conclusions can be made from the data to guide future work on this topic.

For further work on this subject, a saturation curve for *N. oceanica* would be beneficial to guide which lower light intensities should be used in the experiments. This was not done for the preliminary tests as assumptions were made based on previous work and culturing conditions. The typical HL intensity is 750 µE so the LL values were chosen for the preliminary work to consistent of sub-saturating values such as 50 µE which is close to the light level the cells are grown under

(40 μE). The 200 μE and 400 μE were chosen as they are less than the HL value but thought to be sub-saturating. The preliminary data show that this assumption is not true as 400 μE induces the same NPQτ value as 750 μE (data not shown). However, with a saturation curve, the exact levels at which NPQ is low and when it saturates can be used.

In Figure 5-1A, the most interesting features appear at the transition from 750 μE to either 50 μE (orange) or 200 μE (green) at t = 5 min. In the HL to 50 μE transition, there is an immediate decrease in NPQτ similar to that seen in a HL to D transition; however, within 30 seconds, the NPQτ level begins to increase in LL. It continues to rise for the rest of the 20 min LL period until a steady state level is reached. Upon transition from 50 μE to 750 μE at t = 25 min, there is no discernable increase in NPQτ as seen in a typical D to HL transition (dark blue). For the 200 μE LL sequence, there is no decrease in NPQτ at the HL to LL transition, but the value remains constant for several minutes before increasing to a steady state value that is retained through the LL to HL transition. The 400 μE LL sequence follows a similar trend as the 200 μE LL sequence, but due to inconsistency from the growth conditions, it is difficult to see this trend without normalizing all sequences at t = 5 min (data not shown).

Figure 5-1B shows data from the 5 min HL- 5 min LL periodic sequence run using the same range of LL. The trends are very similar to those discussed above; though, the 50 μE sequence (orange) does have a few interesting features to note. First, in the first HL to LL transition at t = 5 min, the immediate decrease in NPQτ is retained but plateaus for ~ 2 minutes before the value begins to increase. It would be interesting to investigate if this slight decrease is related to the acidification of the lumen, which might require time to build up at lower light intensities, or if this is due to VDE being activated in a non-ideal pH environment. The next interesting feature is at the LL to HL transition at t = 10 min. At this transition, there is a slight, rapid increase in NPQτ indicating the pH gradient was sub-saturating before this moment. Finally, at the second HL to LL transition (t = 15 min), there is again a minute, but instantaneous, decrease in NPQτ, signifying a change in the pH gradient across the thylakoid membrane.

These initial data are intriguing and encouraging, yet a few issues should be addressed in future work. One potential explanation for why no significant change in NPQ behavior was in for LL at 200 μE or 400 μE is that the NPQ mechanisms had already been completely activated and saturated, covering any minor relaxation we might see at these values. To test this theory, shorter initial HL excitation periods should be utilized followed by LL.

5.3 Comparing Two-State Versus Three-State Xanthophyll Cycles

The model developed for making quantitative and accurate predictions of predicting *Nannochloropsis oceanica* NPQ[2,10] is a three-state model based on the VAZ cycle. The role of A as a rapidly convertible buffer is critical to the model's success in describing the short-term "memory" of the response to high light. This suggests a two-state system would have very different response to periodic and aperiodic light exposure. Evidence of this is explored in detail in Chapter 4. However, one unanswered question is why have photosynthetic organisms developed two xanthophyll cycles. Additionally, what are the benefits of a two-state system versus a three-state system on adapting to fluctuating light conditions.

Based on the modeling work from Chapter 4, the Dd-Dt cycle appears to respond to changes in light levels, increasing the responsiveness of NPQ. To further test if a two-state system could benefit organisms exposed to rapid light fluctuations, a two-state system needs to be introduced

into a model organism that typically has the VAZ cycle. One way to do this would be to replace the VDE enzyme in *N. oceanica* with the VDE strain from *Mantoniella squamata* or *Ostreococcus lucimarinus*[20–22]. Both species are only able to convert V to A with little to no accumulation of Z in natural conditions.

With the VA-*Nannochloropsis* mutant, a similar battery of tests utilized throughout this thesis would be used to determine the NPQ dynamics. Special attention would be given to observing changes in photoprotective memory. If the VA-*Nannochloropsis* acts like *T. pseudonana*, then we would expect to see a sustained photoprotective memory, even after twenty minutes of dark incubation, unlike what is seen in WT *Nannochloropsis*. In addition to experiments to characterize the NPQ dynamics of VA-*Nannochloropsis*, tests should be run to identify which condition survives in fluctuating growth conditions. By comparing the WT *N. oceanica* to the VA-mutant to *T. pseudonana*, we can determine what conditions are best suited for fluctuating light conditions. The experiments would be similar to those done in Steen, Burlacot et *al* where the algae are grown in a variety of light/dark cycles on agar plates for several days[23]. To fully test if xanthophyll cycle enzymes relate to improved fitness in fluctuating light, the light/dark cycles should range from 1 min to 12 hr periods. For a control, the algae should also be grown in continuous light, which may also indicate which xanthophyll system is more robust in extended light periods.

5.4 Modeling Non-Photochemical Quenching in Plants

The success of a xanthophyll cycle-based model to quantify the mechanism of qE in the single-cell alga *N. oceanica* and its flexibility to describe *T. pseudonana*, which utilizes an entirely different xanthophyll cycle, is encouraging as we endeavor to model the NPQ response in crop plants. However, in order to describe vascular plants, we need to increase the complexity of the model to include more complicated NPQ mechanisms, such as the addition of lutein as quenching carotenoid, state transitions, and photo-inhibitory effects. Utilizing the plant, *Nicotiana benthamiana*, we can extend the existing model by incorporating parameters for lutein-dependent qE, zeaxanthin-dependent quenching (qZ), photoinhibition (qI). *N. benthamiana* is an ideal model organism because many mutants already exist which target specific molecular NPQ components, allowing us to recursively build an intuition for how each component contributes to the WT phenotype. Through subtraction from the WT photoprotective phenotype, we can quantify the extent each unique molecular actor contributes to NPQ. In addition to the added complexities from light intensities and durations, this improved model would be able to describe the NPQ response in fields. We could then alter the model parameters to test how modifications to gene expression could improve photoprotective responses, allowing us to optimize crop yields with guidance.

5.5 References

1. Souza, A. P. D. *et al.* Soybean photosynthesis and crop yield are improved by accelerating recovery from photoprotection. *Science* **377**, 851–854 (2022).
2. Short, A. *et al.* Kinetics of the xanthophyll cycle and its role in photoprotective memory and response. *Nat. Commun.* **14**, 6621 (2023).
3. Zhu, S.-H. & Green, B. R. Photoprotection in the diatom Thalassiosira pseudonana: Role of LI818-like proteins in response to high light stress. *Biochim. Biophys. Acta (BBA) - Bioenerg.* **1797**, 1449–1457 (2010).
4. Steen, C. J., Morris, J. M., Short, A. H., Niyogi, K. K. & Fleming, G. R. Complex Roles of PsbS and Xanthophylls in the Regulation of Nonphotochemical Quenching in Arabidopsis thaliana under Fluctuating Light. *J Phys Chem B* **124**, 10311–10325 (2020).
5. Kaiser, E. *et al.* Dynamic photosynthesis in different environmental conditions. *J Exp Bot* **66**, 2415–2426 (2015).
6. Morales, A. & Kaiser, E. Photosynthetic Acclimation to Fluctuating Irradiance in Plants. *Front. Plant Sci.* **11**, 268 (2020).
7. Slattery, R. A., Walker, B. J., Weber, A. P. M. & Ort, D. R. The impacts of fluctuating light on crop performance. *Plant Physiol* **176**, pp.01234.2017 (2017).
8. MacIntyre, S. Vertical mixing in a shallow, eutrophic lake: Possible consequences for the light climate of phytoplankton. *Limnol. Oceanogr.* **38**, 798–817 (1993).
9. Hintz, N. H., Schulze, B., Wacker, A. & Striebel, M. Ecological impacts of photosynthetic light harvesting in changing aquatic environments: A systematic literature map. *Ecol. Evol.* **12**, e8753 (2022).
10. Short, A. H. *et al.* Xanthophyll-cycle based model of the rapid photoprotection of Nannochloropsis in response to regular and irregular light/dark sequences. *J Chem Phys* (2022) doi:10.1063/5.0089335.
11. Ware, M. A., Belgio, E. & Ruban, A. V. Photoprotective capacity of non-photochemical quenching in plants acclimated to different light intensities. *Photosynth. Res.* **126**, 261–274 (2015).
12. Lazzarin, M., Driever, S., Wassenaar, M., Marcelis, L. F. M. & Ieperen, W. van. Shining light on diurnal variation of non-photochemical quenching: Impact of gradual light intensity patterns on short-term NPQ over a day. *Physiol. Plant.* **176**, e14410 (2024).
13. Ruban, A. V. & Belgio, E. The relationship between maximum tolerated light intensity and photoprotective energy dissipation in the photosynthetic antenna: chloroplast gains and losses. *Philos. Trans. R. Soc. B: Biol. Sci.* **369**, 20130222 (2014).
14. Long, S. P. *et al.* Into the Shadows and Back into Sunlight: Photosynthesis in Fluctuating Light. *Annu. Rev. Plant Biol.* **73**, 617–648 (2022).
15. Graham, P. J., Nguyen, B., Burdyny, T. & Sinton, D. A penalty on photosynthetic growth in fluctuating light. *Sci. Rep.* **7**, 12513 (2017).
16. Kaiser, E., Walther, D. & Armbruster, U. Growth under Fluctuating Light Reveals Large Trait Variation in a Panel of Arabidopsis Accessions. *Plants* **9**, 316 (2020).
17. Alter, P., Dreissen, A., Luo, F.-L. & Matsubara, S. Acclimatory responses of Arabidopsis to fluctuating light environment: comparison of different sunfleck regimes and accessions. *Photosynth. Res.* **113**, 221–237 (2012).
18. Murchie, E. H., Pinto, M. & Horton, P. Agriculture and the new challenges for photosynthesis research. *N. Phytol.* **181**, 532–552 (2009).
19. Murchie, E. H. & Ruban, A. V. Dynamic non-photochemical quenching in plants: from molecular mechanism to productivity. *Plant J* **101**, 885–896 (2020).
20. Goss, R. & Lepetit, B. Biodiversity of NPQ. *J Plant Physiol* **176**, 13–32 (2014).
21. Goss, R., Böhme, K. & Wilhelm, C. The xanthophyll cycle of Mantoniella squamata converts violaxanthin into antheraxanthin but not to zeaxanthin: consequences for the mechanism of enhanced non-photochemical energy dissipation. *Planta* **205**, 613–621 (1998).

22. Frommolt, R., Goss, R. & Wilhelm, C. The de-epoxidase and epoxidase reactions of Mantoniella squamata (Prasinophyceae) exhibit different substrate-specific reaction kinetics compared to spinach. *Planta* **213**, 446–456 (2001).
23. Steen, C. J., Burlacot, A., Short, A. H., Niyogi, K. K. & Fleming, G. R. Interplay between LHCSR proteins and state transitions governs the NPQ response in Chlamydomonas during light fluctuations. *Plant Cell Environ* **45**, 2428–2445 (2022).